ERDC/GSL TR-07-23

Geotechnical and Structures Laboratory

US Army Corps
of Engineers®
Engineer Research and
Development Center

Laboratory Characterization of Gray Masonry Concrete

Erin M. Williams, Stephen A. Akers, and Paul A. Reed

August 2007

ERDC/GSL TR-07-23
August 2007

Laboratory Characterization of Gray Masonry Concrete

Erin M. Williams, Stephen A. Akers, and Paul A. Reed

Geotechnical and Structures Laboratory
U.S. Army Engineer Research and Development Center
3909 Halls Ferry Road
Vicksburg, MS 39180-6199

Final report

Prepared for Headquarters, U.S. Army Corps of Engineers
Washington, DC 20314-1000

Under AT40 Work Unit, Dynamic Behavior of Complex Geologic/Structural Materials

Abstract: Personnel of the Geotechnical and Structures Laboratory, U.S. Army Engineer Research and Development Center, conducted a laboratory investigation to characterize the strength and constitutive property behavior of a gray masonry concrete. A total of 38 mechanical property tests were successfully completed: two hydrostatic compression tests, four unconfined compression (UC) tests, 16 triaxial compression (TXC) tests, two uniaxial strain tests, two uniaxial strain load/biaxial strain unload tests, five uniaxial strain load/constant volume strain loading (UX/CV) tests, two uniaxial strain load/constant strain ratio (UX/SR) tests, three direct pull tests, and two reduced triaxial extension tests. In addition to the mechanical property tests, nondestructive pulse-velocity measurements were performed on each specimen. The TXC tests exhibited a continuous increase in maximum principal stress difference with increasing confining stress. A compression failure surface was developed from the TXC test results at eight levels of confining stress and from the results of the UC tests. The results of the direct pull and reduced triaxial extension tests were used to develop the extension failure surface. The resulting compression and extension failure surfaces were well defined and nonsymmetric about the mean normal stress axis. Good correlations were observed between the stress paths obtained from the UX/CV and UX/SR strain path tests and the failure surface from the TXC test.

Contents

Figures and Tables

Figures

Tables

Preface

This laboratory mechanical property investigation of gray masonry concrete was conducted by personnel of the U.S. Army Engineer Research and Development Center (ERDC) at the Waterways Experiment Station (WES) site. Funding was provided by Headquarters, U.S. Army Corps of Engineers under the Dynamic Behavior of Complex Geologic/Structural Materials Work Unit of the AT40 Weapons Effects and Structural Response Work Package. This study was conducted from November 2003 to February 2004 by staff members of the Impact and Explosion Effects Branch (IEEB), Engineering Systems and Materials Division (ESMD), Geotechnical and Structures Laboratory (GSL), ERDC, under the general direction of Henry S. McDevitt, Jr., Chief, IEEB; Dr. Larry N. Lynch, Chief, ESMD; Dr. William P. Grogan, Deputy Director, GSL; and Dr. David W. Pittman, Director, GSL.

The Principal Investigator for this project was Dr. Stephen A. Akers, IEEB. Erin M. Williams, IEEB, served as co-investigator for this project, processed the material property data, and prepared this report. Laboratory characterization tests were performed by Paul A. Reed, IEEB, under the technical direction of Dr. Akers. Instrumentation support was provided by A. Leroy Peeples, Engineering and Informatic Systems Division, Information Technology Laboratory, ERDC.

COL Richard B. Jenkins was Commander and Executive Director of ERDC. Dr. James R. Houston was Director.

1 Introduction

Background

Personnel of the Geotechnical and Structures Laboratory, U.S. Army Engineer Research and Development Center at the Waterways Experiment Station (WES) site conducted a laboratory investigation to characterize the strength and constitutive property behavior of gray masonry concrete (GMC) for the Dynamic Behavior of Complex Geologic/Structural Materials Work Unit of the AT40 Weapons Effects and Structural Response Work Package. WES personnel conducted a total of 38 mechanical property tests, all of which were successfully completed. The 38 tests consisted of two hydrostatic compression tests, four unconfined compression (UC) tests, 16 triaxial compression (TXC) tests, two uniaxial strain tests, two uniaxial strain load/biaxial strain unload tests, five uniaxial strain load/constant volume strain loading (UX/CV) tests, two uniaxial strain load/constant strain ratio (UX/SR) tests, three direct pull tests, and two reduced triaxial extension tests. In addition to the mechanical property tests, nondestructive pulse-velocity measurements were performed on each specimen.

Purpose and scope

The purpose of this report is to document the results from the laboratory mechanical property tests conducted on the GMC specimens. In addition, results from the nondestructive pulse-velocity measurements are documented. The physical and composition properties, test procedures, and test results are documented in Chapter 2. Comparative plots and analyses of the experimental results are presented in Chapter 3. A summary is provided in Chapter 4.

2 Laboratory Tests

Material description

The test specimens used in this investigation were prepared from samples cored from solid concrete masonry units of GMC. The company that produced the 0.295-scale concrete masonry units used in scaled laboratory experiments also produced the solid standard-size concrete masonry units. The GMC material is a standard commercial material for concrete masonry units. Typically, each solid concrete masonry unit produced six to eight cored test specimens. Additional details are documented in the Specimen Preparation section of this chapter.

Composition property tests

Prior to performing the mechanical property tests, the height, diameter, and mass for each test specimen were determined. These measurements were used to compute the specimen's wet, bulk, or "as-tested" density. Results from these determinations are provided in Table 1. Measurements of posttest water content[1] were conducted in accordance with procedures given in American Society for Testing and Materials (ASTM) D 2216 (ASTM 2002e). Based on the appropriate values of posttest water content, wet density, and an assumed grain density of 2.61 Mg/m^3, values of dry density, porosity, degree of saturation, and volumes of air, water, and solids were calculated (Table 1). Also listed in the table are maximum, minimum, and mean values and the standard deviation about the mean for each quantity. The GMC specimens had a mean wet density of 2.141 Mg/m^3 (based on data from 38 specimens), a mean water content of 2.06 percent, and a mean dry density of 2.100 Mg/m^3 (based on data from 35 specimens).

Ultrasonic pulse-velocity determinations

Prior to performing a mechanical property test, ultrasonic pulse-velocity measurements were collected on each test specimen. This involved measuring the transit distance and time for each P (compressional) or S (shear) pulse to propagate through a given specimen. The velocity was

[1] Water content is defined as the weight of water (removed during drying in a standard oven) divided by the weight of dry solids.

then computed by dividing the transit distance by the transit time. A matching pair of 1 MHz piezoelectric transducers were used to transmit and receive the ultrasonic P waves. A pair of 2.25 MHz piezoelectric transducers were used to transmit and receive the ultrasonic S waves. The transit time was measured with a 100 MHz digital oscilloscope and the transit distance with a digital micrometer. All of these wave-velocity determinations were made under atmospheric conditions, i.e., no prestress of any kind was applied to the specimens. The tests were conducted in accordance with procedures given in ASTM C 597 (ASTM 2002c).

One compressional-wave (P-wave) and one shear-wave (S-wave) velocity were determined axially through each specimen. Radial P- and S-wave velocities were determined for each specimen in the following manner. Six radial P-wave velocities were determined, i.e., two transverse to each other at elevations of 1/4, 1/2, and 3/4 of the specimen height. Two radial S-wave velocities were measured; both of these determinations were made at the mid-height of the specimen transverse to each other. The various P- and S-wave velocities determined for the test specimens are provided in Table 1; the radial-wave velocities listed in Table 1 are the average values.

Mechanical property tests

Thirty-eight mechanical property tests were successfully performed on the GMC specimens to characterize the strength and constitutive properties of the material. All of the mechanical property tests were conducted quasi-statically with axial strain rates on the order of 10^{-4} to 10^{-5} per second and times to peak load on the order of 5 to 30 minutes. Mechanical property data were obtained under several different stress and strain paths. Undrained compressibility data were obtained during the hydrostatic loading phase of the triaxial compression (TXC) tests and from two hydrostatic compression (HC) tests. Shear and failure data were obtained from unconsolidated-undrained TXC tests, the direct pull (DP) tests, and from reduced triaxial extension (RTE) tests. One-dimensional compressibility data were obtained from undrained uniaxial strain (UX) tests with lateral stress measurements or K_o tests. Three different types of undrained strain-path tests were conducted during the test program. All of the strain-path tests were initially loaded under uniaxial strain boundary conditions to a prescribed level of stress or strain. At the end of the UX loading, constant axial to radial strain ratios (ARSR) of 0, -1.33, and -2.0 were applied. The ARSR = 0 path is a constant axial strain

unloading path and produces a forced state of volumetric expansion; these tests will be referred to as UX/BX tests. The UX/SR tests have an ARSR = -1.33, produces a path that has a constant strain ratio when loaded. The ARSR = -2.0 path is a constant volume strain loading path, and these paths will be referred to as UX/CV tests. The terms undrained and unconsolidated signify that no pore fluid (liquid or gas) was allowed to escape or drain from the membrane-enclosed specimens. The completed test matrix is presented in Table 2. Table 2 lists the types of tests conducted, the number of tests, the test numbers for each group, the test numbers of the specimens that had cyclic loading, and the nominal peak radial stress applied to specimens prior to shear loading or during the HC, UX, or strain-path loading.

Specimen preparation

The mechanical property test specimens were cut from sections of GMC using a diamond-bit core barrel by following the procedures provided in ASTM C 42 (ASTM 2002b). The test specimens were cut to the correct length, and the ends were ground flat and parallel to each other and perpendicular to the sides of the core in accordance with procedures in ASTM D 4543 (ASTM 2002f). Prior to testing, the prepared specimens were measured for height, diameter, and weight and were ultrasonically pulsed. This information was used to calculate the composition properties and wave velocities of the specimens. The prepared test specimens had a nominal height of 110 mm and a diameter of 50 mm.

Prior to testing, each specimen was placed between hardened steel top and base caps. With the exception of the UC and DP test specimens, two 0.6-mm-thick membranes were placed around the specimen, then a thick Aqua seal® membrane, and finally the exterior of the outside membrane was coated with a liquid synthetic rubber to inhibit deterioration caused by the confining-pressure fluid (Figure 1). The fluid was a mixture of kerosene and hydraulic oil. Finally, the specimen, along with its top cap and base cap assembly, was placed on the instrumentation stand of the test apparatus, and the instrumentation setup was initiated.

Test devices

Four different sets of test devices were used in this test program. The axial load for all of the UC tests was provided by a 3.3-MN (750,000-lb) loader. The application of load was manually controlled with this test device. No

pressure vessel was required for the UC tests; only a base, load cell, and vertical and radial deformeters were necessary.

Direct pull tests were performed by using the direct pull apparatus, in which end caps were attached to unconfined specimens with a high-modulus high-strength epoxy. A manual hydraulic pump was used to pressurize the direct pull chamber. When the direct pull chamber was pressurized, a piston retracted and produced tensile loading on the test specimen. Measurements for the loading of the specimen were recorded by the load cell.

To perform a RTE test, a static high-pressure triaxial test device (HPTX) was used (Figure 2). This device was manually controlled and can be pressurized up to 100 MPa. The pumping equipment that was used during the operation of this device limited the peak pressure to 70 MPa. When the triaxial extension top cap was used with the HPTX device, independent control of the vertical and lateral stresses was permitted. The specimen top cap was bolted to the extension loading piston, and the surface on top of the piston was pressurized. During a RTE test, the confining pressure (or radial stress) was kept constant while the vertical stress was reduced (Akers, Reed, and Ehrgott 1986).

All of the remaining tests were conducted in a 600-MPa-capacity pressure vessel, and the axial load was provided by an 8.9-MN (2-million-lb) loader. With the 8.9-MN loader, the application of load, pressure, and axial displacement were regulated by a servo-controlled data acquisition system. This servo-controlled system allowed the user to program rates of load, pressure, and axial displacement in order to achieve the desired stress or strain path. Confining pressure was measured external to the pressure vessel by a pressure transducer mounted in the confining fluid line. A load cell mounted in the base of the specimen pedestal was used to measure the applied axial loads inside the pressure vessel (Figure 1).

Outputs from the various instrumentation sensors were electronically amplified and filtered, and the conditioned signals recorded by computer-controlled 16-bit analog-to-digital converters. The data acquisition systems were programmed to sample the data channels every 1 to 5 seconds, convert the measured voltages to engineering units, and store the data for further posttest processing.

Test instrumentation

The vertical deflection measurement system in all the test areas except the DP test area consisted of two linear variable differential transformers (LVDTs) mounted vertically on the instrumentation stands and positioned 180-degrees apart. They were oriented to measure the displacement between the top and base caps, thus providing a measure of the axial deformations of the specimen. For the confined tests, a linear potentiometer was mounted external to the pressure vessel so as to measure the displacement of the piston through which axial loads were applied. This provided a backup to the vertical LVDTs in case they exceeded their calibrated range.

Two different types of radial deflection measurement systems (lateral deformeters) were used in this test program. The output of each deformeter was calibrated to the radial displacement of the two footings that were glued to the sides of the test specimen (Figure 1). These two small steel footings were mounted 180-degrees apart at the specimen's mid-height. The footing faces were machined to match the curvature of the test specimen. A threaded post extended from the outside of each footing and protruded through the membrane. The footings were mounted to the specimen prior to placement of the membrane. Once the membranes were in place, steel caps were screwed onto the threaded posts to seal the membrane to the footing. The lateral deformeter ring was attached to these steel caps with set-screws. The completed specimen lateral deformeter setup is shown in Figure 3.

One type of lateral deformeter consisted of an LVDT mounted on a hinged ring; the LVDT measured the expansion or contraction of the ring. This lateral deformeter was used over smaller ranges of radial deformation when the greatest measurement accuracy was required. This lateral deformeter was used for all of the HC, UC, UX, and strain-path tests and for the TXC tests at confining pressures less than 50 MPa. This design is similar to the radial-deformeter design provided by Bishop and Henkel (1962). When the specimen expanded (or contracted), the hinged-deformeter ring opened up (or closed) causing a change in the electrical output of the horizontally mounted LVDT.

The second type of lateral deformeter, which was used for all of the TXC tests at confining pressures of 50 MPa and greater, consisted of two strain-gauged spring-steel arms mounted on a double-hinged ring; the strain-

gauged arms deflected as the ring expanded or contracted. This lateral deformeter was used when the greatest radial deformation range was required and therefore, was less accurate than the LVDT deformeter. With this deformeter, when the specimen expanded or contracted, the rigid deformeter ring flexed about its hinge causing a change in the electrical output of the strain-gauged spring-arm. The output of the spring-arms was calibrated to the specimen's deformation. Radial measurements were not performed during the DP tests.

Test descriptions

The UC and TXC tests were performed in accordance with ASTM C 39 (ASTM 2002a) and ASTM C 801 (ASTM 2002d), respectively. TXC tests were conducted in two phases. During the first phase, the hydrostatic compression phase, the cylindrical test specimen was subjected to an increase in hydrostatic pressure while measurements of the specimen's height and diameter changes were made. The data are typically plotted as pressure versus volumetric strain, the slope of which, assuming elastic theory, is the bulk modulus, *K*. The second phase of the TXC test, the shear phase, was conducted after the desired confining pressure was applied during the HC phase. While holding the desired confining pressure constant, axial load was increased, and measurements of the changes in the specimen's height and diameter were made. The axial (compressive) load was increased until the specimen failed. The shear data are generally plotted as principal stress difference versus axial strain, the slope of which represents Young's modulus, *E*. The maximum principal stress difference that a given specimen can support or the principal stress difference at 15 percent axial strain during the shear loading, whichever occurs first, is defined as the peak strength.

Note that the UC test is a TXC test in which no confining pressure is applied. The maximum principal stress difference observed during a UC test is defined as the unconfined compressive strength of the material.

Extension data were obtained for GMC by performing direct pull (DP) tests and reduced triaxial extension (RTE) tests. The DP tests have no confining pressure during the tests. To conduct the DP tests, end caps were attached with epoxy to the specimen. The end caps were screwed into the direct pull apparatus, and the specimen was pulled apart vertically when pressure was applied to the piston. The RTE tests were conducted with the HPTX device and the TXE top cap (Figure 2). To begin the RTE

test, the specimen was loaded hydrostatically to a desired confining pressure. After the hydrostatic loading was applied and while the radial stress was held constant, the vertical stress was reduced until the specimen failed. Throughout the RTE test, the specimen's height and diameter changes were recorded (Akers, Reed, and Ehrgott 1986). Extension shear data for the material is generally plotted as principal stress difference versus axial strain.

A uniaxial strain (UX) test was conducted by applying axial load and confining pressure simultaneously so that, as the cylindrical specimen shortened, its diameter remained unchanged, i.e., zero radial strain boundary conditions were maintained. The data are generally plotted as axial stress versus axial strain, the slope of which is the constrained modulus, M. The data are also plotted as principal stress difference versus mean normal stress, the slope of which is twice the shear modulus G divided by the bulk modulus K , i.e., 2G/K, or, in terms of Poisson's ratio ν , $3(1-2\nu)/(1+\nu)$.

The strain-path tests in this test program were conducted in two phases. Initially, the specimen was subjected to a uniaxial-strain loading up to a desired level of mean normal, radial, or axial stress. At the end of the UX loading, constant axial-to-radial-strain ratios of 0, -1.33, or -2.0 were applied; these tests were identified earlier as UX/BX, UX/SR, and UX/CV tests, respectively. In order to conduct these tests, the software controlling the servo-controls had to correct the measured inputs for system compressibility and for the nonlinear calibrations of specific transducers.

Definition of stresses and strains

During the mechanical property tests, measurements were typically made of the axial and radial deformations of the specimen as confining pressure and/or axial load was applied or removed. These measurements along with the pretest measurements of the initial height and diameter of the specimen were used to convert the measured test data to true stresses and engineering strains.[2]

Axial strain, ε_a , was computed by dividing the measured axial deformation, Δh (change in height), by the original height h_o , i.e., $\varepsilon_a = \Delta h/h_o$. Similarly, radial strain, ε_r , was computed by dividing the measured

[2] Compressive stresses and strains are positive in this report.

radial deformation, Δd (change in diameter), by the original diameter d_o, i.e., $\varepsilon_r = \Delta d/d_o$. For this report, volumetric strain was assumed to be the sum of the axial strain and twice the radial strain, $\varepsilon_v = \varepsilon_a + 2\varepsilon_r$.

The principal stress difference, q, was calculated by dividing the axial load by the cross-sectional area of the specimen A, which is equal to the original cross-sectional area, A_o, multiplied by $(1 - \varepsilon_r)^2$. In equation form,

$$q = (\sigma_a - \sigma_r) = \frac{\text{Axial Load}}{\text{A}_\text{o}(1-\varepsilon_r)^2} \tag{1}$$

where σ_a is the axial stress and σ_r is the radial stress. The axial stress is related to the confining pressure and the principal stress difference by

$$\sigma_a = q + \sigma_r \tag{2}$$

The mean normal stress, p, is the average of the applied principal stresses. In cylindrical geometry,

$$p = \frac{(\sigma_a + 2\sigma_r)}{3} \tag{3}$$

Results

Results from all of the mechanical property tests except from the direct pull tests are presented in Plates 1-35. One data plate is presented for each test with reliable results. Results from the HC tests are presented on the plates in four plots, i.e., (a) mean normal stress versus volumetric strain, (b) mean normal stress versus axial strain, (c) radial versus axial strain, and (d) mean normal stress versus radial strain. Each plate for the UC, TXC, UX, strain-paths, and RTE tests displays four plots, i.e., (a) principal stress difference versus mean normal stress, (b) principal stress difference versus axial strain, (c) volumetric strain versus mean normal stress, and (d) volumetric strain versus axial strain.

Table 1. Physical and composition properties of GMC.

Test number	Type of test	Plate no.	Wet density Mg/m³	Posttest water content %	Dry density Mg/m³	Porosity %	Degree of saturation %	Volume of air %	Volume of water %	Volume of solids %	Axial P wave velocity km/s	Radial P wave velocity km/s	Axial S wave velocity km/s	Radial S wave velocity km/s
01	TXC/5	7	2.115	2.45	2.065	20.89	24.22	15.83	5.06	79.11	4.442	4.205	2.593	2.635
02	TXC/5	8	2.164	3.27	2.096	19.70	34.79	12.85	6.85	80.30	4.434	4.338	2.677	2.719
03	TXC/10	9	2.097	2.40	2.048	21.55	22.81	16.63	4.91	78.45	4.338	4.222	2.534	2.595
04	TXC/10	10	2.165	2.83	2.105	19.34	30.81	13.38	5.96	80.66	4.469	4.298	2.639	2.676
05	UX	23	2.200	3.02	2.135	18.20	35.44	11.75	6.45	81.80	4.589	4.447	2.827	2.782
06	UX	24	2.170	2.64	2.114	19.00	29.37	13.42	5.58	81.00	4.456	4.317	2.656	2.729
07	UX/BX	25	2.144								4.422	4.278	2.616	2.686
08	UX/BX	26	2.172	2.83	2.112	19.07	31.34	13.09	5.98	80.93			2.667	2.708
09	UX/CV	27	2.190	2.79	2.130	18.39	32.32	12.44	5.94	81.61	4.506	4.400	2.776	2.715
10	UX/CV	28	2.198	2.84	2.138	18.10	33.53	12.03	6.07	81.90	4.561	4.458	2.834	2.749
11	UX/CV	29	2.198	2.70	2.140	18.02	32.06	12.24	5.78	81.98	4.517	4.387	2.796	2.795
12	UX/CV	30	2.186	2.74	2.128	18.48	31.54	12.66	5.83	81.52	4.554	4.361	2.809	2.709
13	UX/SR	32	2.195	2.73	2.137	18.13	32.17	12.30	5.83	81.87	4.585	4.426	2.781	2.745
14	UX/CV	31	2.192	2.72	2.134	18.25	31.79	12.45	5.80	81.75	4.513	4.391	2.749	2.763
15	UX/SR	33	2.169	3.00	2.106	19.31	32.71	13.00	6.32	80.69	4.455	4.412	2.678	2.675
16	UC	3	2.170	2.27	2.122	18.70	25.75	13.89	4.82	81.30	4.499	4.361	2.705	2.700
17	UC	4	2.093	1.75	2.057	21.20	16.98	17.60	3.60	78.80	4.383	4.238	2.609	2.590
18	UC	5	2.155	2.14	2.110	19.17	23.54	14.66	4.51	80.83	4.580	4.334	2.733	2.696
19	UC	6	2.091	1.83	2.054	21.32	17.62	17.56	3.76	78.68	4.383	4.174	2.605	2.586
20	RTE/65	34	2.133								4.472	4.343	2.636	2.742
21	RTE/65	35	2.076								4.317	4.185	2.548	2.563
22	DP		2.144	1.56	2.111	19.13	17.21	15.83	3.29	80.87	4.540	4.412	2.755	2.753
23	DP		2.177	1.67	2.141	17.98	19.89	14.40	3.58	82.02	4.531	4.421	2.734	2.777
24	DP		2.057	1.29	2.031	22.18	11.81	19.56	2.62	77.82	4.469	4.130	2.545	2.564
25	TXC/20	11	2.179	1.51	2.147	17.75	18.26	14.51	3.24	82.25	4.570	4.432	2.719	2.784

26	TXC/20	12	2.096	1.32	2.069	20.72	13.18	17.99	2.73	79.28	4.404	4.258	2.642	2.620
27	TXC/50	13	2.083	1.37	2.055	21.27	13.24	18.45	2.82	78.73	4.329	4.221	2.605	2.602
28	TXC/50	14	2.054	1.37	2.026	22.37	12.41	19.60	2.78	77.63	4.230	4.087	2.495	2.497
29	TXC/100	15	2.078	1.40	2.049	21.48	13.36	18.61	2.87	78.52	4.325	4.189	2.559	2.630
30	TXC/100	16	2.175	1.69	2.139	18.06	20.01	14.45	3.61	81.94	4.579	4.451	2.770	2.783
31	TXC/200	17	2.184	1.58	2.150	17.64	19.26	14.24	3.40	82.36	4.582	4.425	2.816	2.764
32	TXC/200	18	2.163	1.60	2.129	18.45	18.46	15.04	3.41	81.55	4.497	4.393	2.686	2.724
33	TXC/300	19	2.100	1.44	2.070	20.69	14.40	17.71	2.98	79.31	4.356	4.200	2.644	2.640
34	TXC/300	20	2.080	1.34	2.052	21.37	12.87	18.62	2.75	78.63	4.274	4.152	2.535	2.585
35	TXC/400	21	2.169	1.65	2.134	18.24	19.31	14.72	3.52	81.76	4.536	4.424	2.754	2.764
36	TXC/400	22	2.142	.1.47	2.110	19.14	16.21	16.04	3.10	80.86	4.452	4.348	2.620	2.613
37	HC	1	2.146	1.44	2.115	18.96	16.07	15.91	3.05	81.04	4.502	4.387	2.719	2.725
38	HC	2	2.074	1.31	2.047	21.56	12.44	18.88	2.68	78.44	4.359	4.142	2.579	2.632
N			38	35	35	35	35	35	35	35	37	37	38	38
Mean			2.141	2.06	2.100	19.54	22.49	15.21	4.33	80.46	4.460	4.315	2.675	2.685
Stdv			0.046	0.649	0.038	1.459	7.981	2.439	1.397	1.459	0.096	0.108	0.093	0.077
Max			2.200	3.27	2.150	22.37	35.44	19.60	6.85	82.36	4.589	4.458	2.834	2.795
Min			2.054	1.29	2.026	17.64	11.81	11.75	2.62	77.63	4.230	4.087	2.495	2.497

Table 2. Completed GMC test matrix.

Type of test	No. of tests	Test nos.	Cycled tests nos.	Nominal peak radial stress, MPa
Hydrostatic compression	2	37, 38	38	500
Triaxial compression	4	16-19		0
	2	1, 2		5
	2	3, 4	4	10
	2	25, 26	26	20
	2	27, 28	28	50
	2	29, 30	29	100
	2	31, 32	31	200
	2	33, 34		300
	2	35, 36	36	400
UX strain	2	5, 6	6	500
UX/BX	1	7		50
	1	8		100
UX/CV	1	11		50
	2	9, 10		100
	1	12		150
	1	14		200
UX/SR	2	13, 15		
Direct pull extension	3	22-24		0
Reduce triaxial extension	2	20, 21		65
Total # tests:	38			

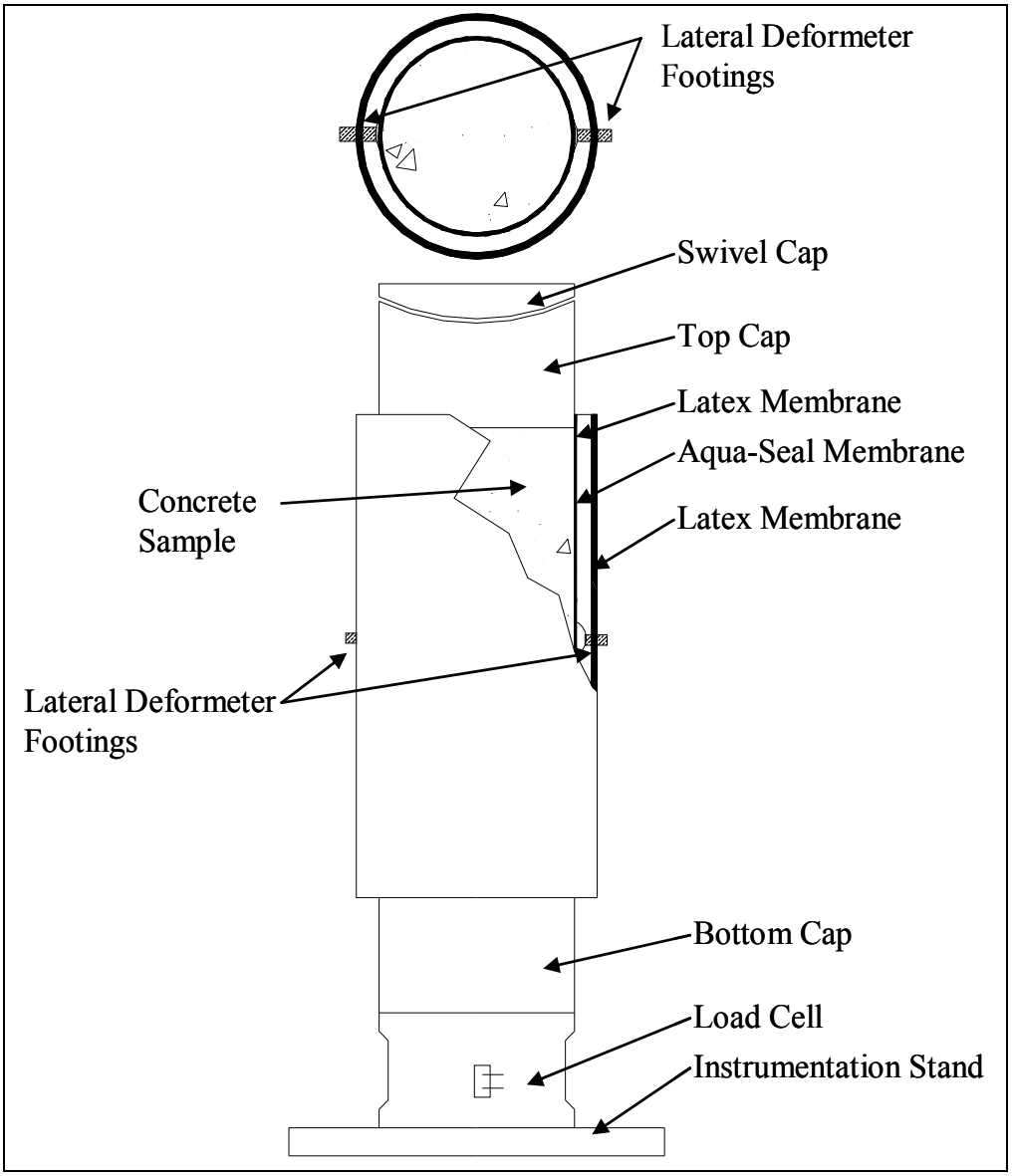

Figure 1. Typical test specimen setup.

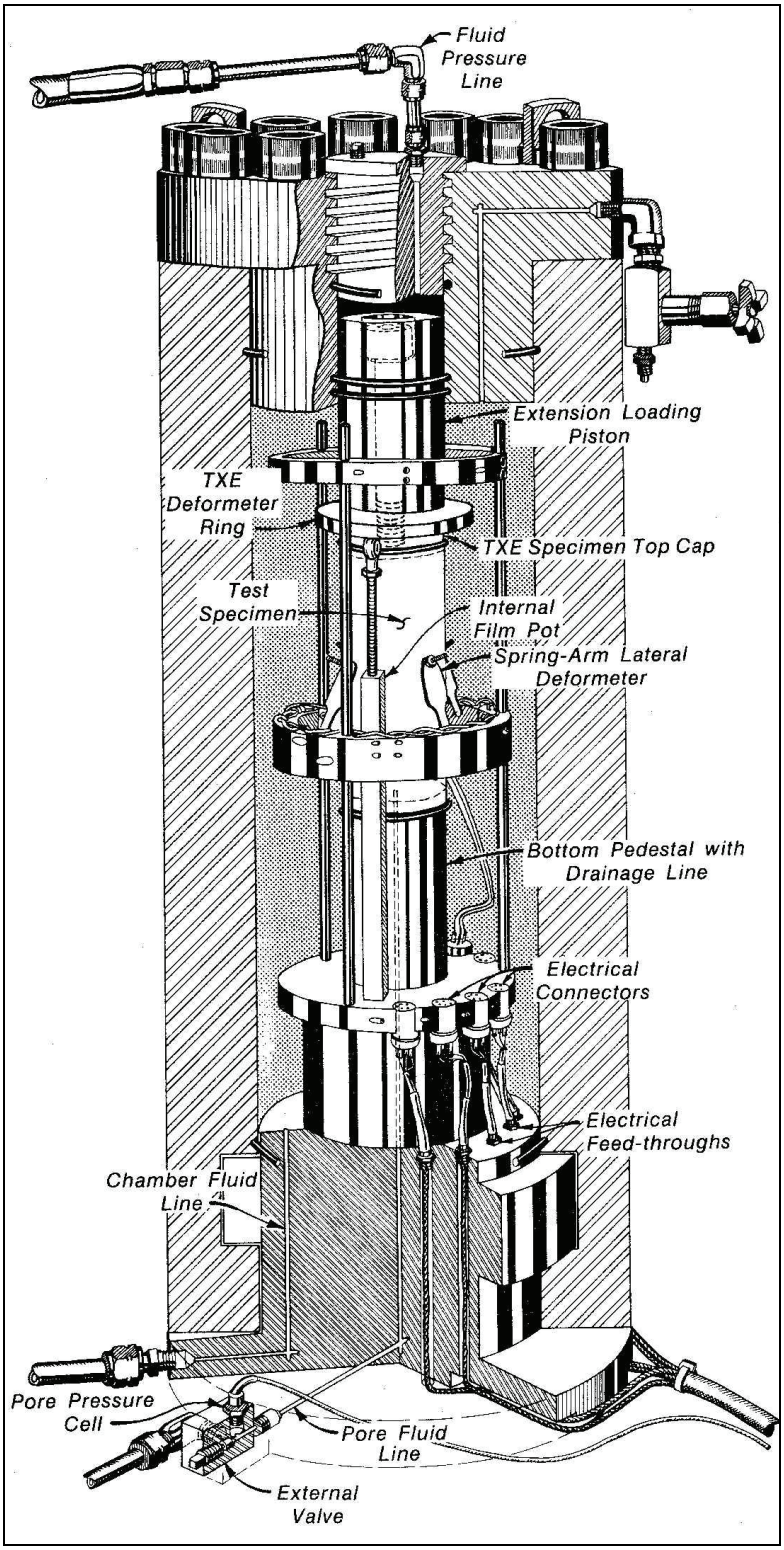

Figure 2. HPTX test device with TXE top cap.

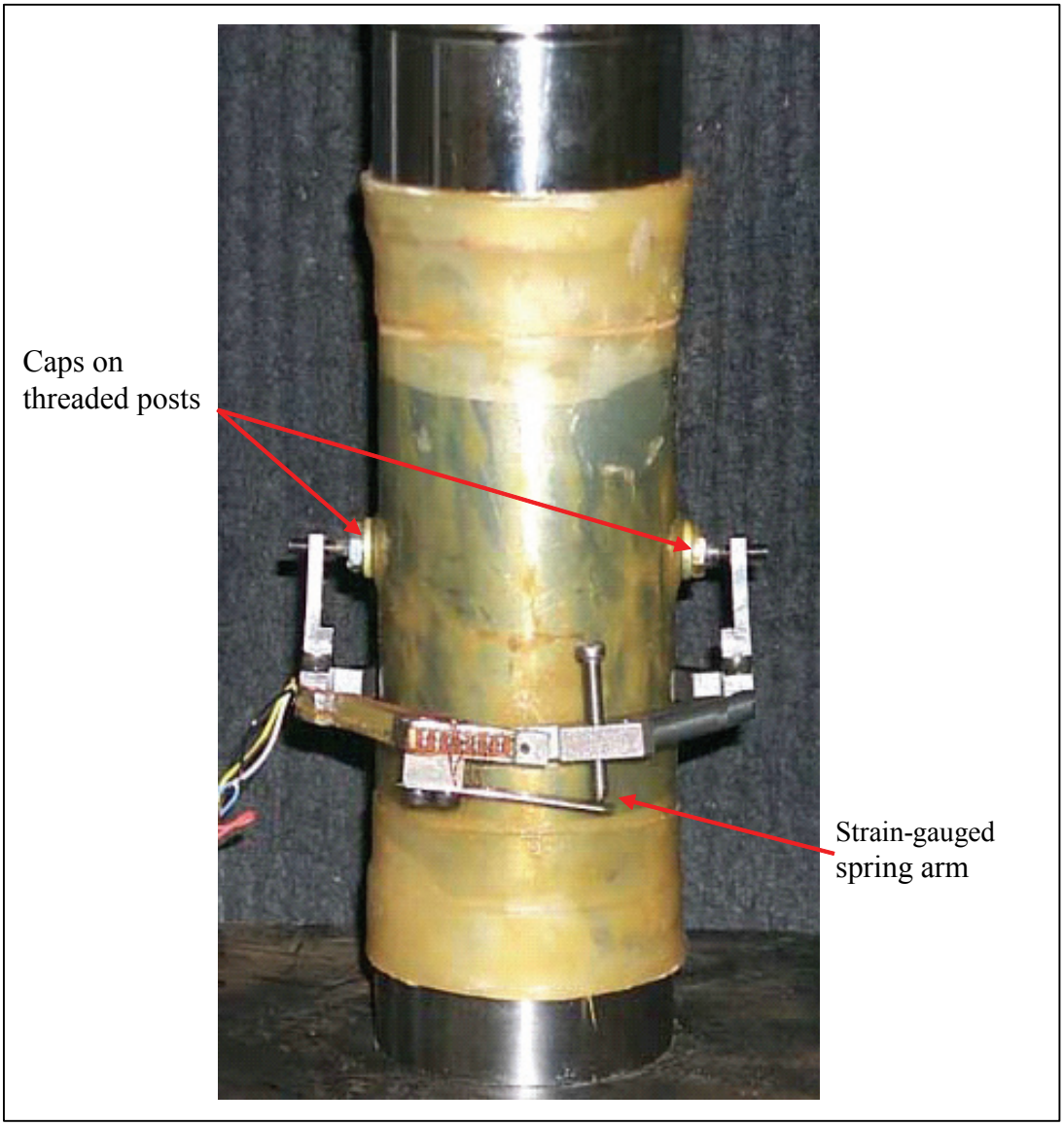

Figure 3. Spring-arm lateral deformeter mounted on test specimen.

3 Analysis of Test Results

Introduction

An analysis of the results from laboratory tests conducted on GMC is presented in this chapter. The purpose of this investigation was to characterize the strength and constitutive properties of the material. As described in Chapter 2, a total of 38 mechanical property tests were conducted in this investigation; all were successfully completed. The analysis in this chapter is based on the results from the following numbers and types of tests: two HC tests, four UC tests, sixteen TXC tests, two UX tests, two UX/BX tests, five UX/CV tests, two UX/SR tests, three DP tests, and two RTE tests.

Hydrostatic compression test results

Undrained compressibility data were obtained from two HC tests and during the hydrostatic loading phases of the 16 TXC tests. The pressure-volume data from the two HC tests are plotted in Figure 4. Unload-reload cycles were applied to HC test specimen 38 in order to obtain unload-reload data at intermediate levels of confining stress. The initial dry densities of the specimens for HC tests 37 and 38 were 2.115 and 2.047 Mg/m^3 respectively. It appears that HC compressibility is affected by initial dry density, i.e., increased compressibility with decreased dry density. Figure 5 presents the pressure time-histories for the HC tests. During HC test 38, the pressure was intentionally held constant for a period of time prior to the unloading cycles. During each hold in pressure, the volumetric strains continue to increase, which indicates that GMC is susceptible to creep (Figure 4). At the peak of the first cycle, the pressure was held at 255 MPa for 242 sec, during which time a volumetric strain of 0.57 percent occurred. During the second cycle, the pressure was held at 510 MPa for 413 sec, and a volume strain of 0.72 percent occurred.

Pressure-volume data obtained during the hydrostatic loading phases of the TXC tests at and above 100 MPa are shown in Figure 6. No significant scatter occurred in the pressure-volume data for these TXC tests. The slight differences during the initial loading are a result of the initial dry densities, which ranged from 2.049 to 2.159 Mg/m^3. The results plotted in Figure 6 indicate that GMC begins to exhibit inelastic strains at a pressure

level of approximately 43 MPa and at a volumetric strain of approximately 0.41 percent. These are the pressure and strain levels at which the pressure-volume response and the initial bulk modulus begin to soften appreciably. Based on the data from HC tests 37 and 38 and the hydrostatic loading of TXC tests in Figure 7, the initial elastic bulk modulus for GMC is approximately 10.4 GPa.

Triaxial compression test results

Shear and failure data were successfully obtained from four unconfined compression tests and 16 unconsolidated-undrained TXC tests. Recall from Chapter 2 that the second phase of the TXC test, the shear phase, is conducted after the desired confining pressure was applied during the HC phase. The UC tests are a special type of TXC test without the application of confining pressure. Results from the UC tests are plotted in Figures 8 and 9, and results from the TXC tests are plotted in Figures 10-25. In all the figures, the axial and volumetric strains at the beginning of the shear phase were set to zero, i.e., only the strains during shear are plotted.

Stress-strain data from the four UC tests in Figures 8 and 9 are plotted as principal stress difference versus axial strain during shear and as principal stress difference versus volumetric strain during shear, respectively deformeters instead of strain gauges were used to measure the axial and radial strains of the UC test specimens. During the UC tests, no attempt was made to capture the post-peak (or softening) stress-strain behavior of this material. The mean unconfined strength of GMC determined from all of the specimens was 33.7 MPa. The UC test results demonstrate some variations. Specimens 16 and 18 have similar strengths while specimens 17 and 19 are similar. The dry densities of the specimens likely caused the variation. Test specimens 16 and 18 had dry densities of 2.122 and 2.110 Mg/m^3 while the dry densities for tests specimens 17 and 19 were 2.057 and 2.054 Mg/m^3. This same trend will be seen in the following figures in that the dry density of the specimen affects the specimen's strength, i.e., specimens with higher dry densities should have higher strengths for a given level of confining pressure.

Figures 10-25 present the results from the TXC tests conducted at nominal confining pressures of 5, 10, 20, 50, 100, 200, 300, and 400 MPa. The TXC results are plotted as principal stress difference versus axial strain during shear and as principal stress difference versus volumetric strain during shear. The results are very good considering the inherent

variability of the initial wet and dry densities and water contents of the specimens. The wet densities of the specimens ranged from 2.054 to 2.184 Mg/m^3, the dry densities ranged from 2.026 to 2.150 Mg/m^3, and the water contents ranged from 1.32 to 3.27 percent.

A few comments should also be made concerning the unloading results. The final unloading stress-strain responses at axial strains approaching 15 percent are less reliable than the unloadings at axial strains less than 11 percent. The internal vertical deformeters go out of range at axial strains of approximately 11 percent. After that, an external deformeter with less resolution is used to measure axial displacement. During the initial unloadings, the creep strains are greater in magnitude than the recovered elastic strains. This behavior results in a net increase in axial strain (for example) during the initial unloading, rather than an expected decrease in axial strain (test 31 in Figure 20 shows this behavior). The net increase in axial strain is the slight bump that appears during the initial unloading.

Results of TXC tests conducted at a constant confining pressure of 5 MPa are shown in Figures 10 and 11. The dry densities for specimens 01 and 02 were 2.065 and 2.096 Mg/m^3, respectively. Both figures for the tests at 5 MPa exhibit increasing peak principal stress difference with increasing initial dry density. The volumetric response in Figure 11 indicates that the material initially compacted until just below the peak principal stress difference, then began to dilate. At 5 MPa confining pressure, the material is still in the elastic region.

Figures 12 and 13 display the results of TXC tests conducted at 10 MPa confining pressure. Test specimen 04 had a higher than average value of initial dry density (2.105 Mg/m^3) than test specimen 03 (2.048 Mg/m^3) resulting in a higher peak principal stress difference for 04 (Figure 12). Little post-peak data were obtained for the specimens. The volumetric response data in Figure 13 indicate that at 10 MPa confining pressure, the specimens compacted until just below the peak principal stress difference then began to dilate.

Test results for TXC tests conducted at a confining pressure of 20 MPa are shown in Figures 14 and 15. Test specimen 25 had a higher than average value of initial dry density (2.145 Mg/m^3) than test specimen 26 (2.069 Mg/m^3) resulting in a higher peak principal stress difference for specimen

25 (Figure 14). Little post-peak data was obtained for test specimen 25 because equipment problems occurred after reaching the peak principal stress difference. Post-peak data were obtained for test specimen 26, but it displayed no strain hardening; therefore, at 20 MPa confining pressure, GMC is still considered brittle. At this confining pressure level, the material compacted until below the peak principal stress difference when it started to dilate.

Results of TXC tests conducted at a confining pressure of 50 MPa are shown in Figures 16 and 17. Figure 16 displays a ductile shear response, i.e., the stress-strain curves exhibit strain hardening. Since the tests at 20 MPa displayed brittle behavior (the material strain softens and little valid post-peak stress or strain data are acquired), a brittle-to-ductile transition occurs between 20 and 50 MPa. The brittle-to-ductile transition occurs when the material flows at a near constant value of principal stress difference. Figure 17 displays volumetric dilation of about 1 percent just prior to peak strength for specimen 28.

Figures 18 and 19 display the results of TXC tests conducted at 100 MPa confining pressure. Test specimen 29 had a lower than average value of initial dry density (2.049 Mg/m^3) than test specimen 30 (2.139 Mg/m^3) resulting in a higher peak principal stress difference for specimen 30 (Figure 18). Figure 18 displays a ductile shear response. The volumetric response data in Figure 19 indicates that at 100 MPa confining pressure, the specimens compacted until just below the peak principal stress difference then began to dilate.

Results of TXC tests conducted at confining pressures of 200, 300, and 400 MPa are shown in Figures 20-21, 22-23, and 24-25, respectively. The qualitative responses at these three levels of confining pressure are essentially the same. The shear responses were predominately ductile, peak strength increased with increased level of confining pressure, and volumetric dilation just prior to peak strength was between 0.5 and 1.5 percent for each set of data. At confining pressures of 200 and 400 MPa each specimen had a higher than average dry density while at the confining pressure of 300 MPa the specimens had a lower than average dry density. After completing the TXC tests, it was determined that none of the specimens reached full saturation during the shear loading. The stress-strain curves continued to exhibit increases in principal stress difference over the entire range of imposed confining stresses.

For comparison purposes, stress-strain curves from selected TXC tests at confining pressures equal to or less than 50 MPa are plotted in Figure 26 and selected tests at confining pressures greater than 50 MPa are plotted in Figure 27. Stress-strain data from the TXC tests in Figures 26 and 27 are plotted in Figures 28 and 29, respectively, as principal stress difference versus volumetric strain during shear. One should note that the initial loading of the TXC stress-strain curves (Figures 26-27) are a function of the material's initial volume changes during shear, which in turn are a function of the specimens' position on the material's pressure-volume curve at the start of shear. As confining pressure increases, the initial loading of the material softens as the stress state moves into the crush regime of the pressure-volume curve, and then stiffens again as the material approaches void closure, i.e., the point at which all of the specimen's air-porosity is crushed out. At confining pressures of 5, 10, and 20 MPa, the specimens' initial volume changes are basically within the elastic regime of the pressure-volume curve, which results in the stiff initial loading of the stress-strain curves. The TXC tests conducted at a confining pressure of 50 MPa had a softer response (lower moduli) during the initial shear loading than the tests at 5, 10, and 20 MPa (Figure 26). The tests conducted at a confining pressure of 300 MPa had the softest initial loading results in stress difference-axial strain space (Figures 29 and 30). The test specimens at 300 MPa (with the lower than average initial densities) also had the softest response in stress difference-volume strain space (see Figure 31). The TXC tests conducted at 400 MPa exhibited increasingly stiffer initial loading, and the results were all stiffer than the tests at 300 MPa. The subsequent increase in initial loading with increasing confining pressure during shear is directly related to the increasing stiffness in the pressure-volume response of the concrete.

Results from TXC tests at confining pressures from 5 to 400 MPa are plotted in Figure 32 as radial strain during shear versus axial strain during shear. A contour of zero volumetric strain during shear is also plotted on this figure. When the instantaneous slope of a curve is shallower than the contour of zero volumetric strain, the specimen is in a state of volume compression; when steeper, the specimen is in a state of dilation or volume expansion. Data points plotting below the contour signify that a test specimen dilated, and the current volume of the specimen is greater than the volume at the start of shear. The plotted results show that the specimens tested at 5, 10, 20, and one test from both 50 and 100 MPa

dilated while the majority of the specimens maintained volume compression during shear.

The failure data from all of the UC and TXC tests are plotted in Figure 33 as principal stress difference versus mean normal stress; one stress path at each confining stress is also plotted. In Figure 34, a recommended failure surface is plotted with the failure points. The quality of the failure data is very good; the data exhibits very little scatter. It is important to note that the failure points exhibit a continuous increase in maximum principal stress difference with increasing values of mean normal stress. The response data from the 400 MPa TXC tests indicate that at a mean normal stress of approximately 616 MPa, the concrete still has not reached void closure and is far from full saturation. Concrete materials can continue to gain strength with increasing pressure until all of the air porosity in the concrete has been crushed out, i.e., when void closure is reached. It is important to recognize that void closure can be attained during the shear loading phase of the TXC tests as well as under hydrostatic loading conditions. At levels of mean normal stress above void closure, the failure surface will have a minimal slope.

Although it is difficult to show with the TXC data, this material is subject to significant shear-induced volumetric strains. This means that a significant portion of the volume changes observed in Figure 32 are due to shear and not changes in pressure. In an attempt to show this behavior, the pressure-volume data from two TXC tests are compared in Figure 35 to the pressure-volume data from the HC tests. The data from the TXC tests were plotted until the specimens began to dilate, i.e., only the compressive volumetric strains during the HC and shear phases were plotted. It is clear from this figure that the pressure-volume response from the TXC tests at 300 and 400 MPa (initial dry density of 2.070 and 2.110 Mg/m^3, respectively) exhibits larger volumetric strains from shear loading than the HC tests 37 and 38 (initial dry density of 2.115 and 2.047 Mg/m^3, respectively). HC test 38 exhibits a larger amount of volumetric strain when compared to test 37. The two TXC tests display larger volumetric strains due to compressive shear-induced volume changes during the TXC tests.

Reduced triaxial extension test results

Extension stress-strain and failure data were successfully obtained from five direct pull tests and three unconsolidated-undrained RTE tests. The

DP tests are a special type of RTE test without the application of confining pressure. Results from the DP tests are plotted in Figure 36, results from the RTE tests are plotted in Figures 37-38, and the recommended failure surfaces from the triaxial test results are plotted in Figure 39. Data from the DP tests exhibit some scatter. The stress-strain data in Figure 37 displays the RTE test results conducted at confining pressures of approximately 65 MPa. All of the RTE specimens fractured. Test specimens 20 and 21 exhibit slight variations during the loading that were caused by the confining pressure and the manual operation of the equipment used for RTE tests. Only the DP, RTE, and UC tests included in this test program used manual operation rather then a servo-controlled data acquisition system to control the load and confining pressure. Figure 39 displays failure data from the UC, TXC, DP, and RTE tests, and the recommended compression and extension failure surfaces for GMC. The resulting compression and extension failure surfaces were well defined and nonsymmetric about the mean normal stress axis. GMC can withstand more deviatoric stress in compression than extension before failure occurs, which is typical behavior for concrete materials.

Uniaxial strain test results

One-dimensional compressibility data were obtained from two undrained uniaxial strain (UX) tests with lateral stress measurements. Data from the tests are plotted in Figures 40-42; the stress-strain data from the UX tests are plotted in Figure 40, the pressure-volume data in Figure 41, and the stress paths with the failure surface data in Figure 42. The UX responses in Figures 40 and 41 are initially very stiff due to the cement in the GMC material. When the cement was crushed, the compressibility responses softened, and the material compacted significantly. As the material became denser, compressibility stiffened, i.e., a slight increase occurred in the compressibility of the material with lower the dry density. Specimen 05 had an initial dry density of 2.135 Mg/m^3 while specimen 06 had an initial dry density of 2.114 Mg/m^3. Specimen 06 compressed more than specimen 05 during the UX loading (Figures 40 and 41).

From the UX stress-strain loading data (Figure 40), an initial constrained modulus of 22.6 GPa was calculated. UX data may also be plotted as principal stress difference versus mean normal stress; the slope of an elastic material in this space is 2G/K. A initial shear modulus of 9.1 GPa was calculated from the initial constrained modulus and the initial elastic bulk modulus (10.4 GPa) determined from the HC and TXC tests. These

two values may be used to calculate any of the other initial elastic constants, e.g., the Young's modulus is 21.2 GPa and Poisson's ratio is 0.16.

The UX stress paths in Figure 42 have a steep initial path until almost reaching the TXC recommended failure surface. The stress paths soften after the material is crushed causing the data to lie well below the failure surface. The pressure-volume responses from HC and UX tests are compared in Figure 43. Below a volumetric strain of about 5 percent, the HC test results are stiffer than the UX data. This implies that the UX state of stress is providing additional shear-induced compaction to the specimens even at low levels of stress.

Strain path test results

Three different types of strain-path tests were conducted in this test program. UX/BX refers to tests with uniaxial strain loading followed by constant axial strain unloading. UX/CV refers to tests with uniaxial strain loading followed by constant volume strain loading. UX/SR refers to tests with uniaxial strain loading then continued loading along a constant ratio of axial strain to radial strain (ARSR) of -1.33.

Two UX/BX tests were conducted to a peak axial stress of approximately 50 MPa and 100 MPa. Data from the tests are plotted in Figures 44-47; the stress-strain data from the UX/BX tests are plotted in Figure 44, the pressure-volume data in Figure 45, the stress paths with the failure surface data in Figure 46, and the strain paths in Figure 47. The stress-strain responses of the material (Figure 44) displays variations during the UX loading that are likely a function of the test specimens' initial dry densities; unfortunately the dry density for specimen 07 is unknown because the specimen leaked but the wet densities can also be used to evaluate test data. The wet density for test specimen 07 is 2.144 Mg/m^3 and the wet density for test specimen 08 is 2.172 Mg/m^3. The higher density of specimen 08 resulted in steeper loading path than that of test specimen 07. The stress-strain curves illustrate that the specimens were allowed to creep under zero-radial-strain boundary conditions prior to initiating the BX unloading. The pressure-volume data presented in Figure 45 illustrates the large amount of volume recovery that occurs during the BX unloading. The specimens recovered all the compressive volumetric strain and dilated about one percent volume strain. The stress-paths plotted in Figure 46 are typical of most concretes. At the end of the UX loading and prior to the BX unloading, some stress relaxation occurred in the system; hence, the

slight unload just after peak stress (Figure 46). During the unloading, the stress-paths show a small increase in principal stress difference followed by a significant decrease in stress difference with decreasing mean normal stress. This unloading appears to follow a limiting surface, which is normally the material's failure relation (the TXC recommend failure surface in most cases). In this case, the BX unloading exceeds the failure surface by an unusually large amount that, at this time, cannot be explained. Figure 47 shows the strain paths that were followed during the two tests.

Results from five UX/CV tests conducted to four different levels of peak axial stresses during the initial UX phase are shown in Figures 48-51. The stress-strain data from the UX/CV tests are plotted in Figure 48, the pressure-volume data in Figure 49, the stress paths with the failure surface data in Figure 50, and the strain paths in Figure 51. The CV portions of the stress path data in Figure 50 initially exhibit an increase in stress difference with a slight decrease in mean normal stress then follow the failure relation. For this series of tests, the CV portions of the data provide an excellent confirmation of the failure relation by following along the recommended TXC failure surface. The servo-controlled system lost control during the changed from UX loading to constant volume strain loading for test specimen 10. Control was regained but the plots display irregularities caused by the servo-controlled system not initially maintaining constant volume strain loading.

Data was obtained from two UX/SR tests that were loaded to two different levels of peak axial stress during the initial UX phase. Data from the tests are plotted in Figures 52-55; the stress-strain data from the UX/SR tests are plotted in Figure 52, the pressure-volume data in Figure 53, the stress paths with the failure surface data in Figure 54, and the strain paths in Figure 55. Specimen 13 was tested at an axial to radial strain ratios (ARSR) of -1.32 rather than -1.33 because of a programming error. The plotted stress paths (Figure 54) demonstrate increasing values of principal stress difference and decreasing values of mean normal stress after the SR loading initiates. After reaching the material's limiting surface, both stress difference and mean normal stress decrease. The stress paths in Figure 54 confirm that the limiting surface for the UX/SR tests is similar to the material's recommended TXC failure surface.

Comparison plots of the results of selected UX/BX, UX/CV, and UX/SR are plotted in Figures 56-59; the stress-strain data are plotted in Figure 56,

the pressure-volume data are plotted in Figure 57, the stress-paths with the failure surface are plotted in Figure 58, and the strain-paths are plotted in Figure 59. The following statements provide an interpretation of the measured pressure-volume data during the strain paths. When loading along the constant volume strain path, the specimens want to increase in volume due to the material's inherent shear-induced dilation characteristics. Increasing levels of pressure are required to maintain constant volume boundary conditions (Figure 57). The material's behavior while loading along a constant strain ratio path displays decreasing pressure and decreasing volumetric strain. The specimen does not want to expand faster than the boundary conditions permit unlike the specimens loaded along the constant-volume strain path. To maintain the boundary conditions during the UX/SR tests, the pressure is reduced. The boundary conditions applied during the BX unloading require significant amounts of volume expansion. To maintain the boundary conditions, pressure must be reduced. In Figure 58, one stress path for each of the different strain path tests and the TXC failure surface are overlaid to illustrate the merger of the data in the vicinity of a failure surface. The convergence of the data from the UX/CV tests and the UX/SR tests validates the TXC failure data. The UX/BX test data does not validate the failure surface developed from the TXC test data.

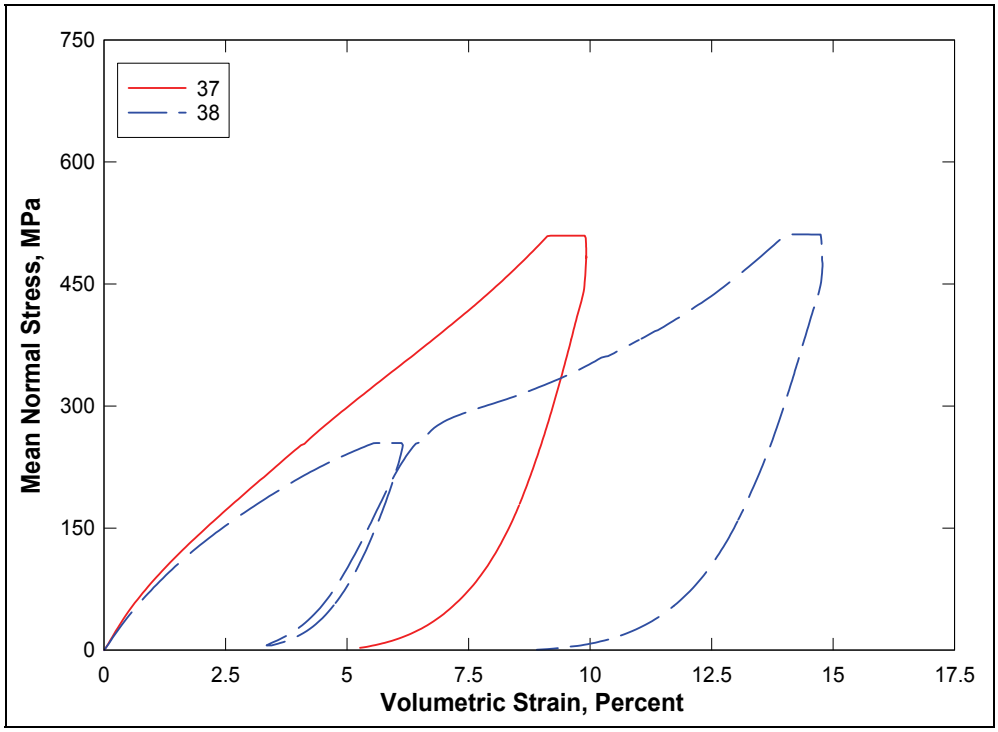

Figure 4. Pressure-volume responses from the HC tests.

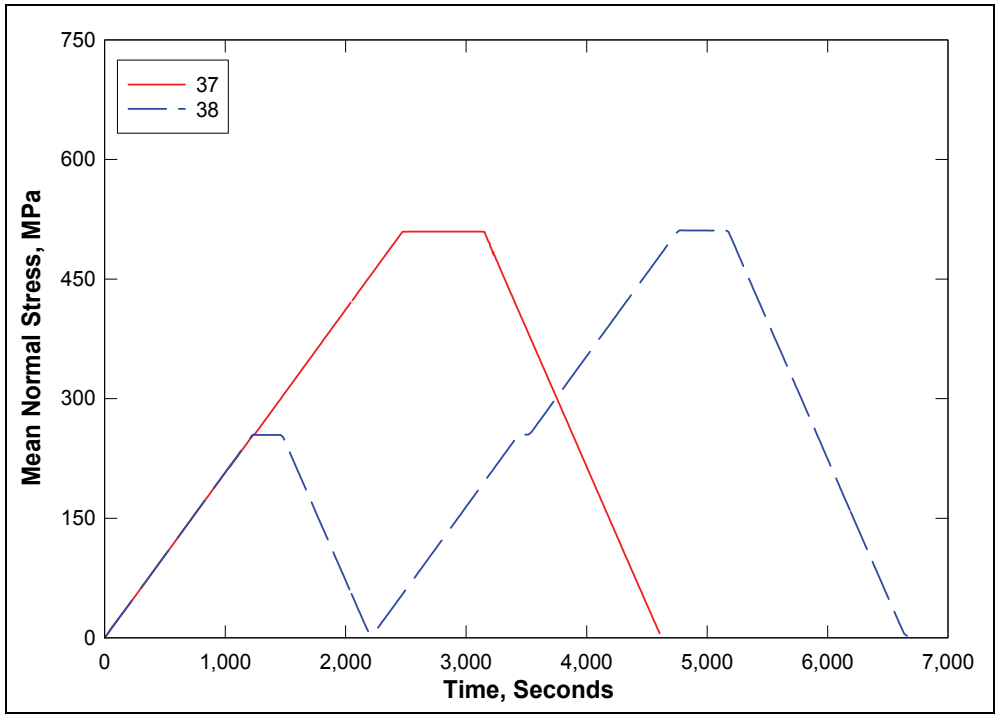

Figure 5. Pressure time-histories from the HC tests.

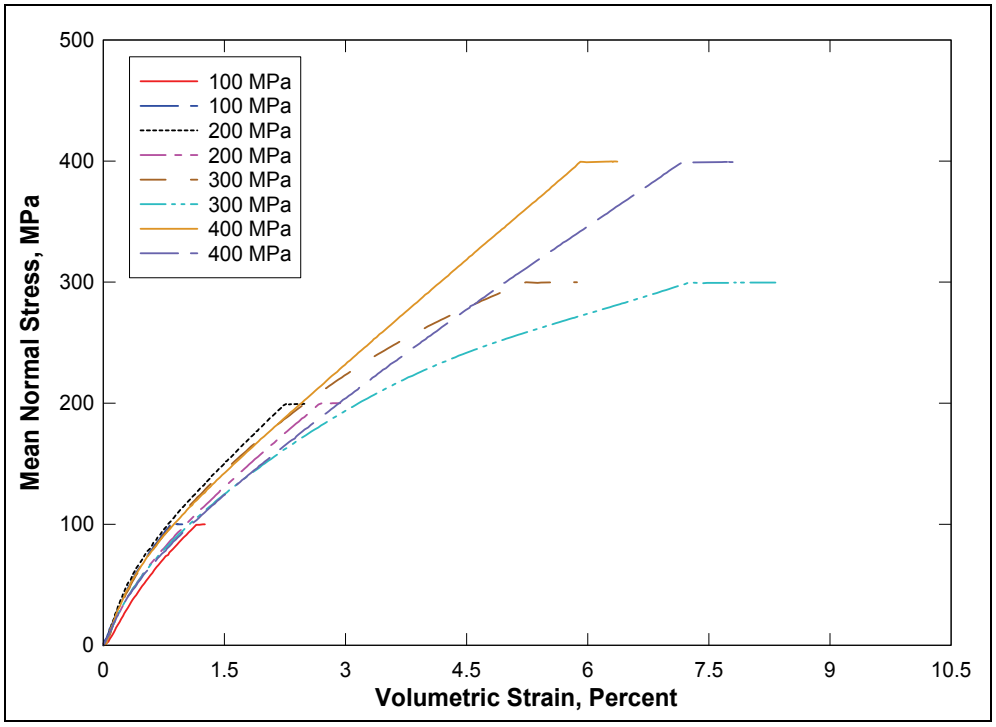

Figure 6. Pressure-volume responses from selected TXC tests.

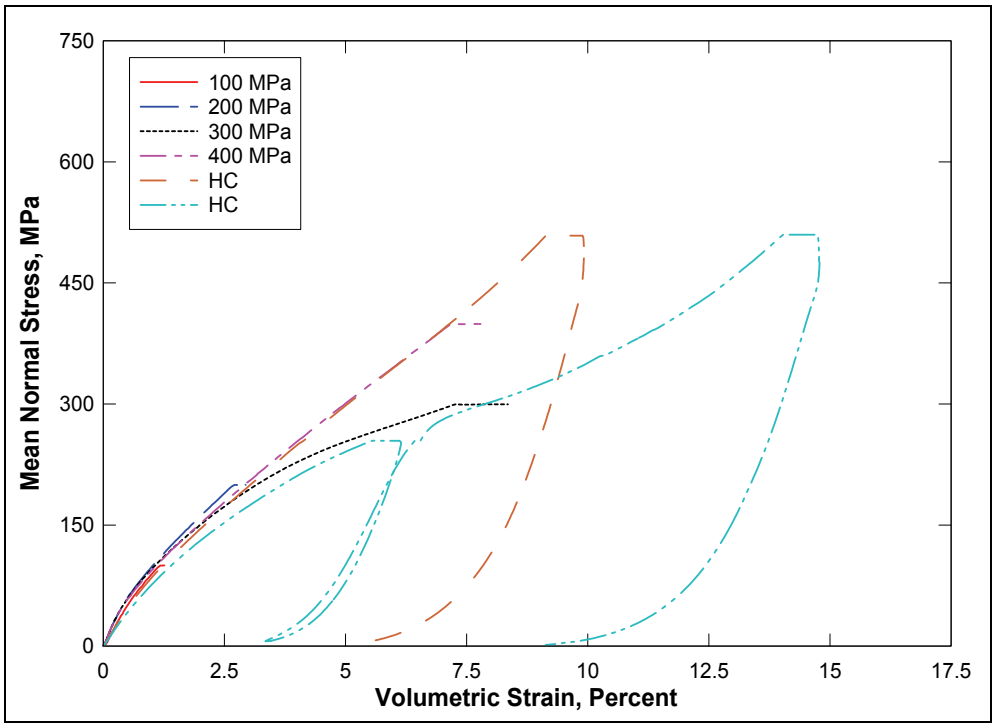

Figure 7. Pressure-volume responses from HC and selected TXC tests.

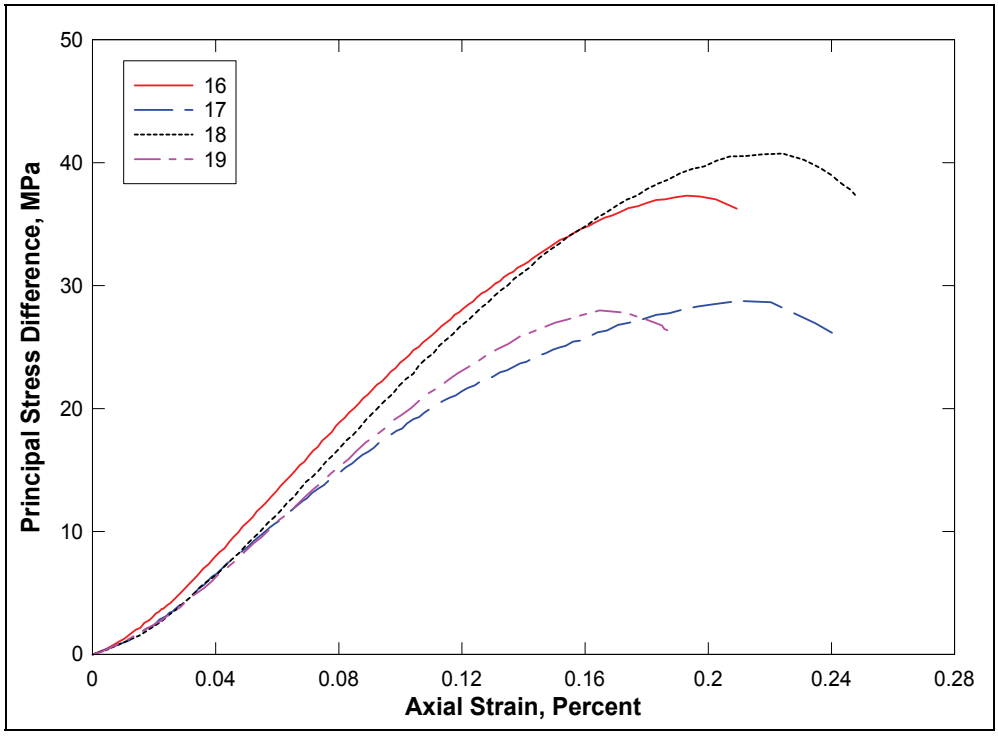

Figure 8. Stress-strain curves from UC tests.

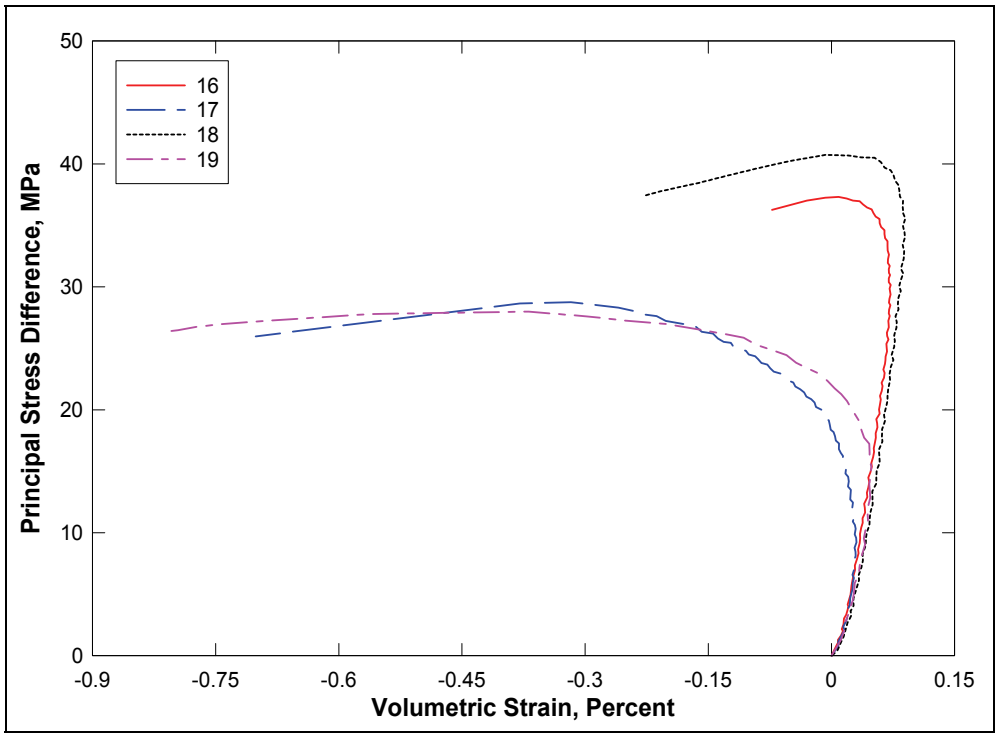

Figure 9. Stress difference-volumetric strain during shear from UC tests.

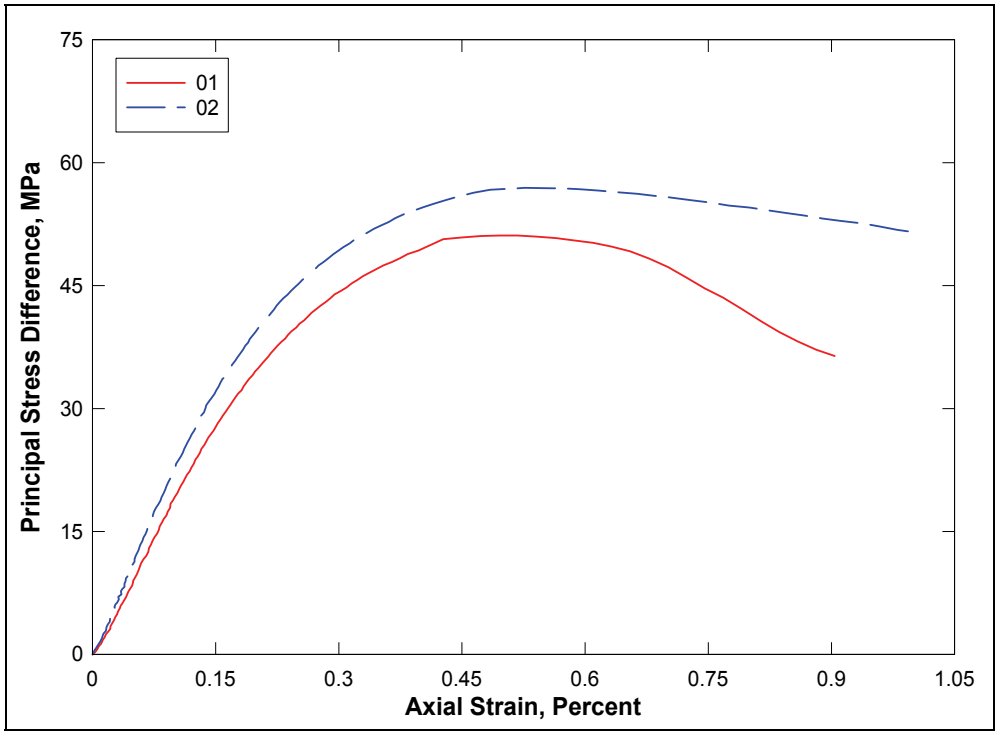

Figure 10. Stress-strain curves from TXC tests at a confining pressure of 5 MPa.

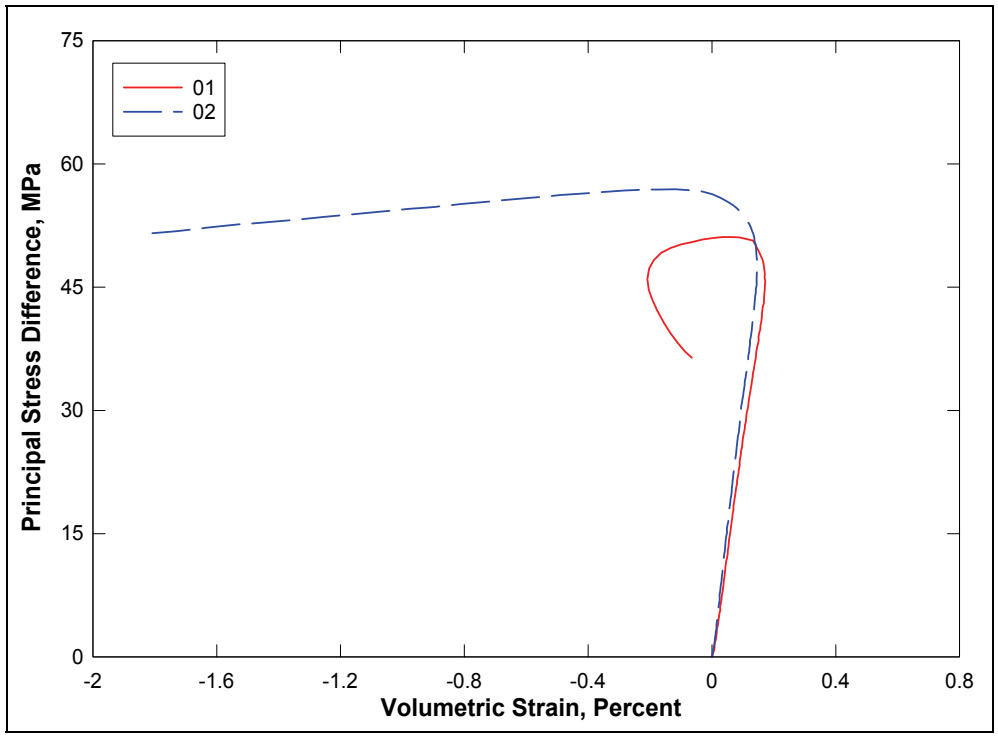

Figure 11. Stress difference-volumetric strain during shear from TXC tests at a confining pressure of 5 MPa.

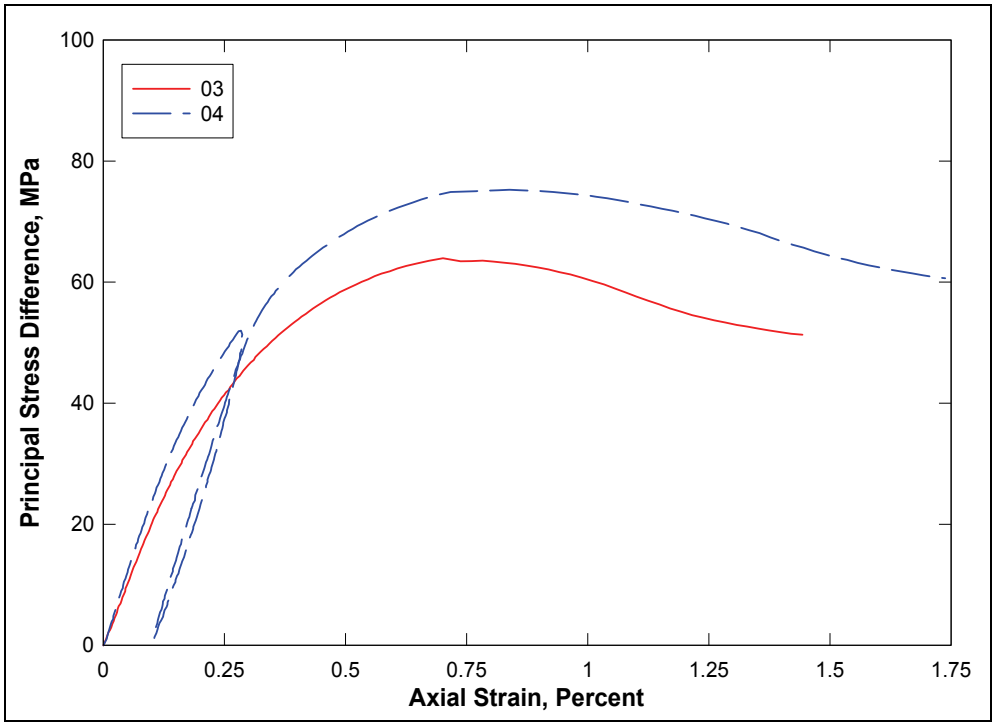

Figure 12. Stress-strain curves from TXC tests at a confining pressure of 10 MPa.

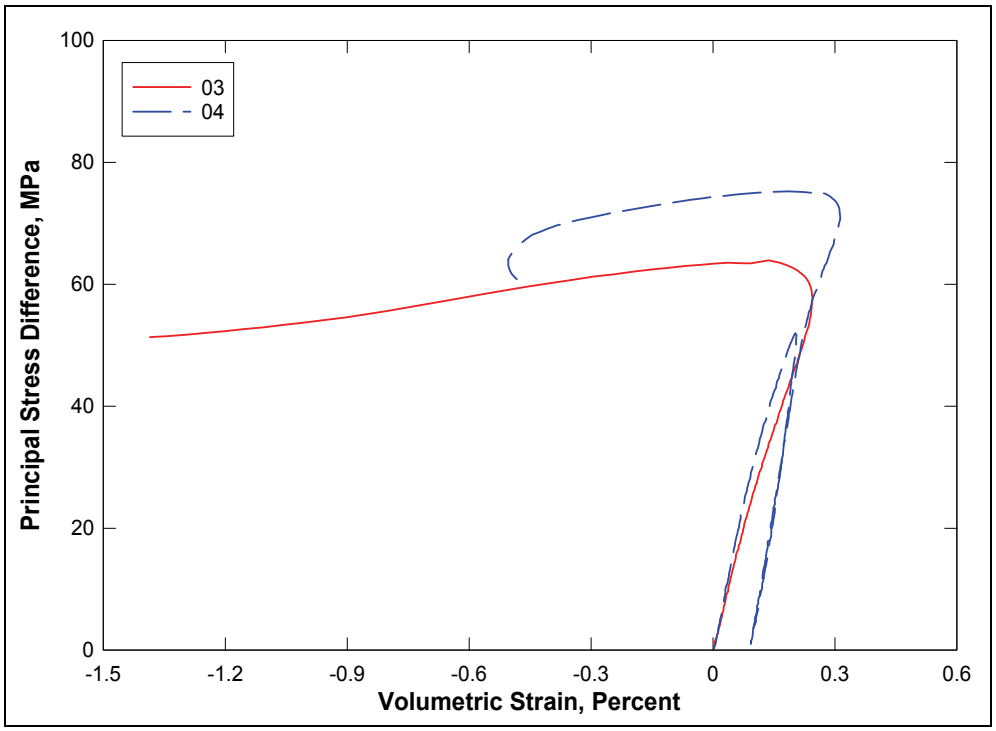

Figure 13. Stress difference-volumetric strain during shear from TXC tests at a confining pressure of 10 MPa.

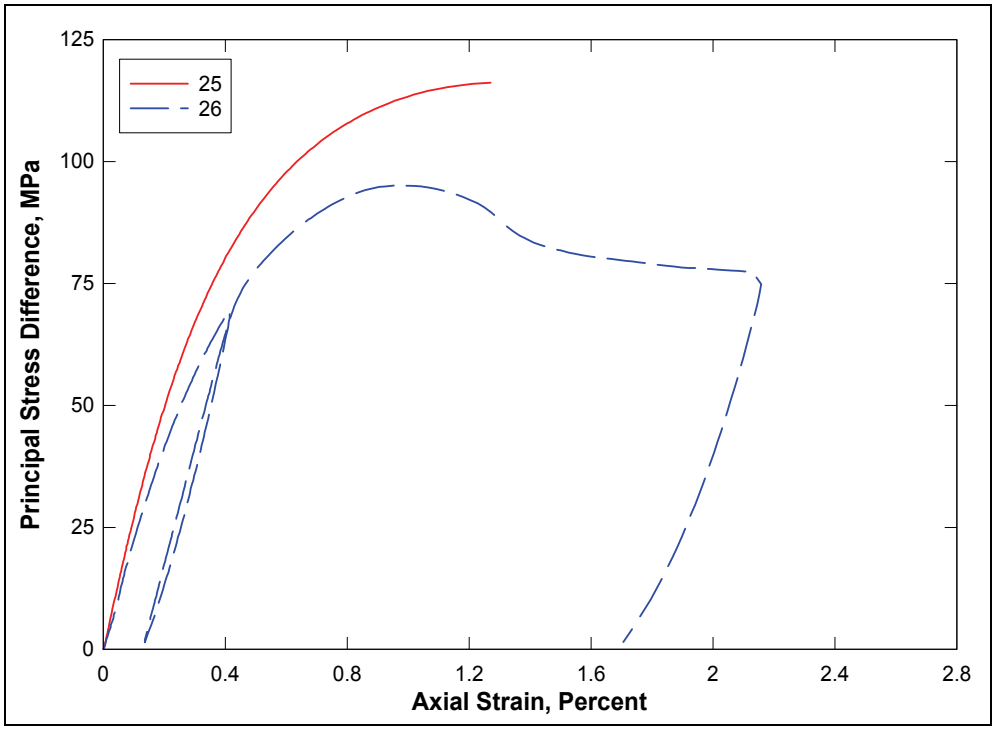

Figure 14. Stress-strain curves from TXC tests at a confining pressure of 20 MPa.

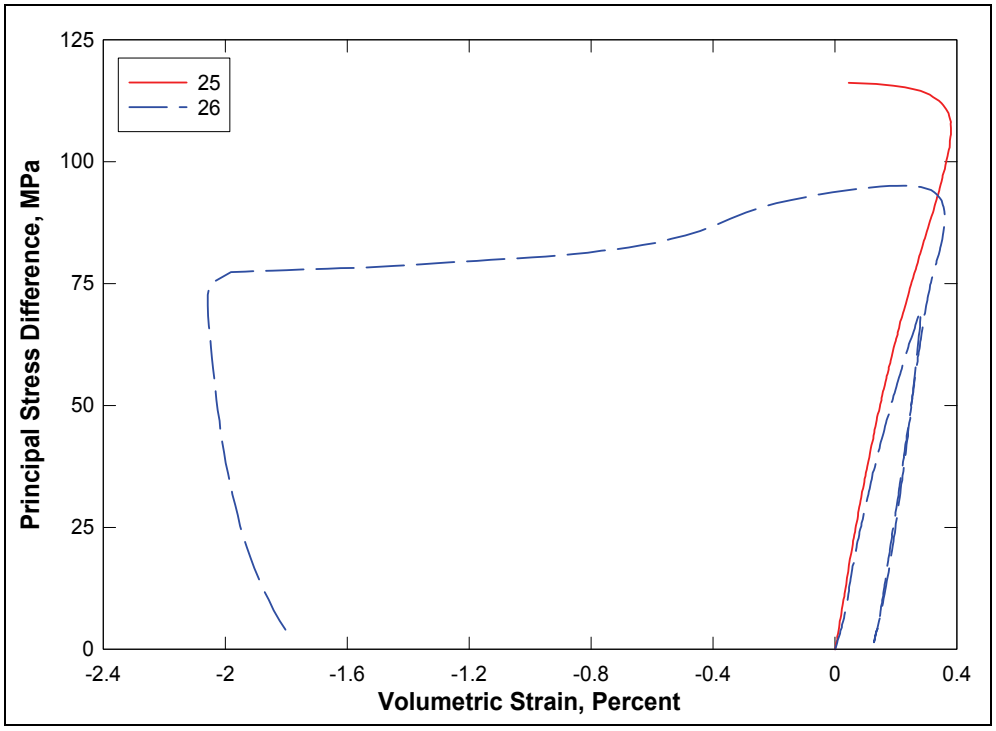

Figure 15. Stress difference-volumetric strain during shear from TXC tests at a confining pressure of 20 MPa.

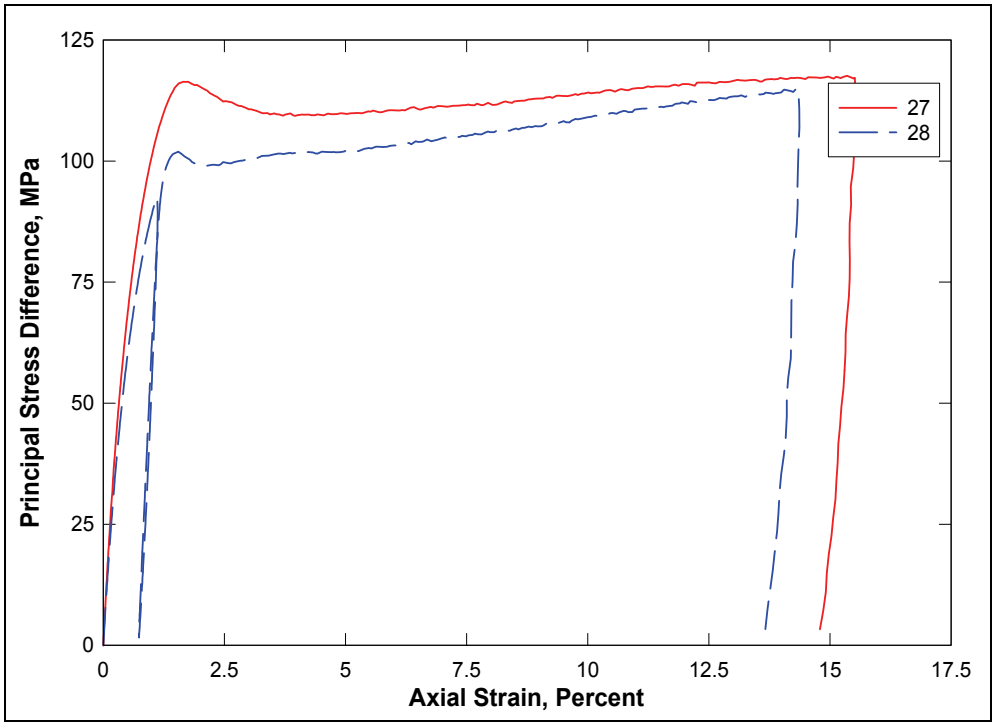

Figure 16. Stress-strain curves from TXC tests at a confining pressure of 50 MPa.

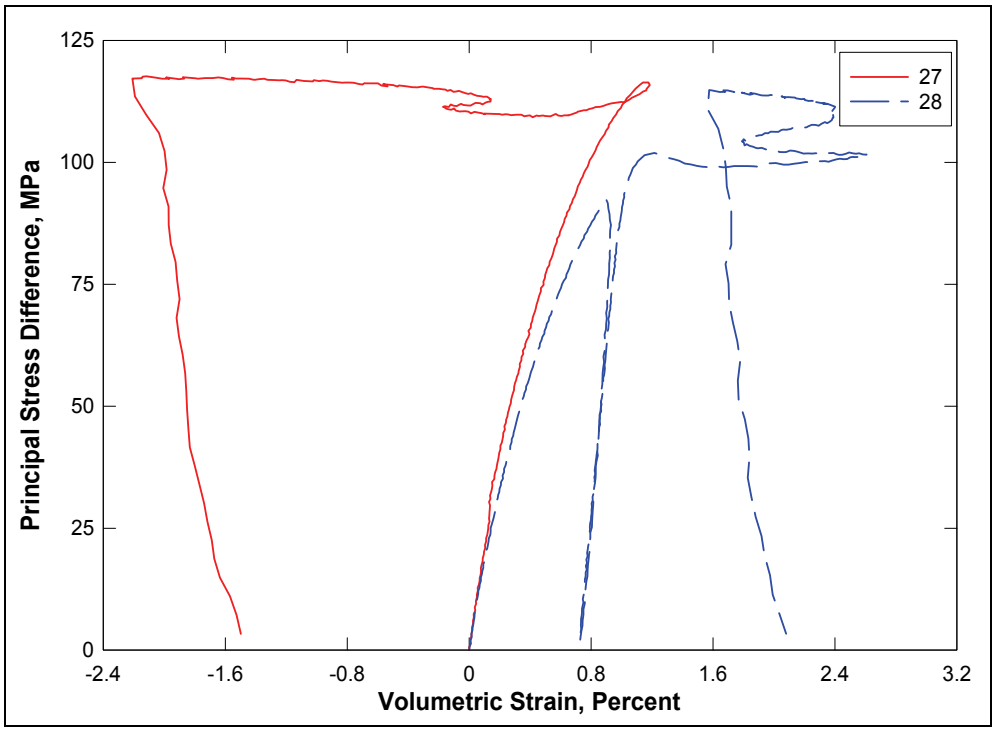

Figure 17. Stress difference-volumetric strain during shear from TXC tests at a confining pressure of 50 MPa.

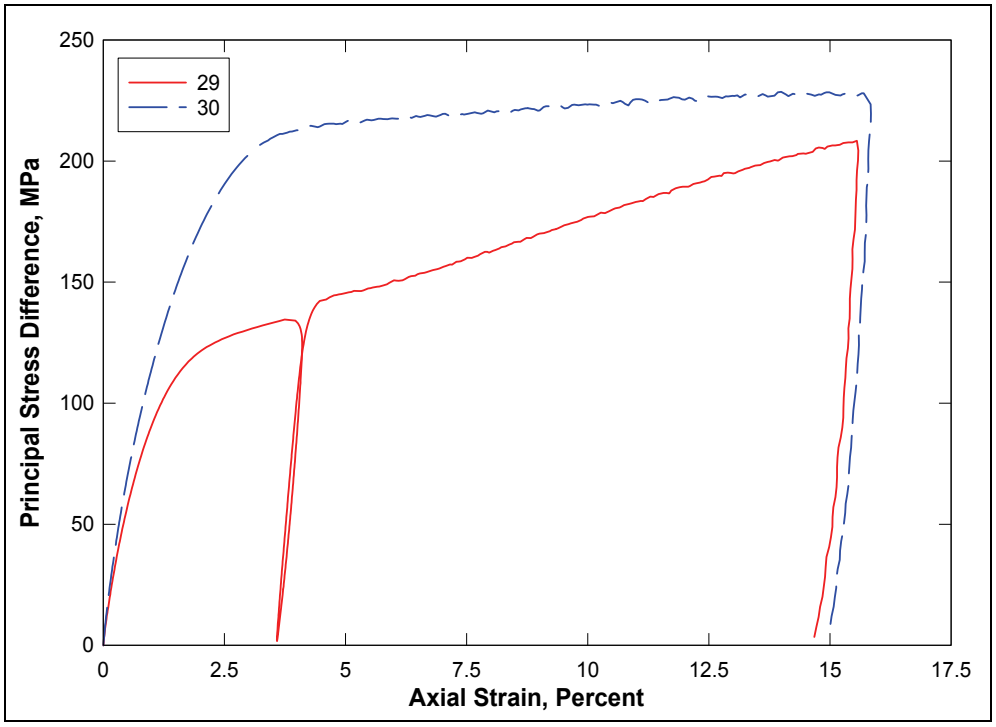

Figure 18. Stress-strain curves from TXC tests at a confining pressure of 100 MPa.

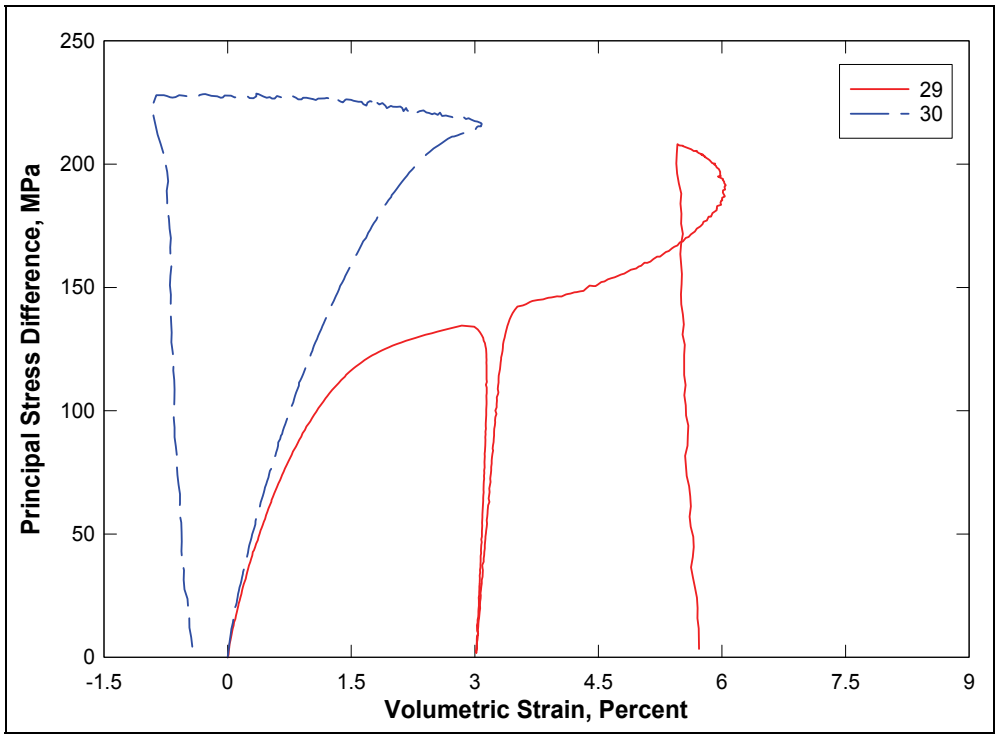

Figure 19. Stress difference-volumetric strain during shear from TXC tests at a confining pressure of 100 MPa.

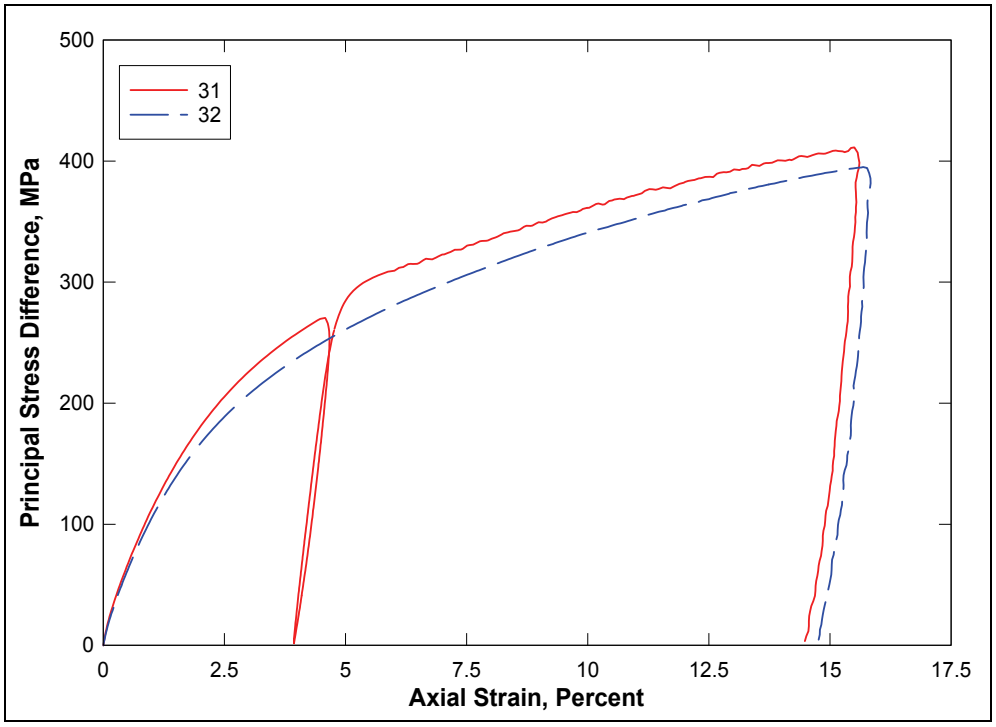

Figure 20. Stress-strain curves from TXC tests at a confining pressure of 200 MPa.

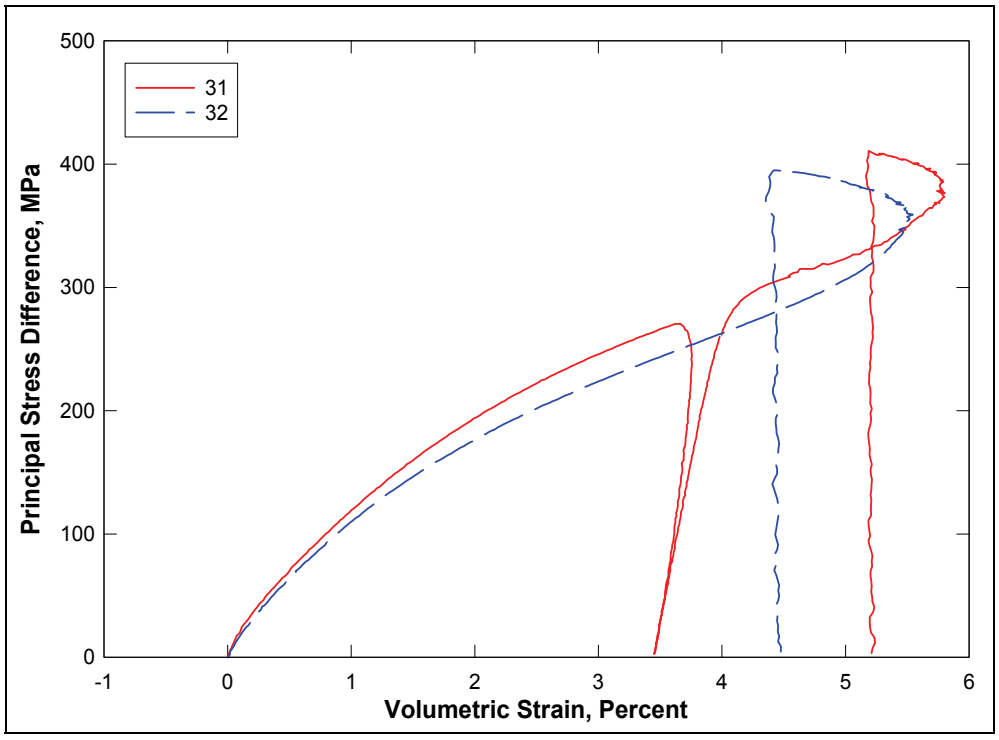

Figure 21. Stress difference-volumetric strain during shear from TXC tests at a confining pressure of 200 MPa.

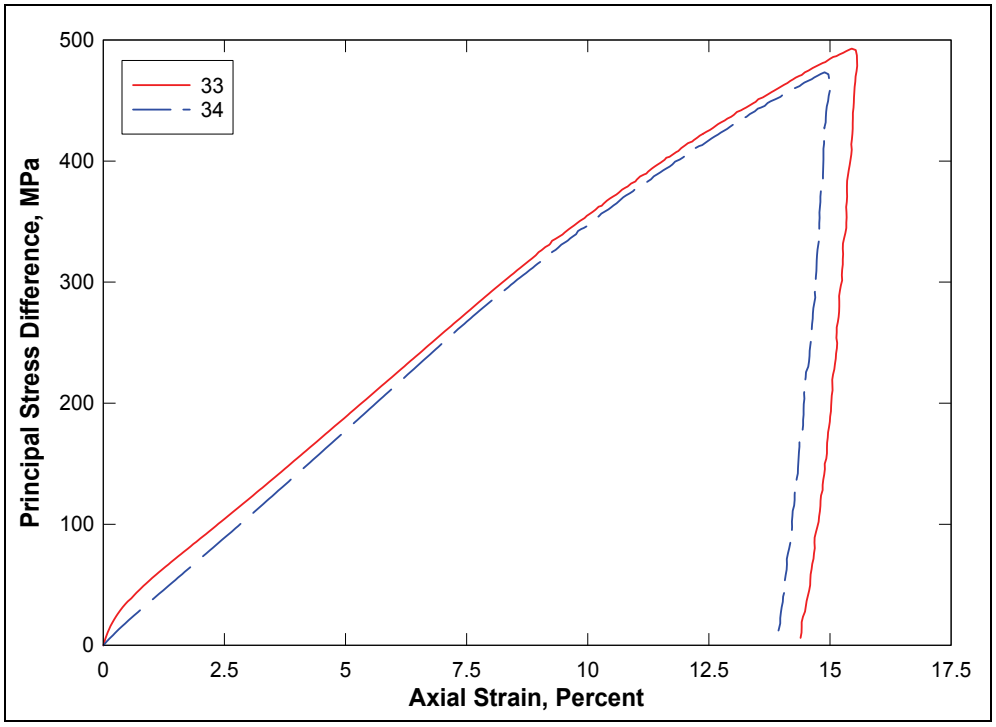

Figure 22. Stress-strain curves from TXC tests at a confining pressure of 300 MPa.

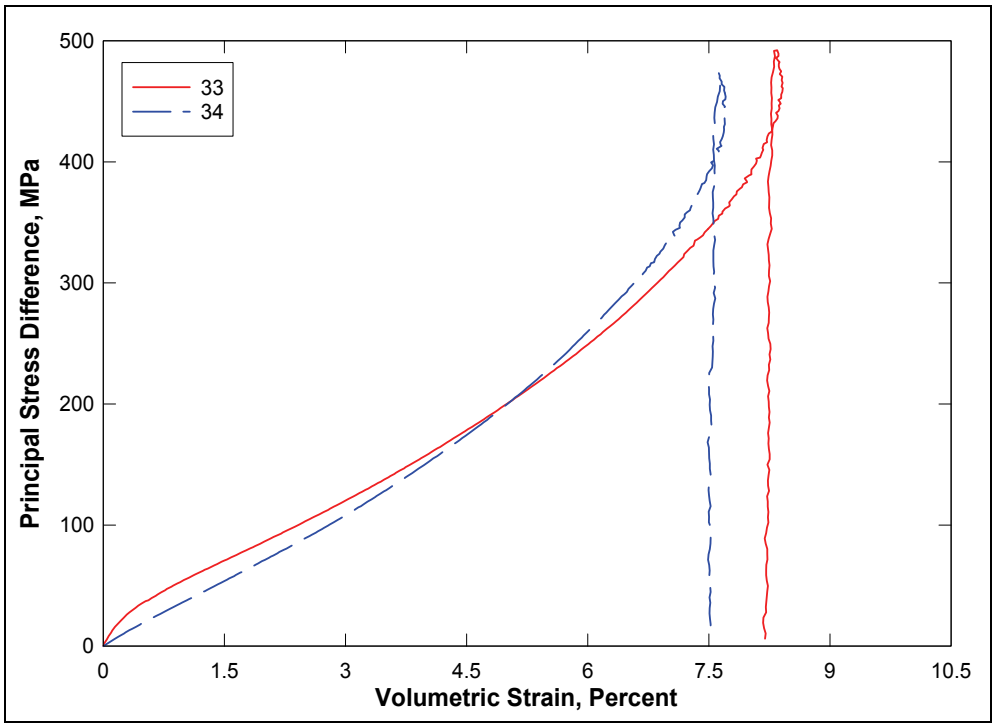

Figure 23. Stress difference-volumetric strain during shear from TXC tests at a confining pressure of 300 MPa.

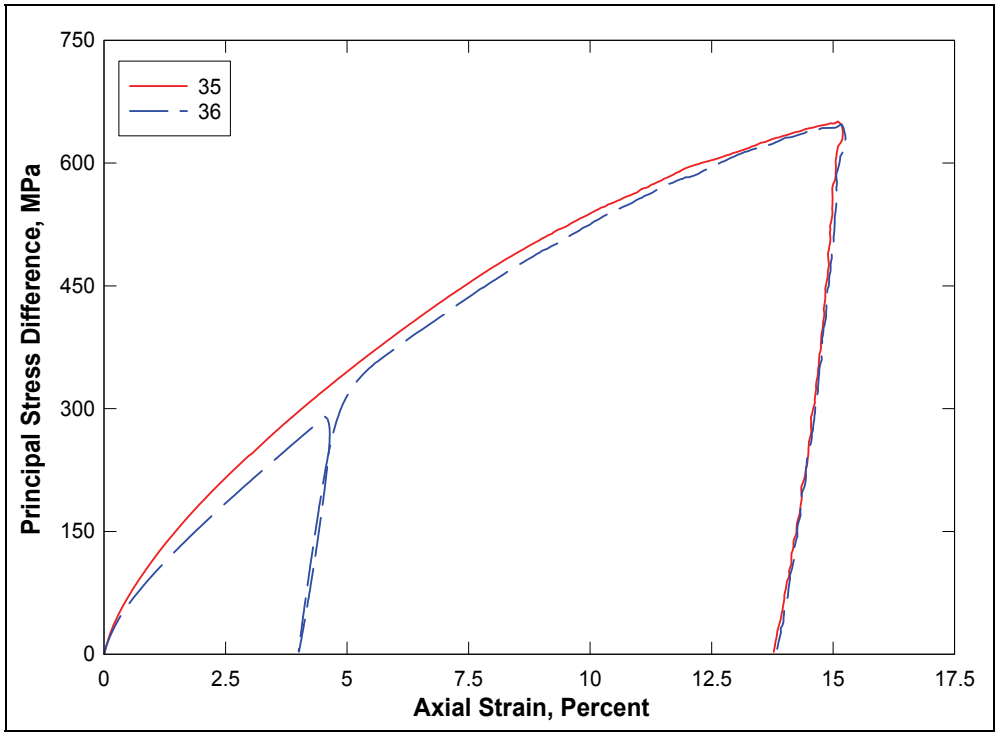

Figure 24. Stress-strain curves from TXC tests at a confining pressure of 400 MPa.

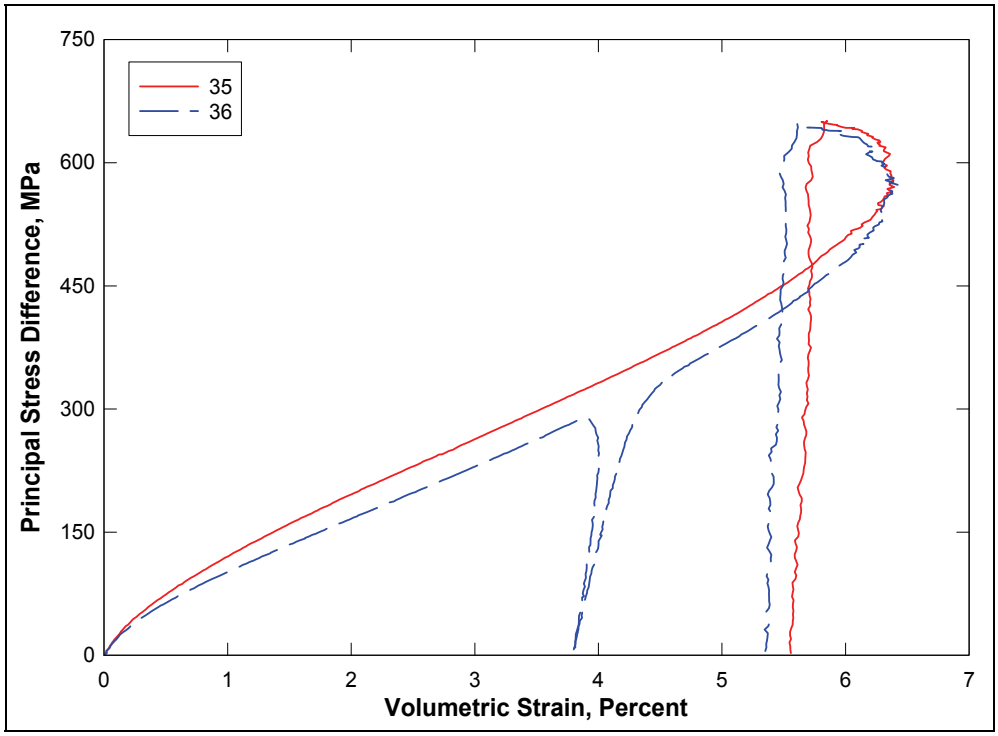

Figure 25. Stress difference-volumetric strain during shear from TXC tests at a confining pressure of 400 MPa.

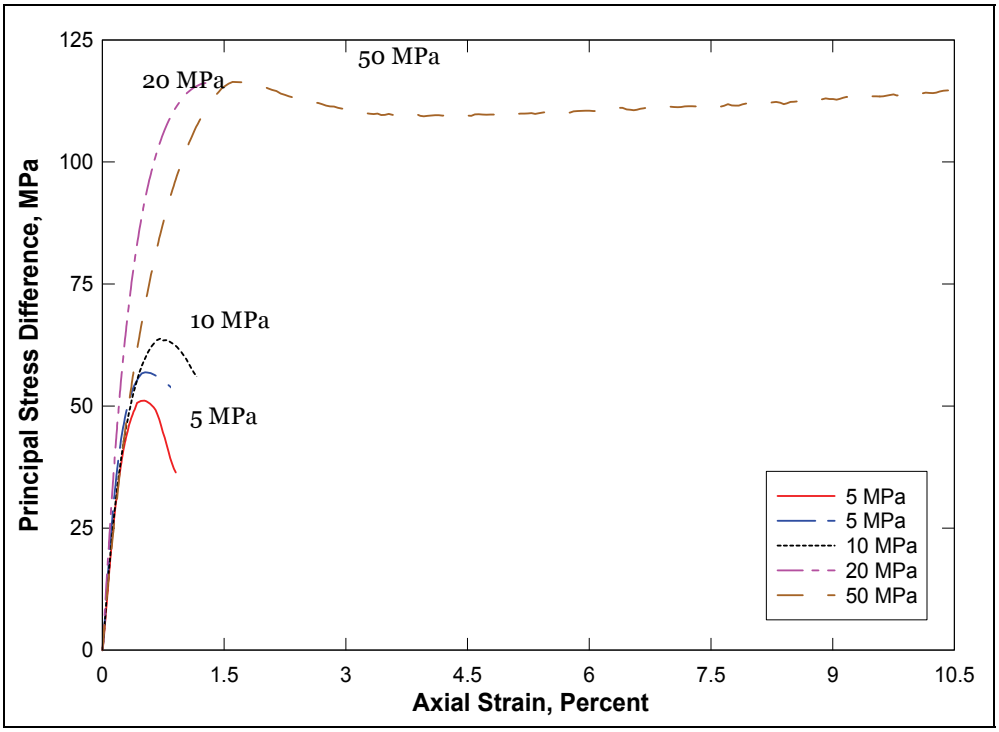

Figure 26. Stress-strain data from TXC non-cyclic tests at confining pressures between 5 and 50 MPa.

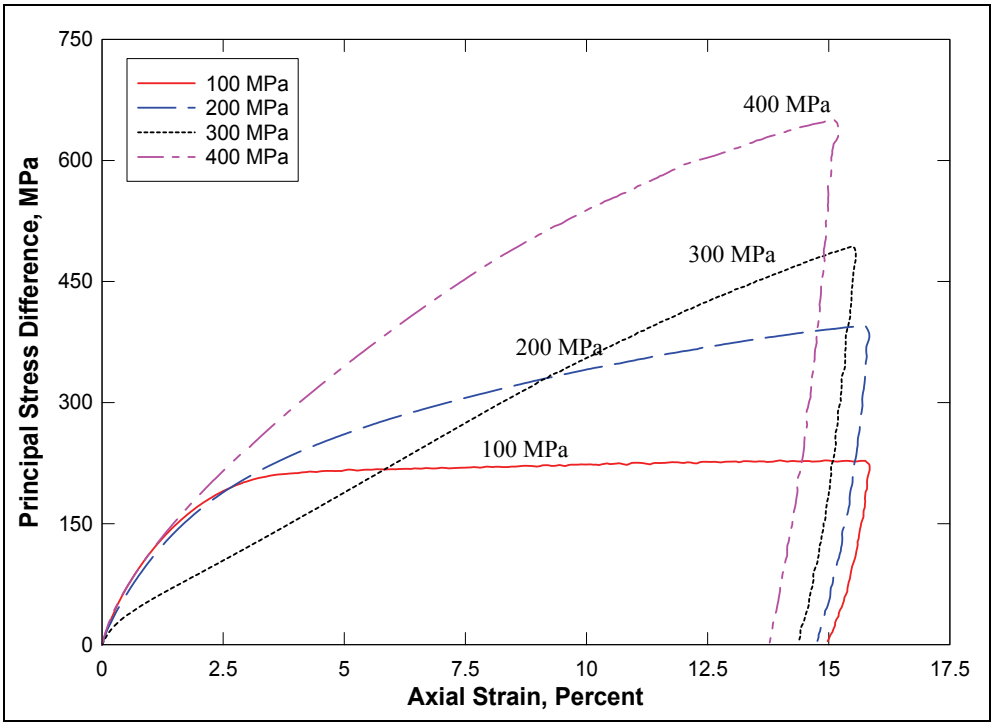

Figure 27. Stress-strain data from TXC non-cyclic tests at confining pressures between 100 and 400 MPa.

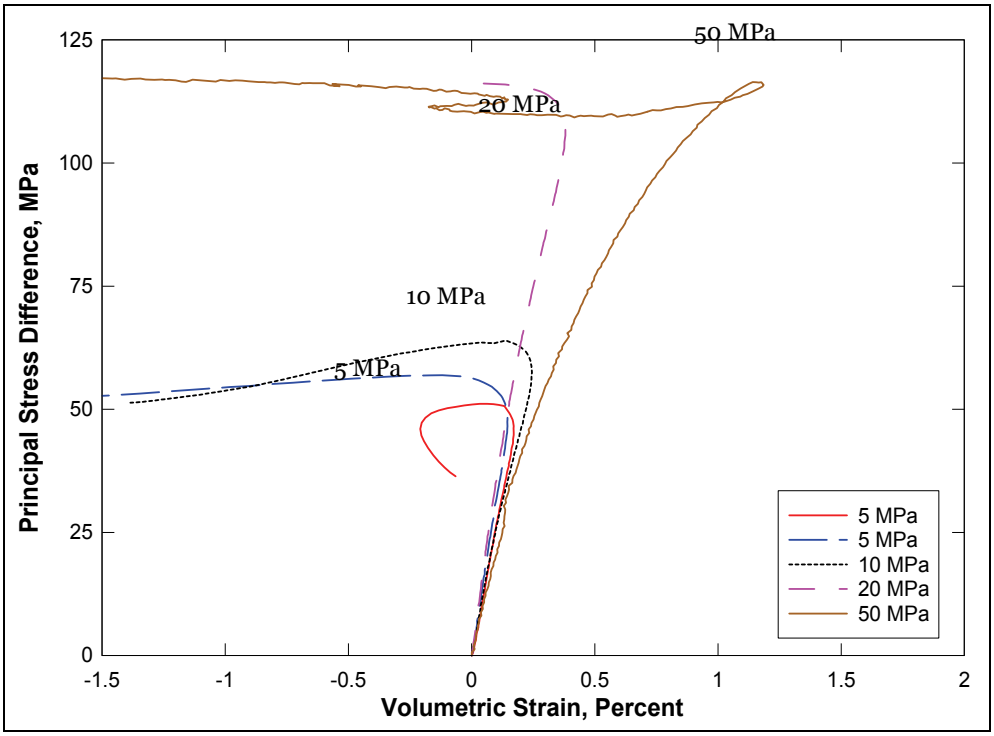

Figure 28. Stress difference-volumetric strain during shear from TXC non-cyclic tests at confining pressures between 5 and 50 MPa.

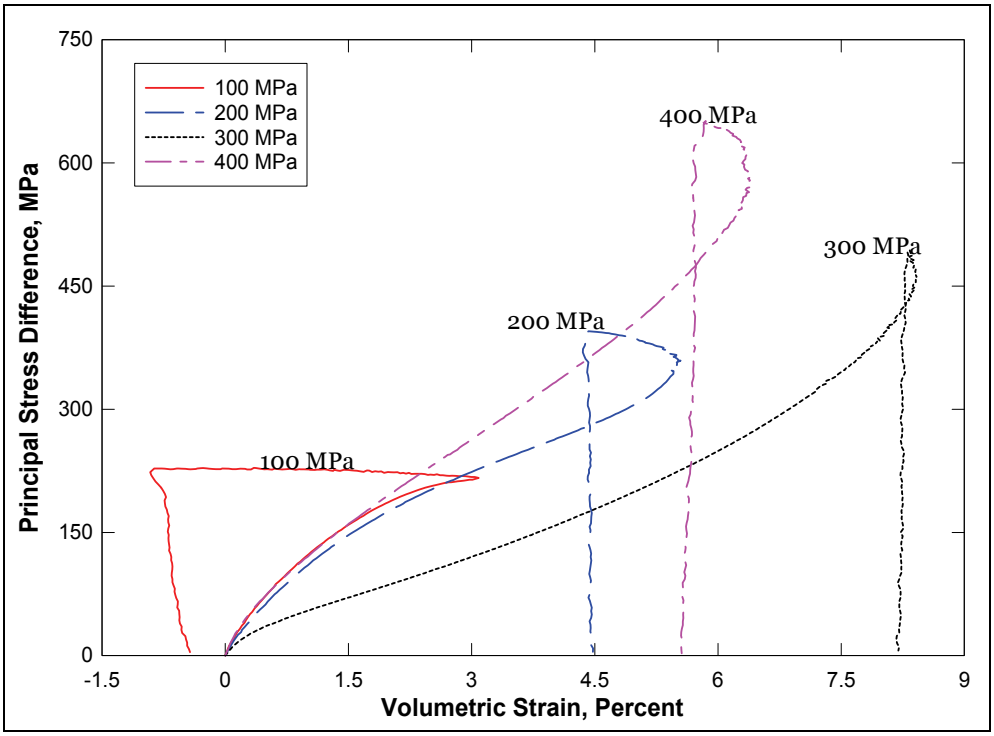

Figure 29. Stress difference-volumetric strain during shear from TXC non-cyclic tests at confining pressures between 100 and 400 MPa.

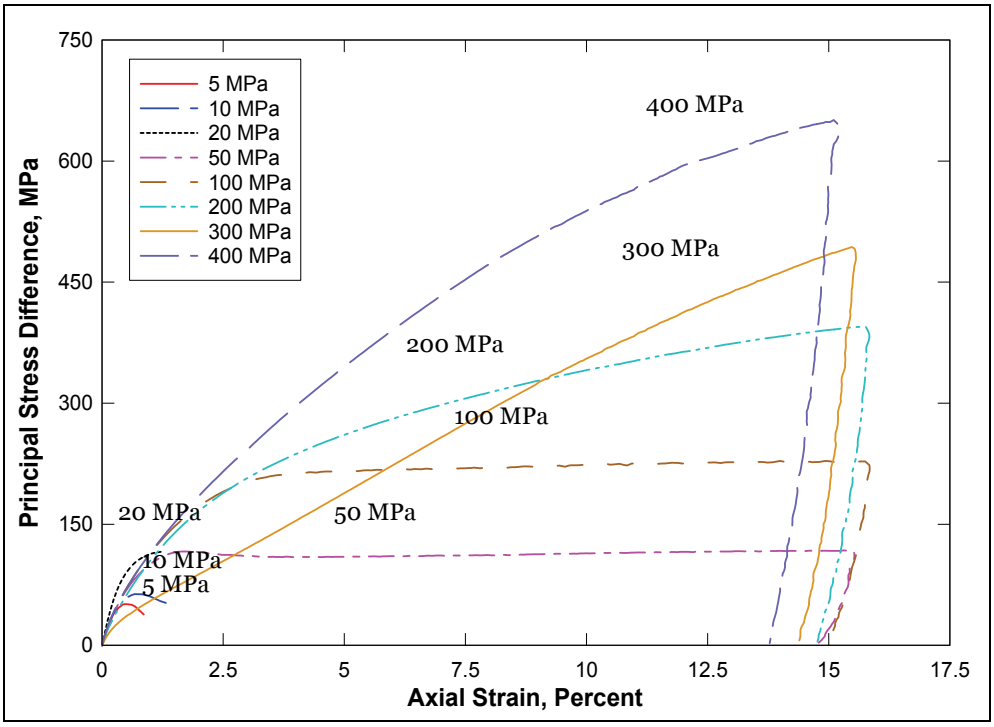

Figure 30. Stress-strain data from non-cyclic TXC tests at confining pressures between 5 and 400 MPa.

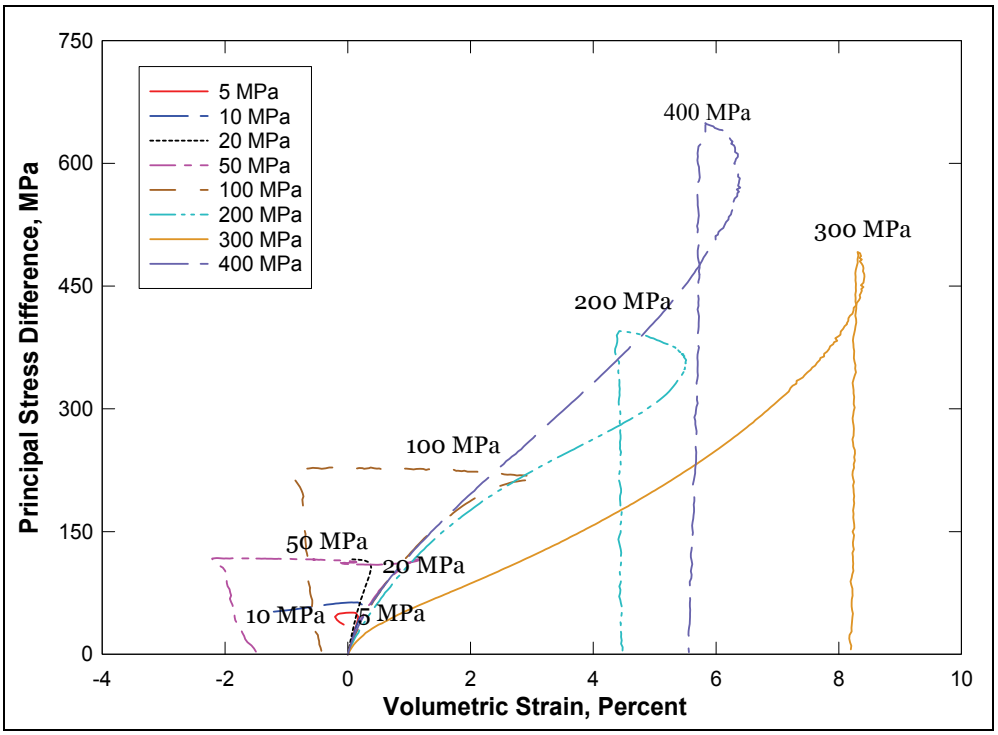

Figure 31. Stress difference-volumetric strain during shear from non-cyclic TXC tests at confining pressures between 5 and 400 MPa.

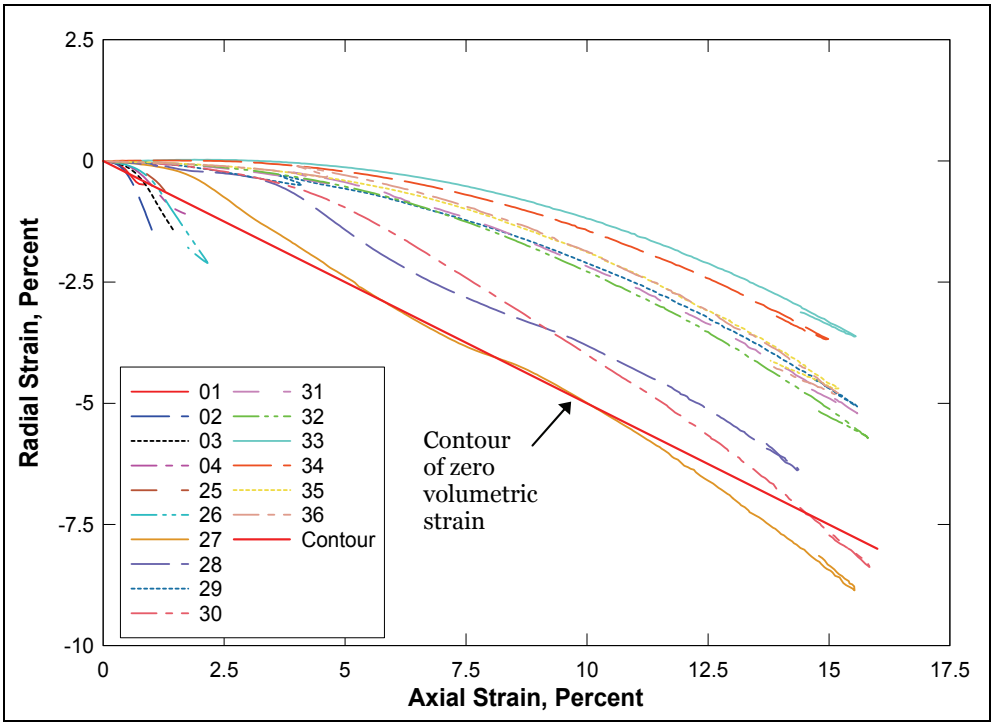

Figure 32. Radial strain-axial strain data during shear from TXC tests at confining pressures between 5 and 400 MPa.

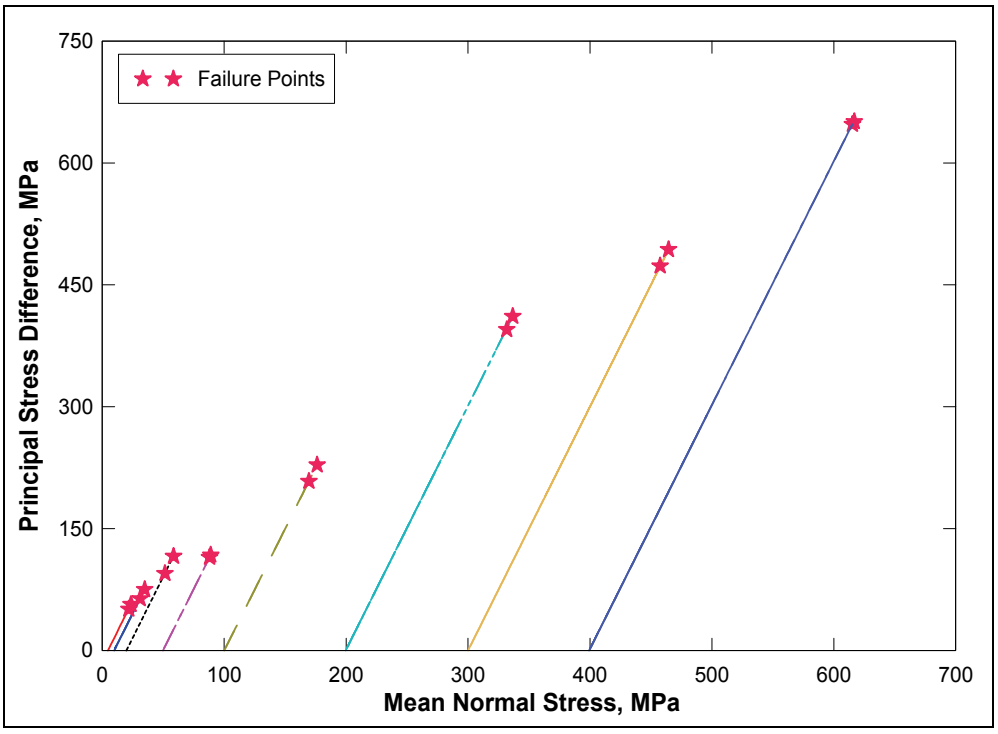

Figure 33. Failure data shear from TXC tests at confining pressures between 5 and 400 MPa.

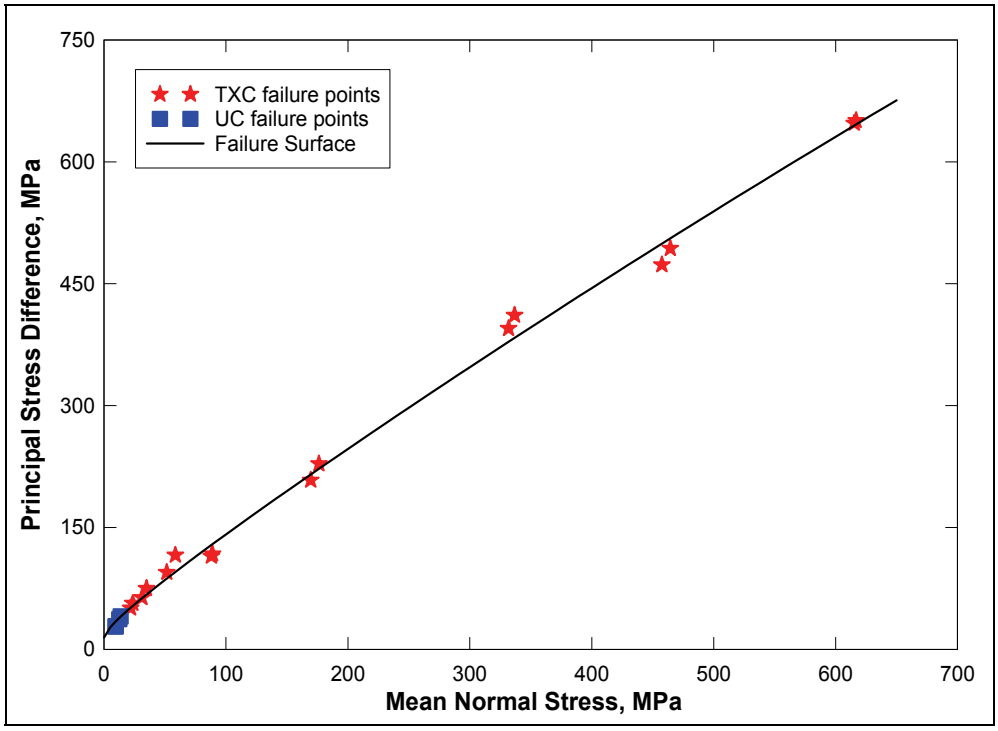

Figure 34. Failure data from UC and TXC tests and recommended failure surface.

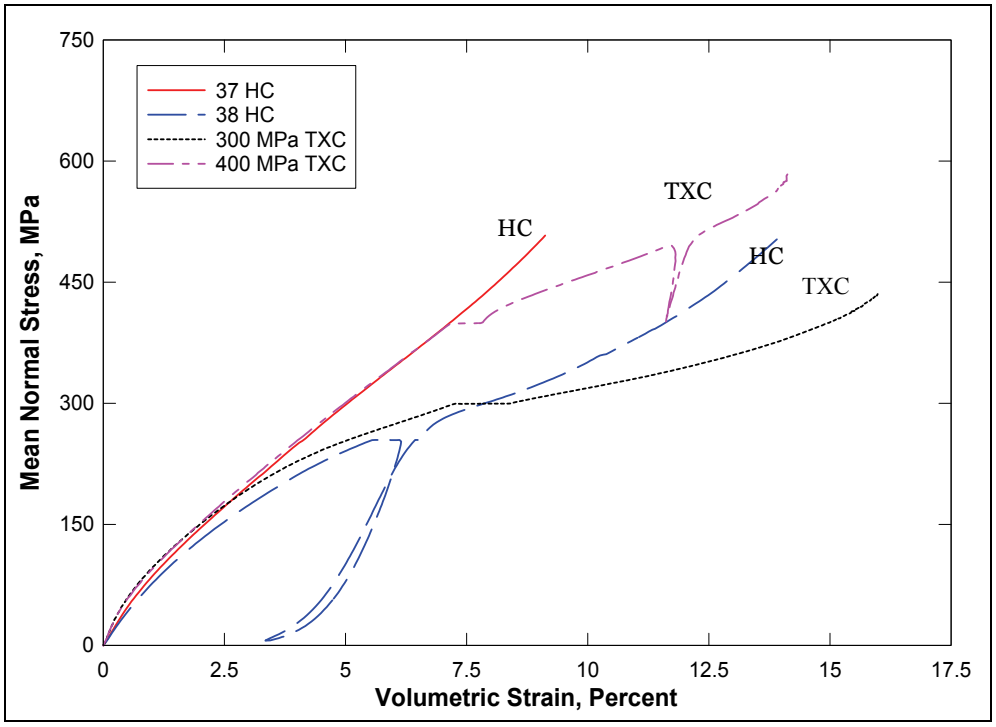

Figure 35. Pressure-volumetric strain data from HC and selected TXC tests.

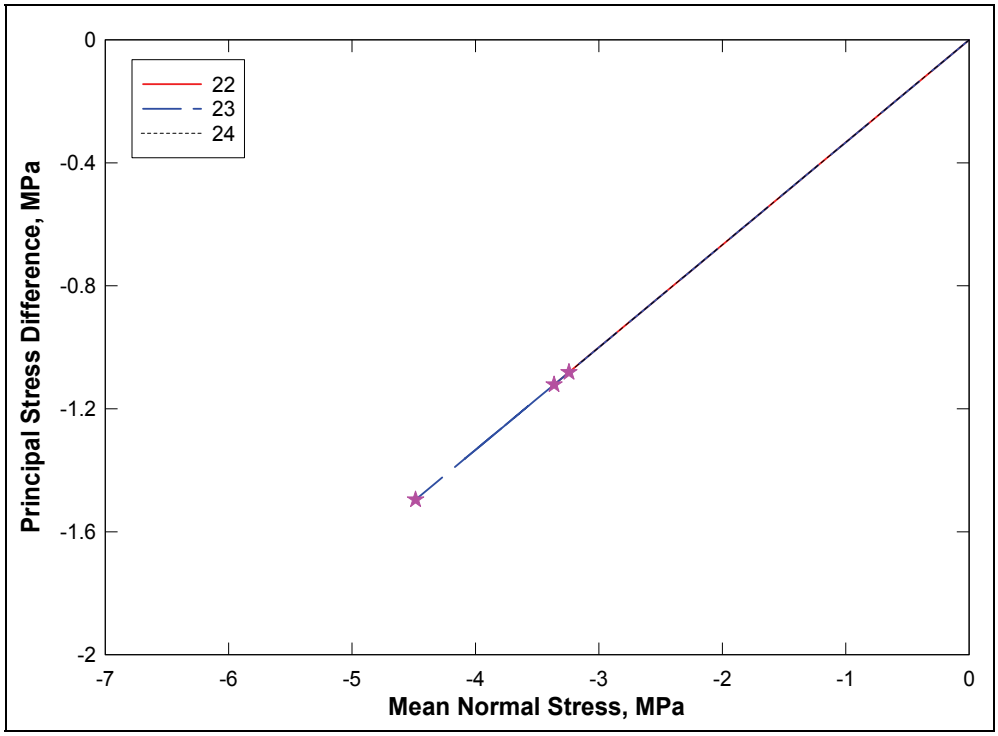

Figure 36. Stress paths and failure data from DP tests.

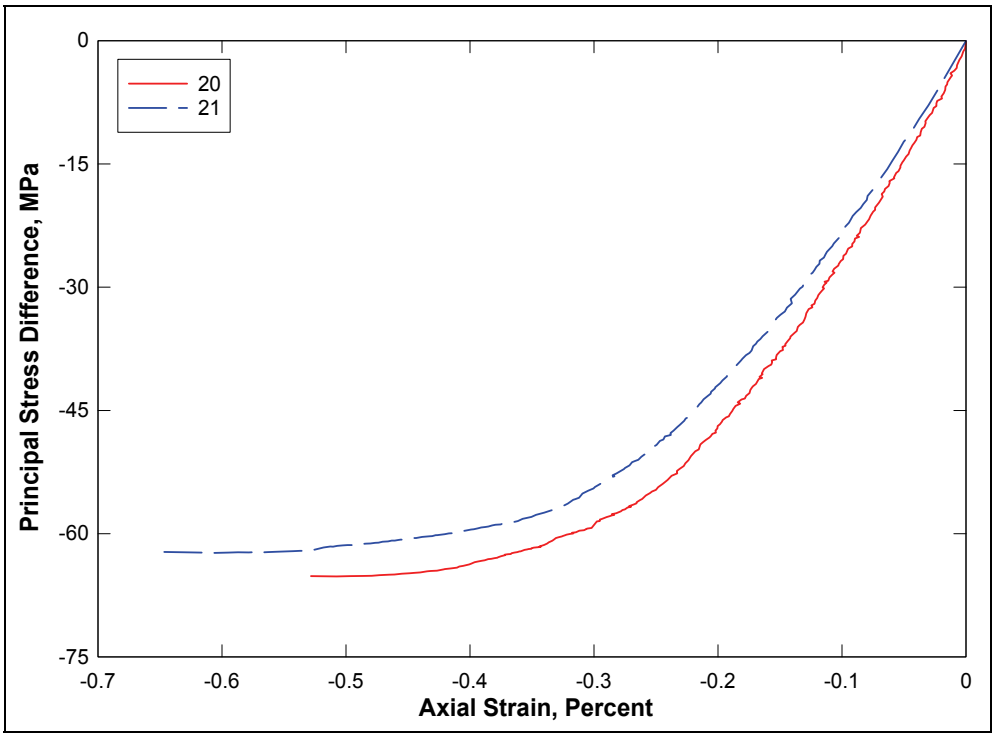

Figure 37. Stress-strain data from RTE tests.

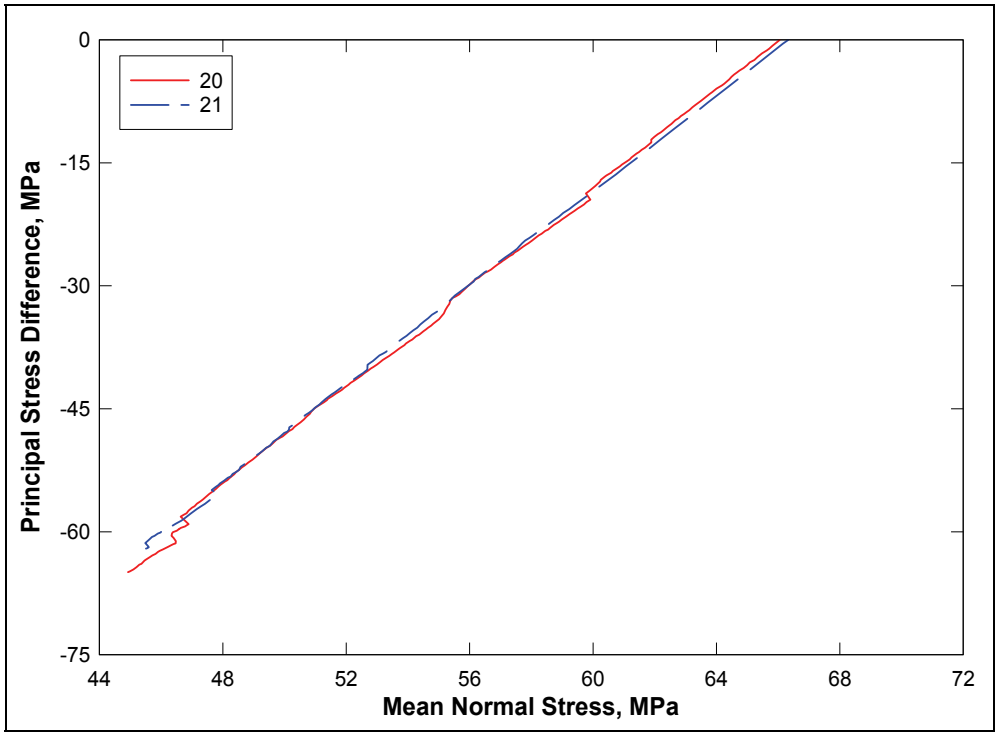

Figure 38. Stress path data from RTE tests.

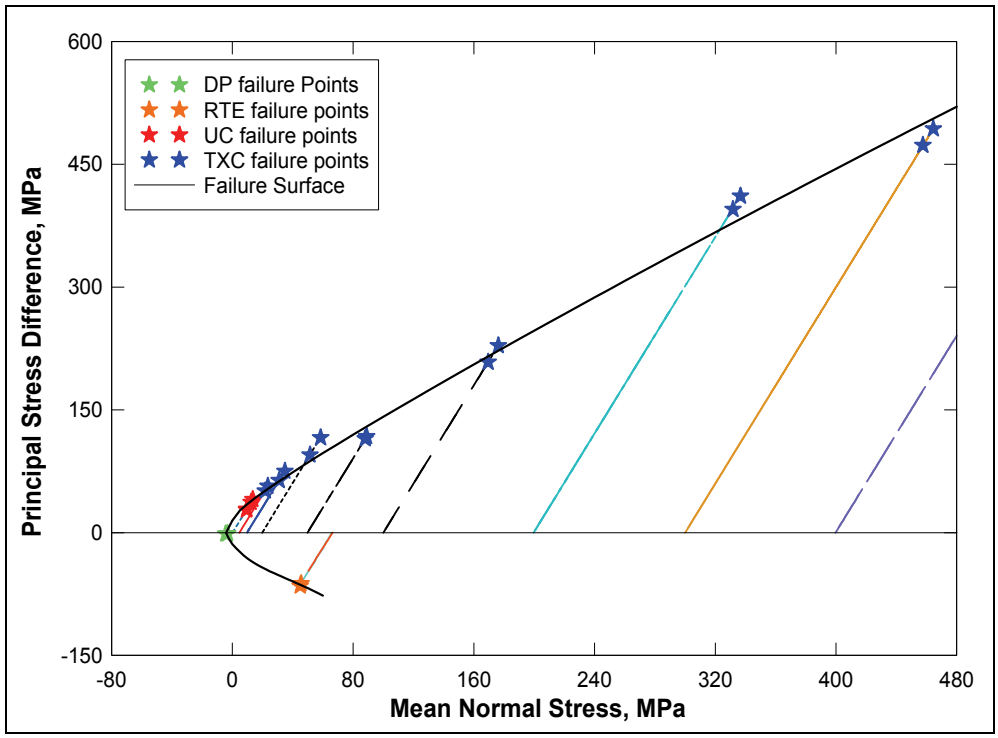

Figure 39. Failure surfaces and stress paths from UC tests, DP tests, RTE tests, and the TXC tests between 0 MPa to 100 MPa.

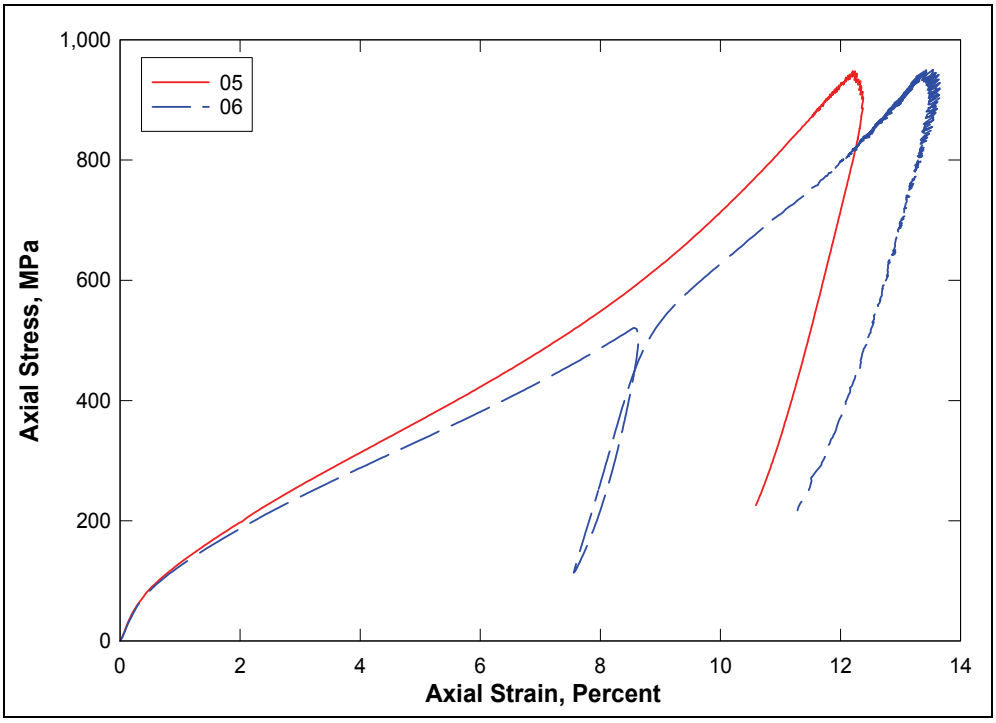

Figure 40. Stress-strain curves from UX tests.

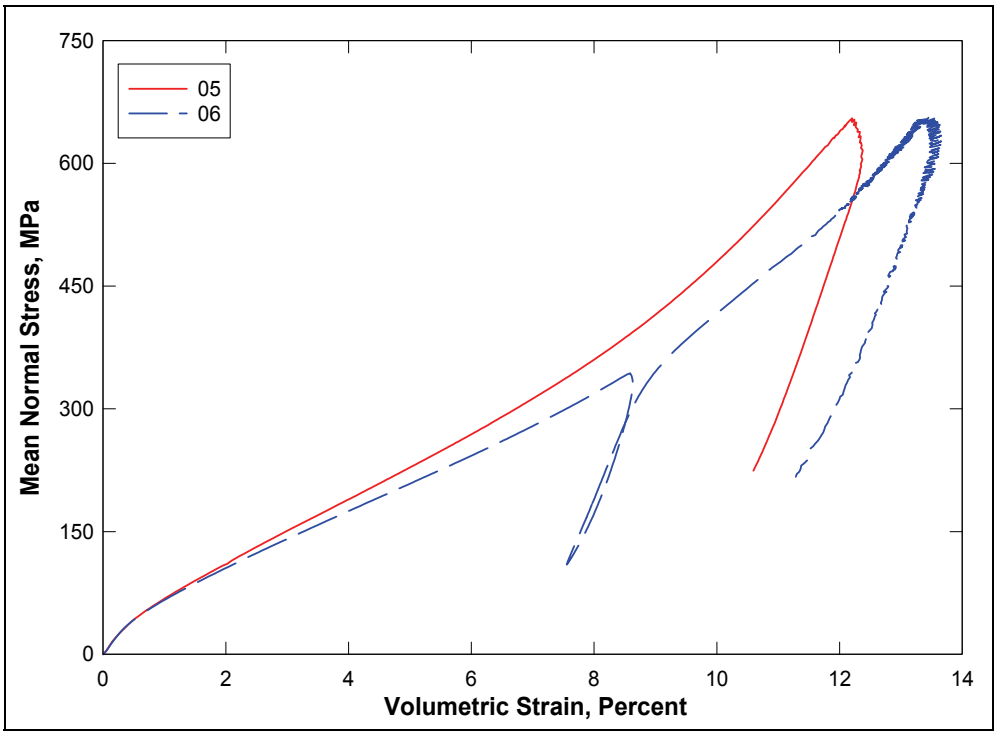

Figure 41. Pressure-volume data from UX tests.

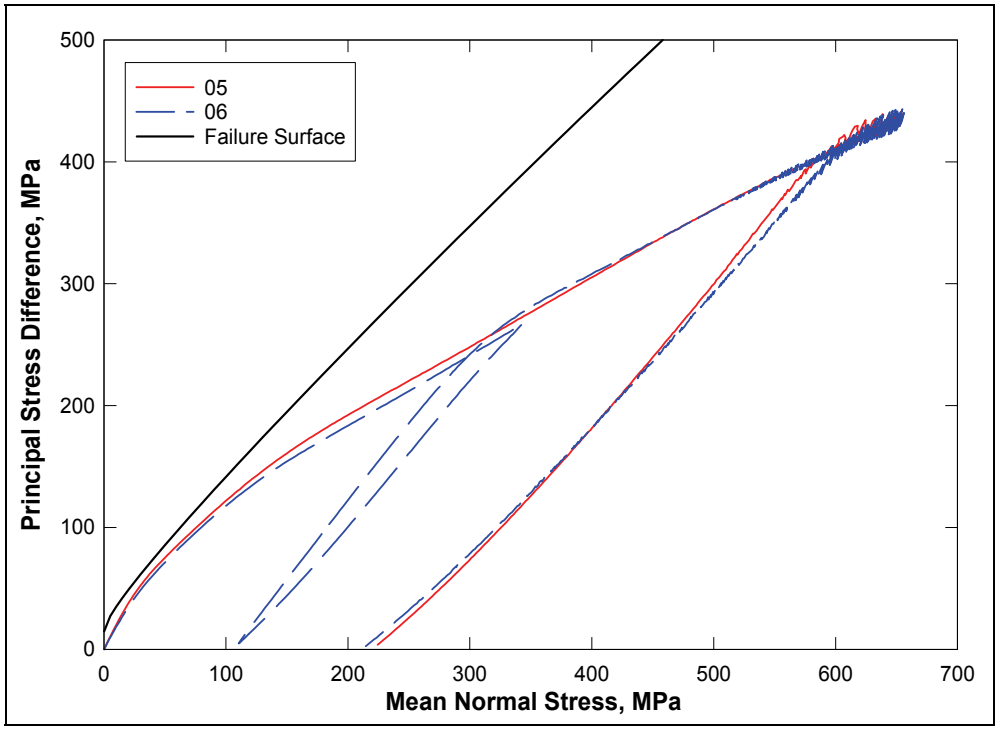

Figure 42. Stress paths from UX tests and failure surface from TXC tests.

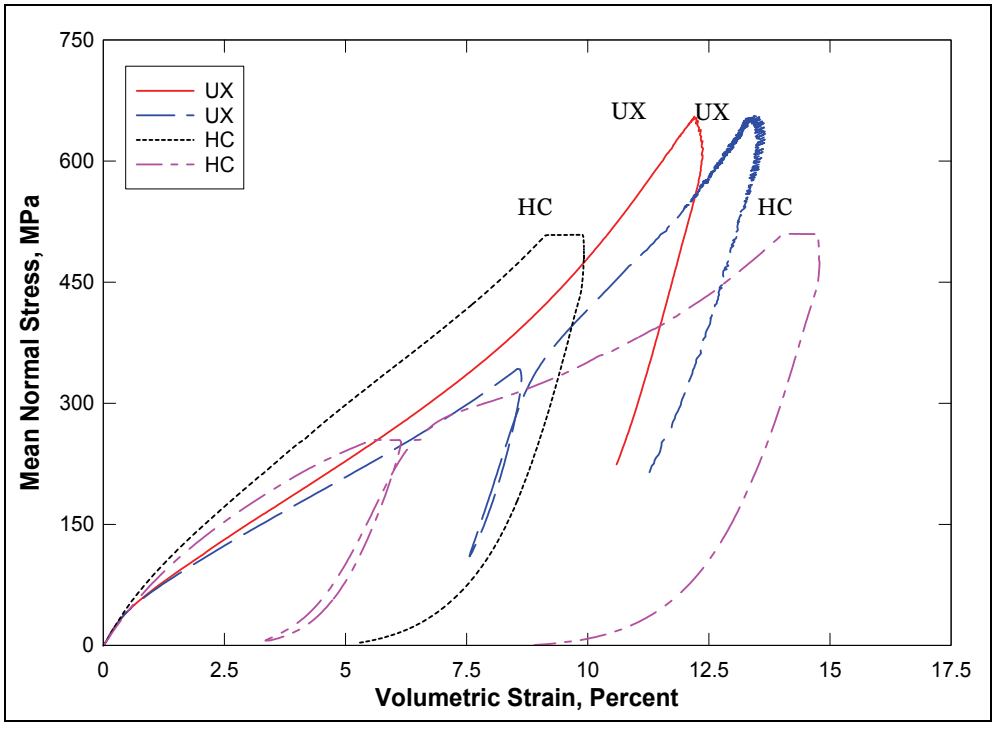

Figure 43. Comparison of pressure-volume data from HC and UX tests.

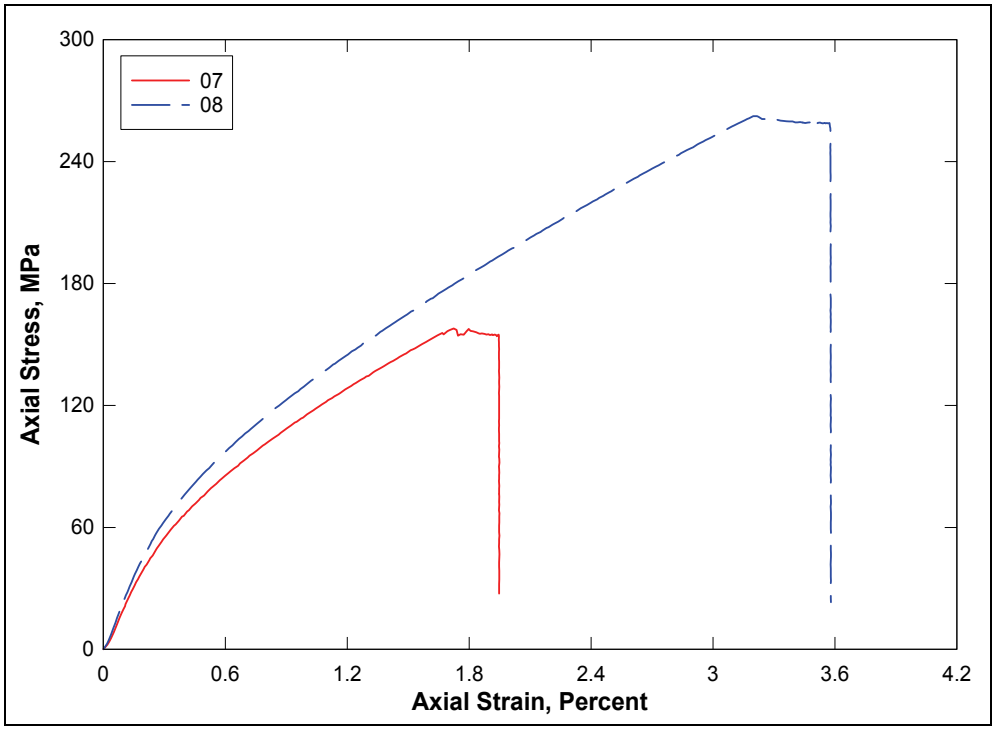

Figure 44. Stress-strain curves from UX/BX tests.

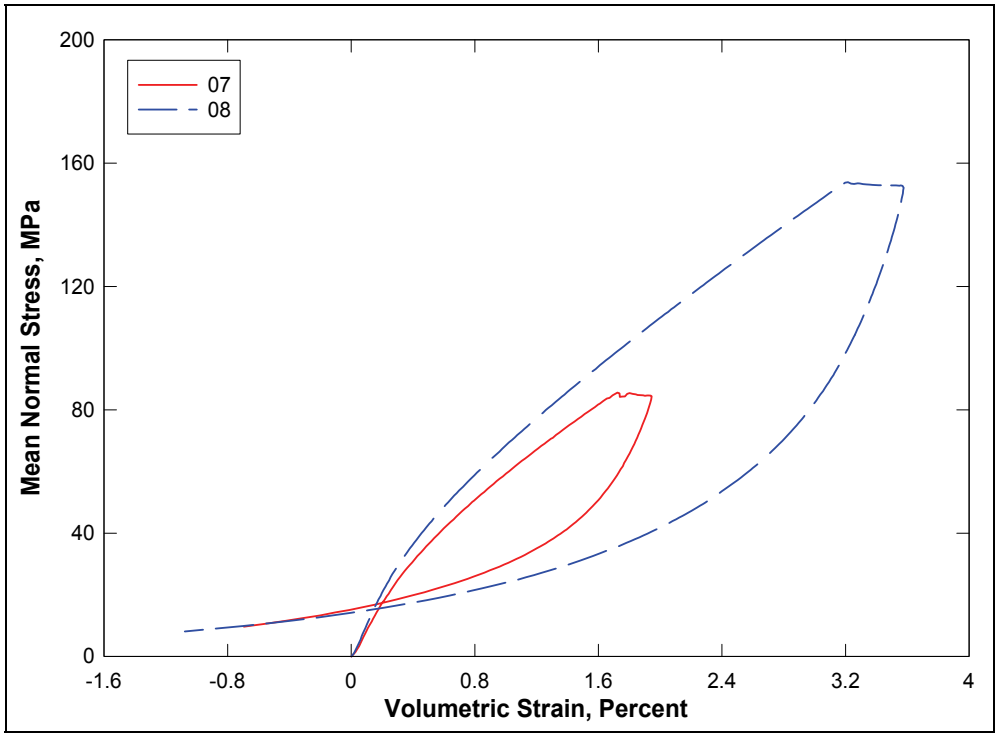

Figure 45. Pressure-volume data from UX/BX tests.

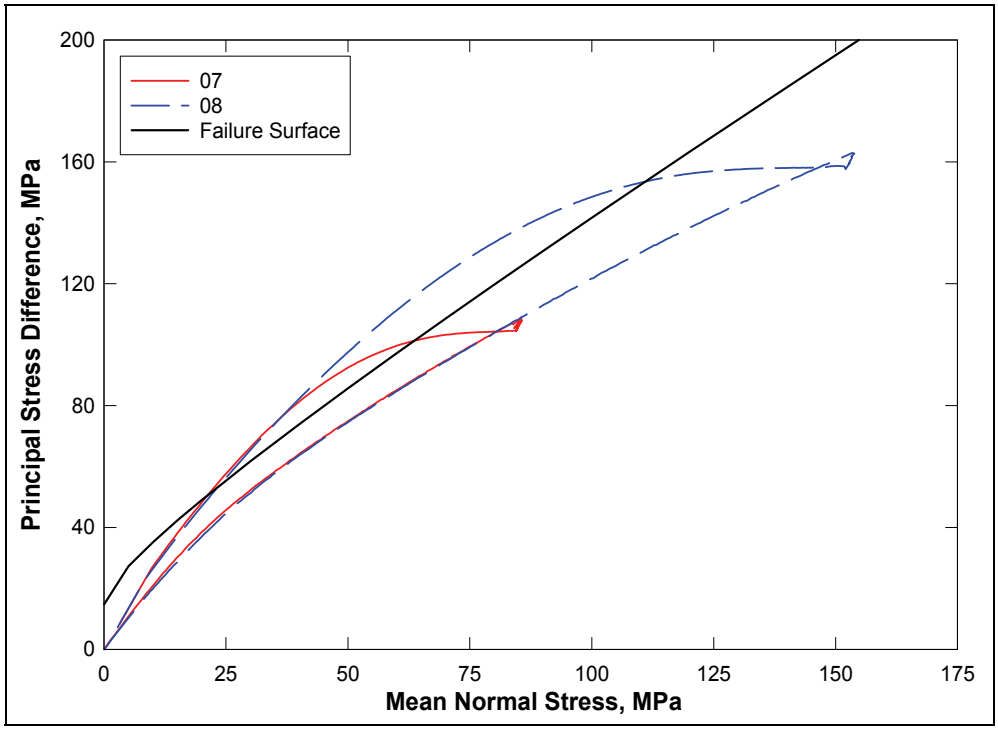

Figure 46. Stress paths from UX/BX tests and failure surface from TXC tests.

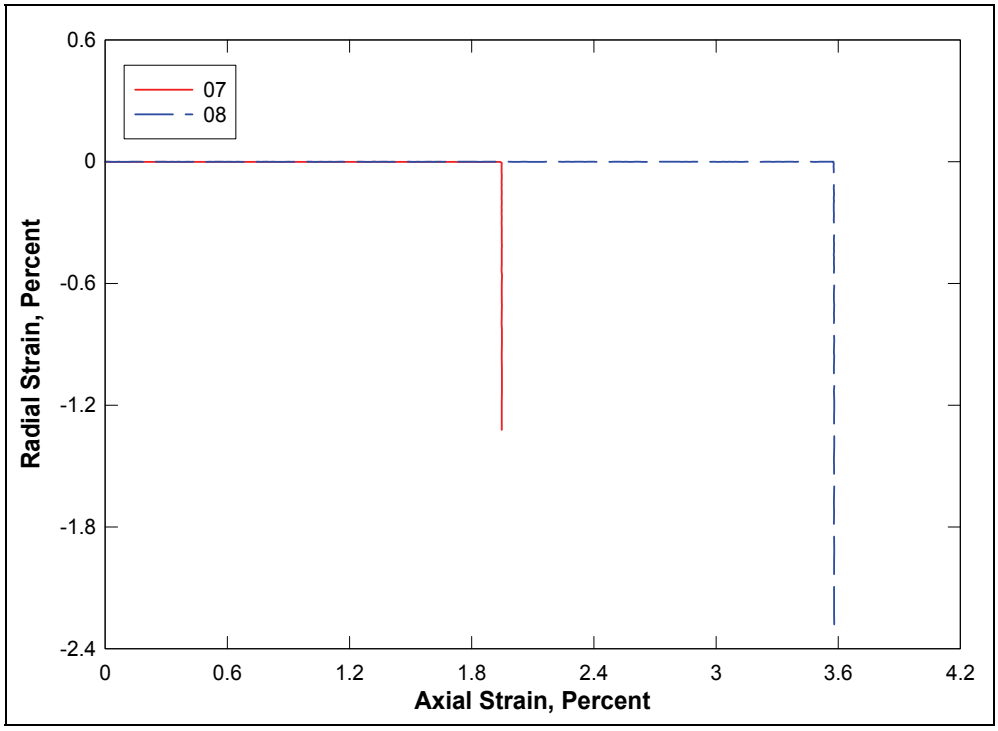

Figure 47. Strain paths from UX/BX tests.

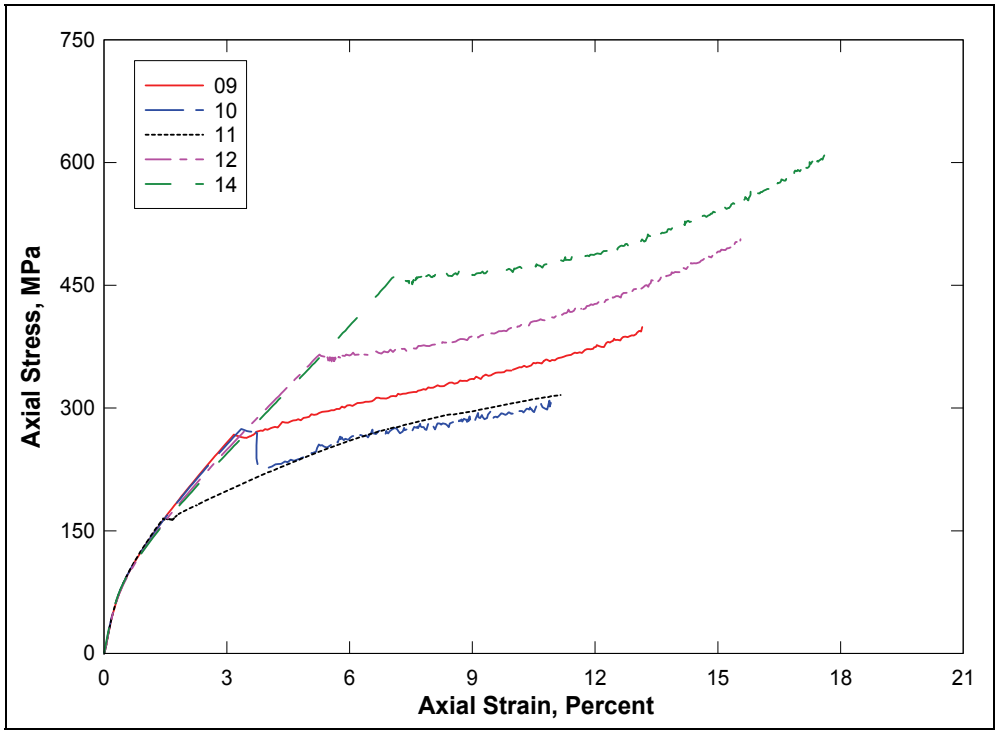

Figure 48. Stress-strain curves from UX/CV tests.

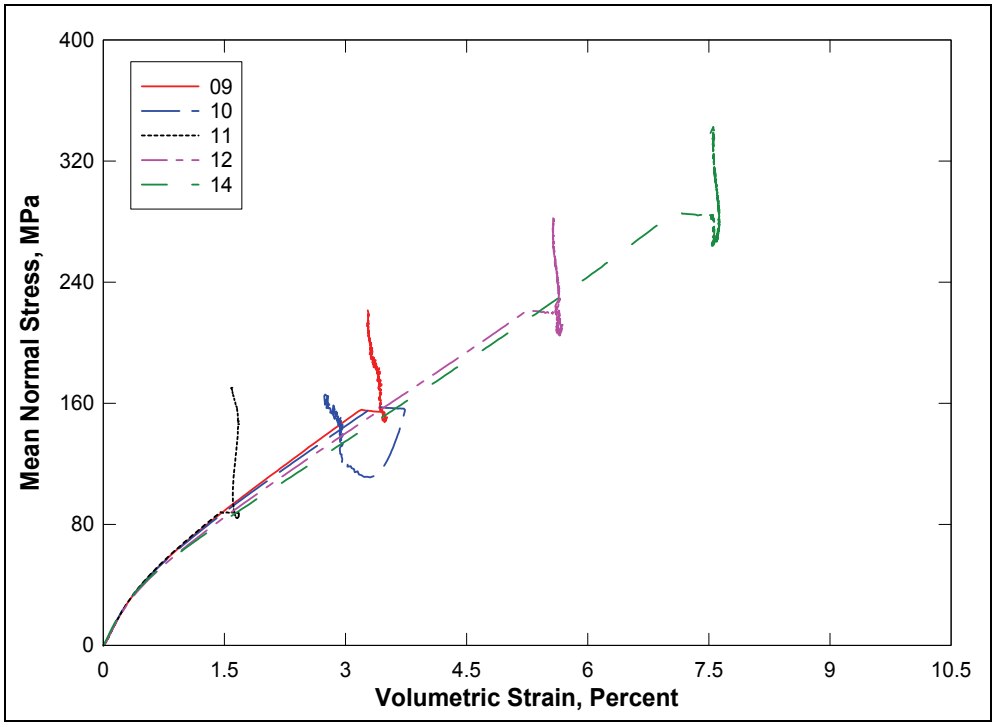

Figure 49. Pressure-volume data from UX/CV tests.

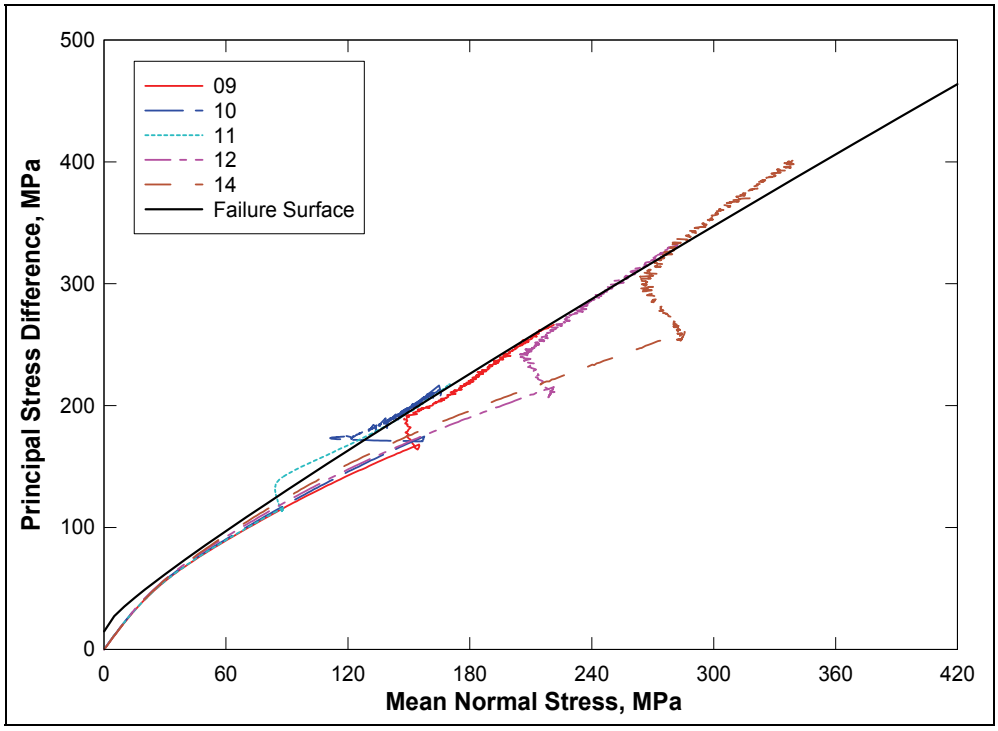

Figure 50. Stress paths from UX/CV tests and failure surface from TXC tests.

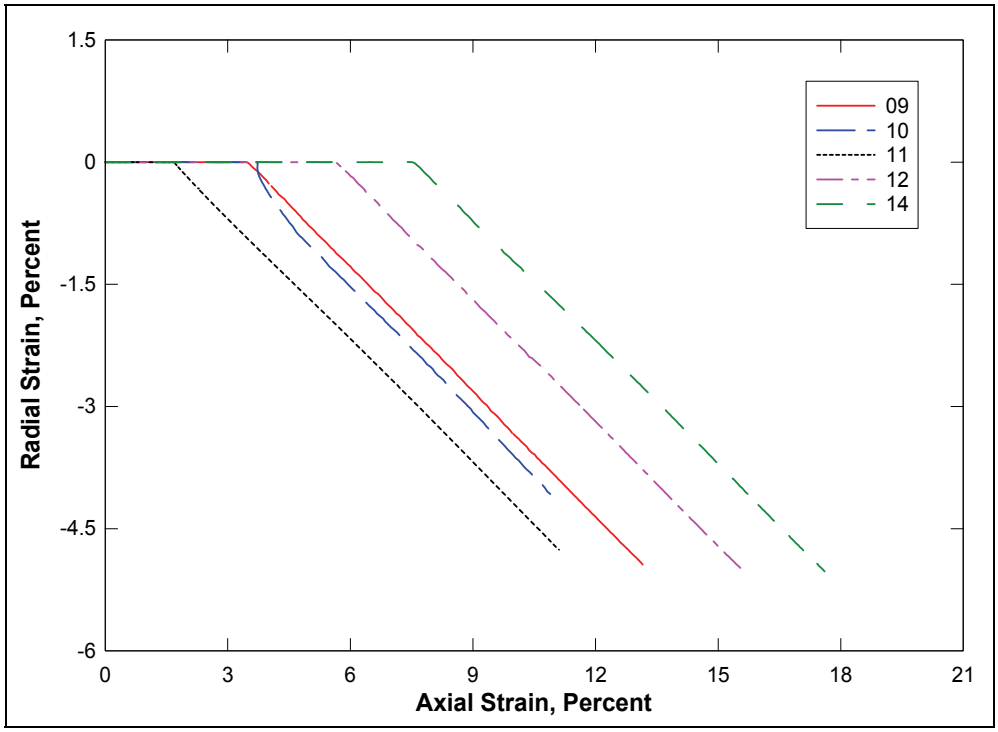

Figure 51. Strain paths from UX/CV tests.

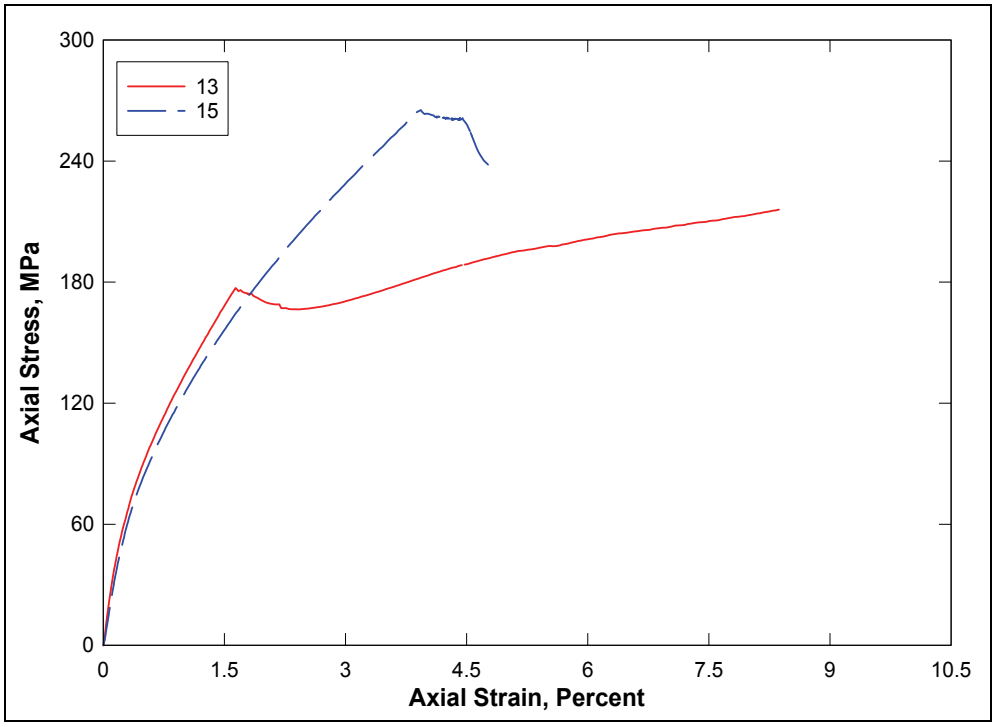

Figure 52. Stress-strain curves from UX/SR tests.

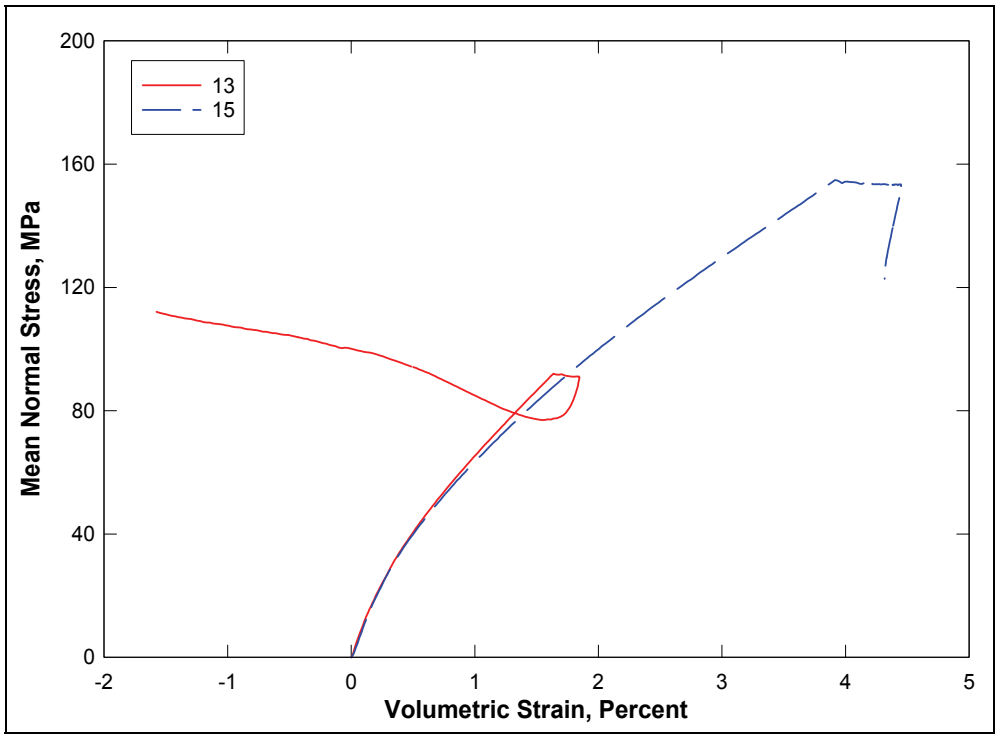

Figure 53. Pressure-volume data from UX/SR tests.

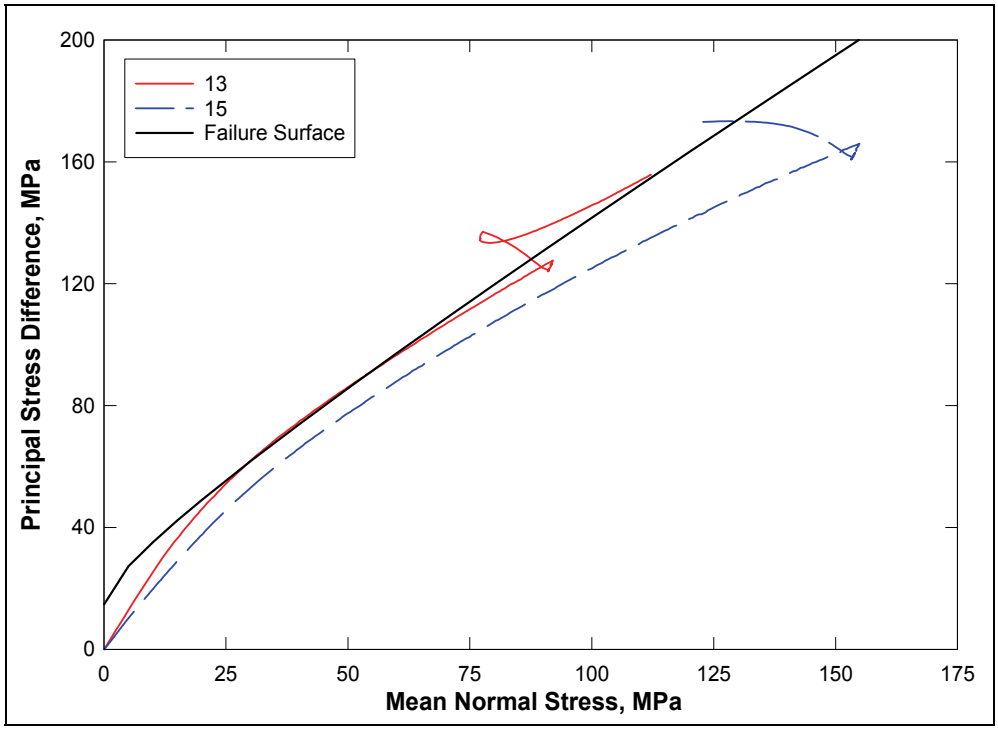

Figure 54. Stress paths from UX/SR tests and failure surface from TXC tests.

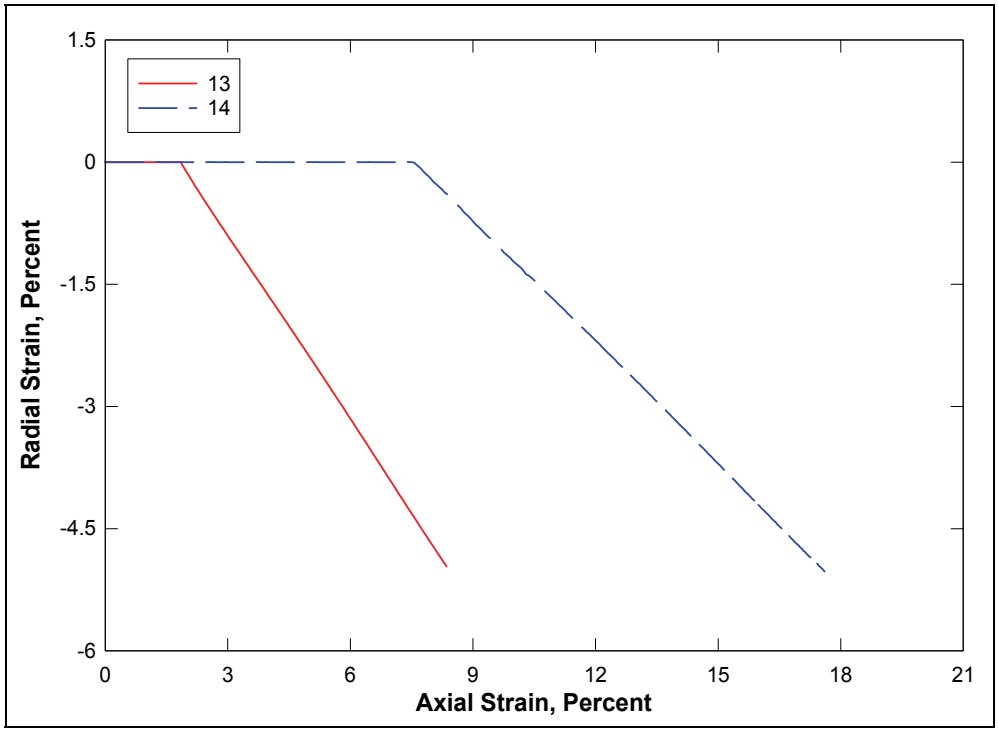

Figure 55. Strain paths from UX/CV tests.

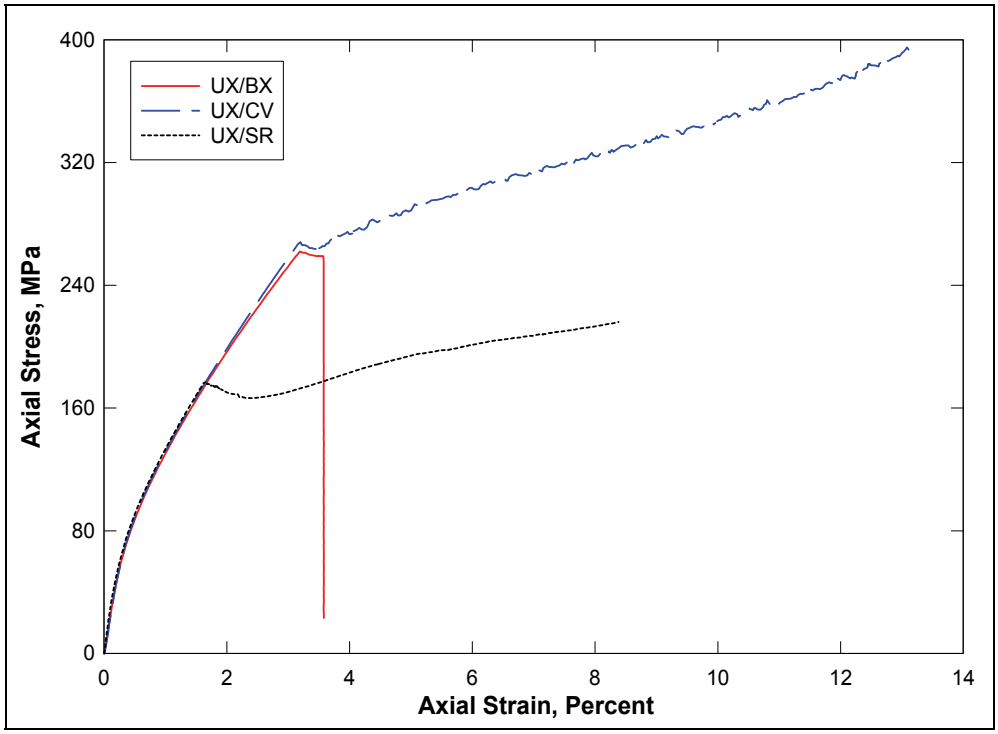

Figure 56. Stress-strain curves from selected UX, UX/BX, UX/CV, and UX/SR tests.

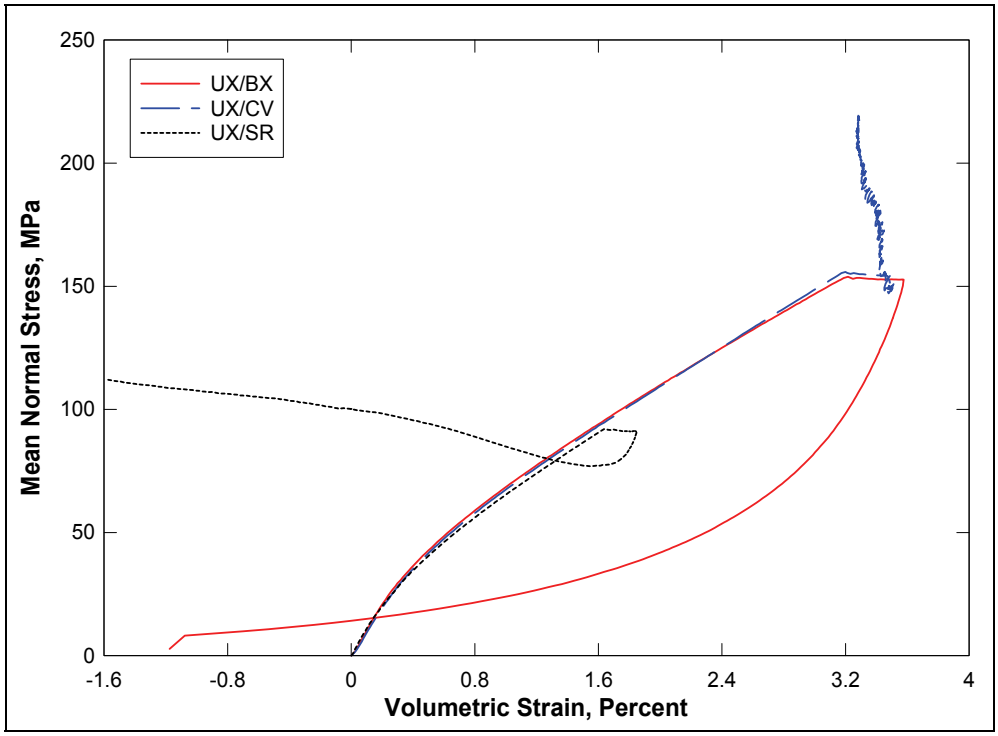

Figure 57. Pressure-volume data from selected UX/BX, UX/CV, and UX/SR tests.

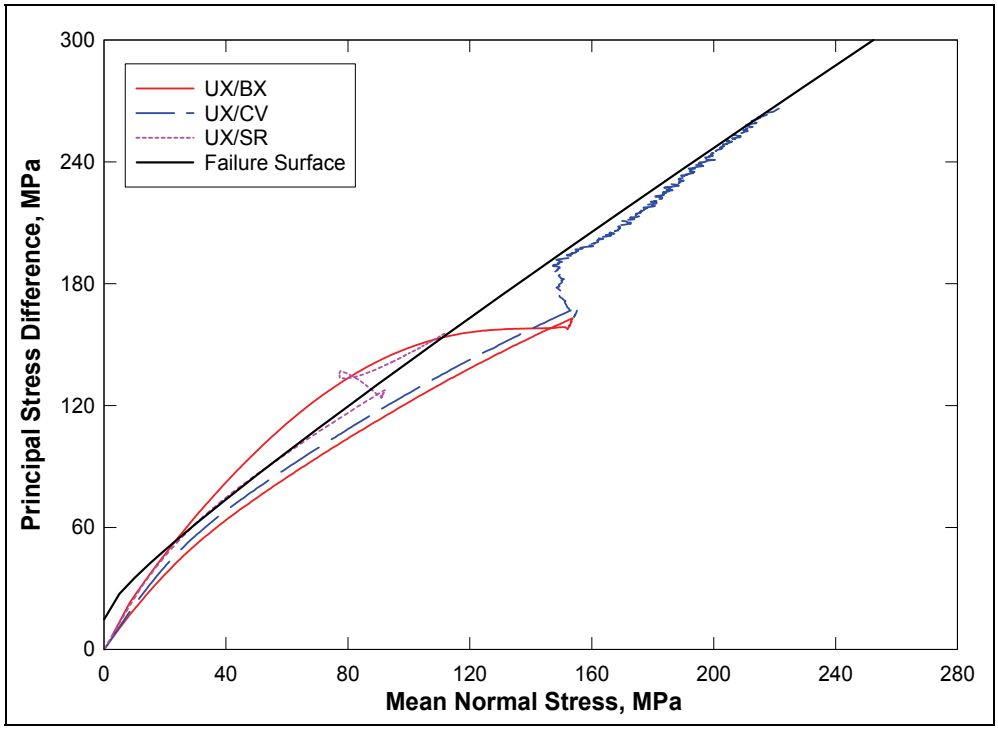

Figure 58. Stress paths from selected UX/BX, UX/CV, and UX/SR tests and failure surface from TXC tests.

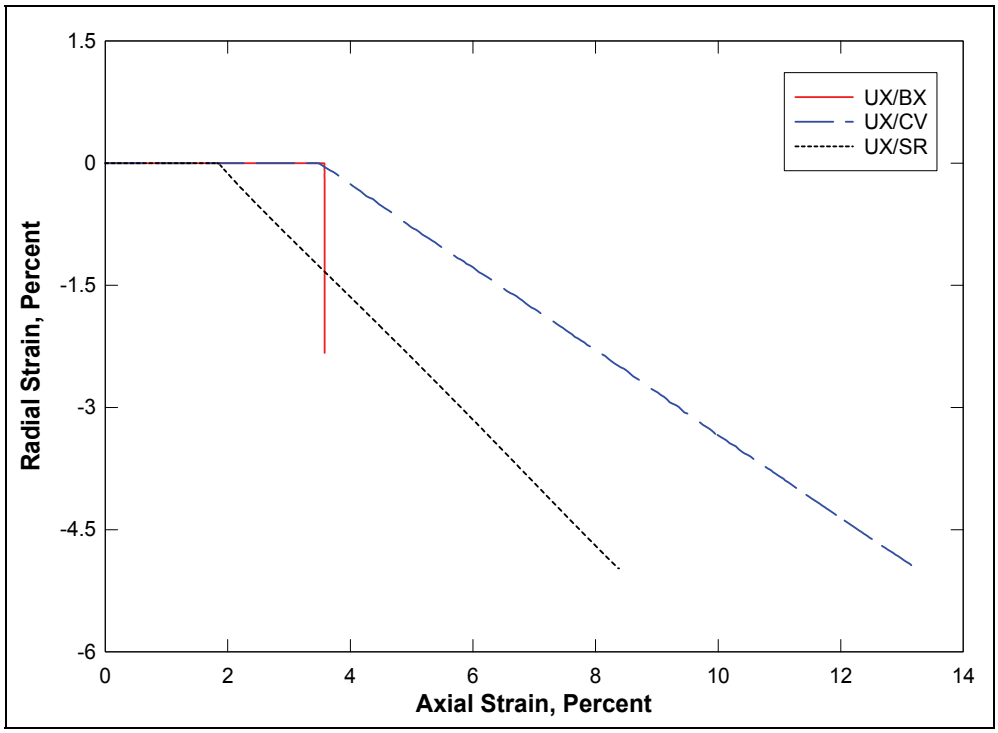

Figure 59. Strain paths from selected UX/BX, UX/CV, and UX/SR tests.

4 Summary

Personnel in the Geotechnical and Structures Laboratory of the US Army Engineer Research and Development Center at the Waterways Experiment Station conducted a laboratory investigation to characterize the strength and constitutive property behavior of Gray Masonry concrete (GMC). ERDC conducted 38 successful mechanical property tests consisting of two hydrostatic compression tests, four unconfined compression tests, sixteen triaxial compression tests, two uniaxial strain tests, two uniaxial strain load/biaxial strain unload tests, five uniaxial strain load/constant volume strain tests, two uniaxial strain load/strain ratio strain tests, three direct pull tests, and two reduced triaxial retention tests. In addition to the mechanical property tests, nondestructive pulse-velocity measurements were performed on each specimen.

In general, the overall quality of the test data was very good; limited scatter was observed in the data over repeated loading paths. The compressibility of GMC is affected by initial dry density, i.e., increased compressibility with decreased dry density. The initial loading HC and UX compressibility responses were very stiff due to the cemented nature of the GMC material. Comparisons of the volumetric responses from the HC and UX tests showed that the GMC material exhibited increased compaction under shear-induced loading from the UX tests when compared to results from HC tests in which no shear-induced loading occurred. Creep was observed during the HC and UX tests. The TXC tests exhibited a continuous increase in maximum principal stress difference with increasing confining stress. TXC tests exhibited primarily compressive volume strains during shear. A compression failure surface was developed from the TXC test results at eight levels of confining stress and from the results of the UC tests. The DP and RTE tests exhibited lower absolute values of principal stress difference than comparable TXC tests. The results for the DP and RTE tests were used to develop the extension failure surface. The resulting compression and extension failure surfaces were well defined and nonsymmetric about the mean normal stress axis. During UX/BX tests, stress relaxation was evident during the change from uniaxial strain loading to biaxial strain unloading. Good correlations were observed between the stress paths obtained from the UX/CV and UX/SR strain path tests and the failure surface from the TXC test.

References

Akers, S. A., P. A. Reed, and J. Q. Ehrgott. 1986. *WES High-Pressure Uniaxial Strain and Triaxial Shear Test Equipment*. Miscellaneous Paper SL-86-11. Vicksburg, MS: U.S. Army Engineer Waterways Experiment Station.

American Society for Testing and Materials. 2002. *2002 Annual Book of ASTM Standards*. Philadelphia, PA.

a. Designation C 39-01. Standard test method for compressive strength of concrete specimens.
b. Designation C 42-99. Standard test method for obtaining and testing drilled cores and sawed beams of concrete.
c. Designation C 597-97. Standard test method for pulse velocity through concrete.
d. Designation C 801-98. Standard test method for determining the mechanical properties of hardened concrete under triaxial loads.
e. Designation D 2216-98. Standard test method for laboratory determination of water (moisture) content of soil and rock by mass.
f. Designation D 4543-01. Standard test method for preparing rock core specimens and determining dimensional and shape tolerances.

Bishop, A. W., and D. J. Henkel. 1962. *The measurement of soil properties in the triaxial test*. London: Edward Arnold, Ltd. 72-74.

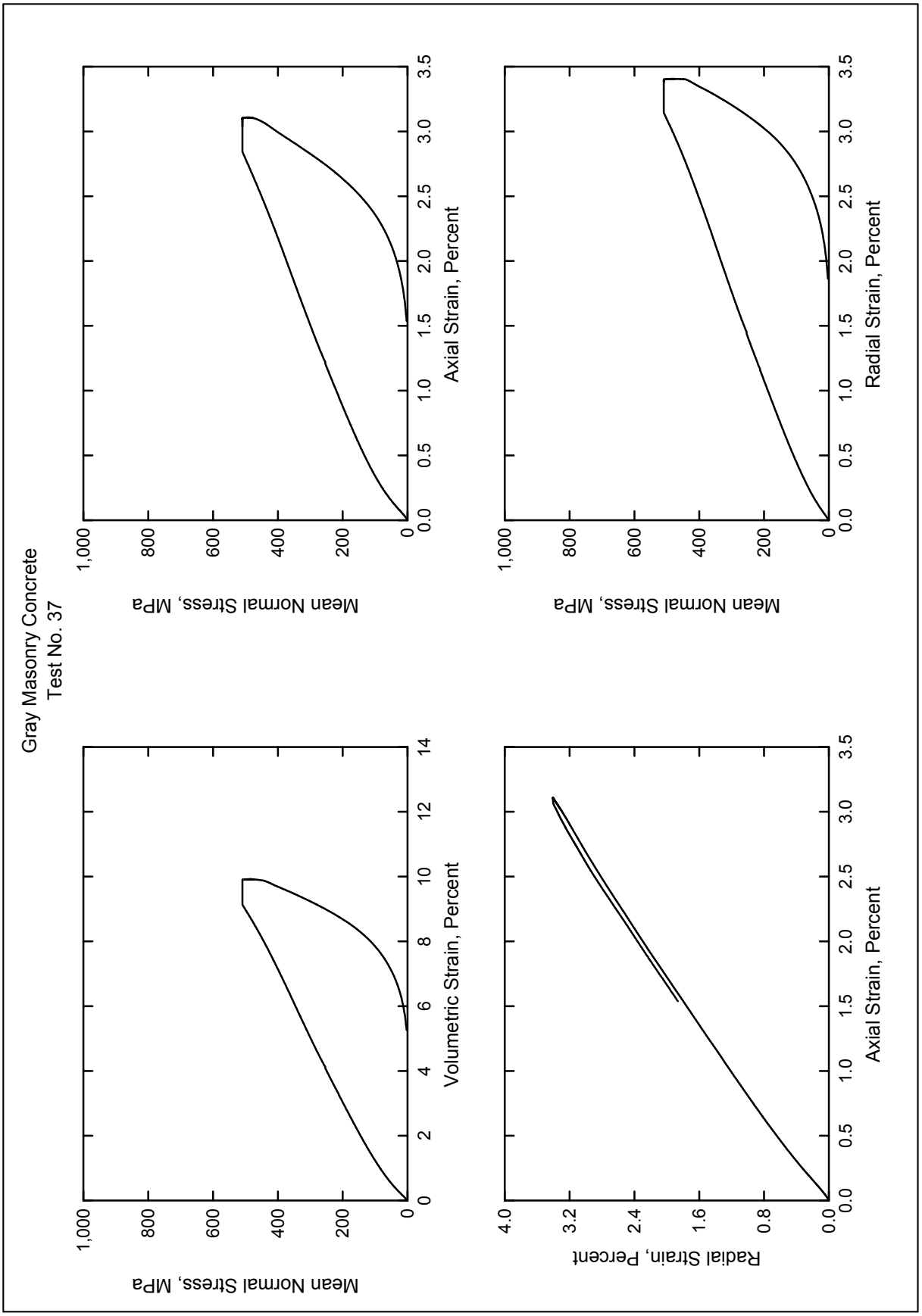
Gray Masonry Concrete
Test No. 37
Mean Normal Stress, MPa
Axial Strain, Percent
Mean Normal Stress, MPa
Radial Strain, Percent
Mean Normal Stress, MPa
Volumetric Strain, Percent
Radial Strain, Percent
Axial Strain, Percent

Plate 1

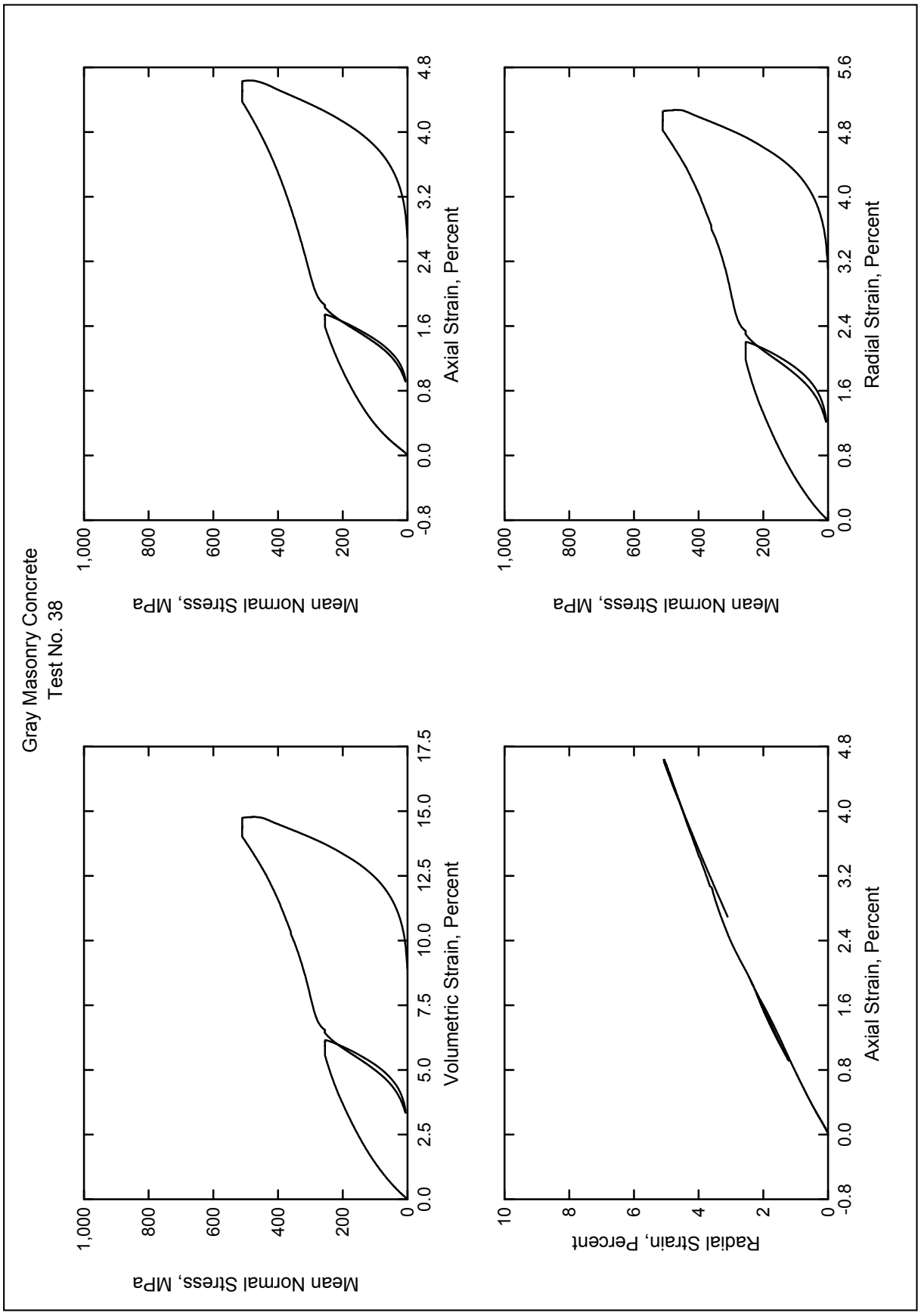
Gray Masonry Concrete
Test No. 38
Mean Normal Stress, MPa
Axial Strain, Percent
Mean Normal Stress, MPa
Radial Strain, Percent
Mean Normal Stress, MPa
Volumetric Strain, Percent
Radial Strain, Percent
Axial Strain, Percent

Plate 2

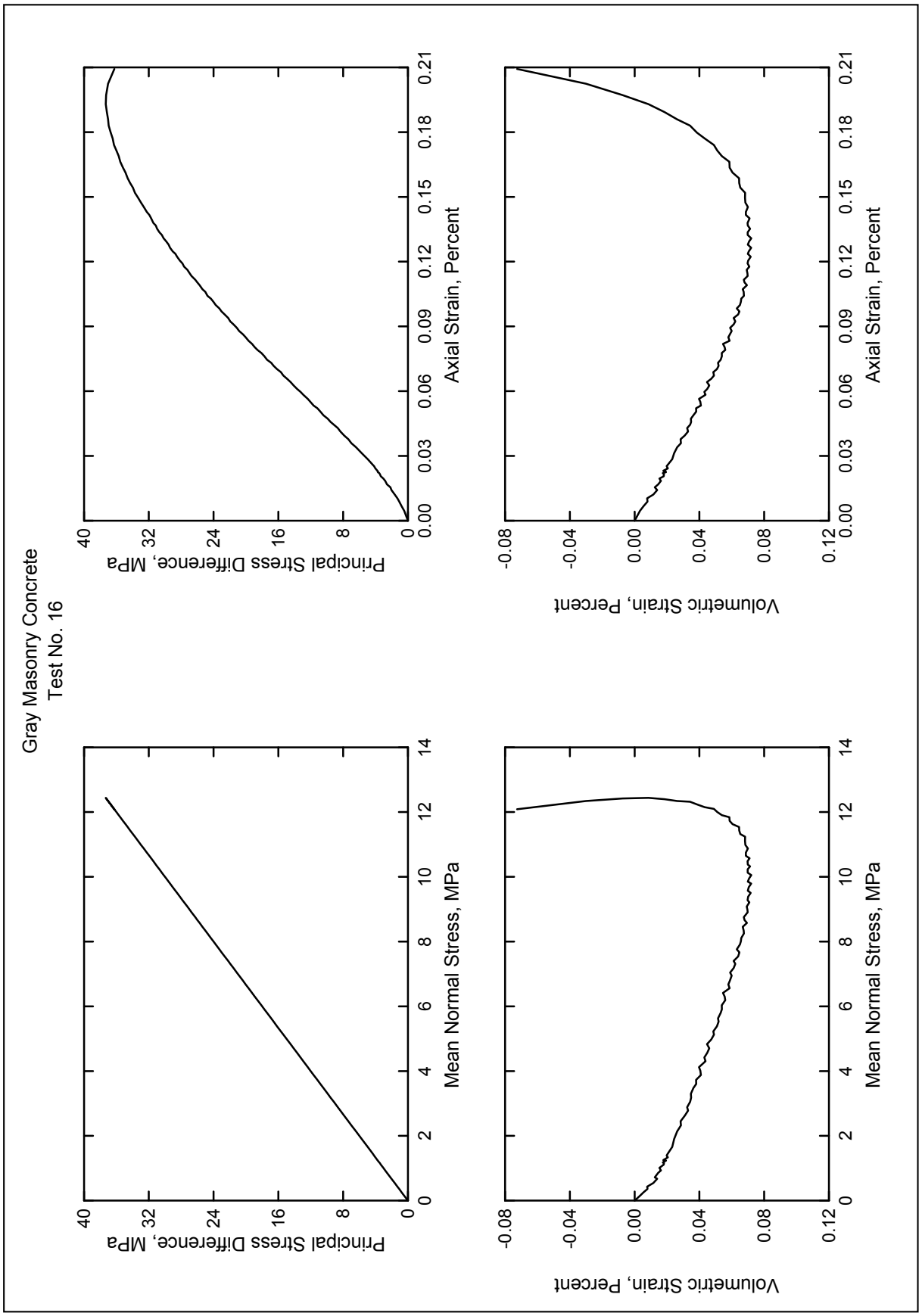
Gray Masonry Concrete
Test No. 16
Principal Stress Difference, MPa
Axial Strain, Percent
Volumetric Strain, Percent
Axial Strain, Percent
Principal Stress Difference, MPa
Mean Normal Stress, MPa
Volumetric Strain, Percent
Mean Normal Stress, MPa

Plate 3

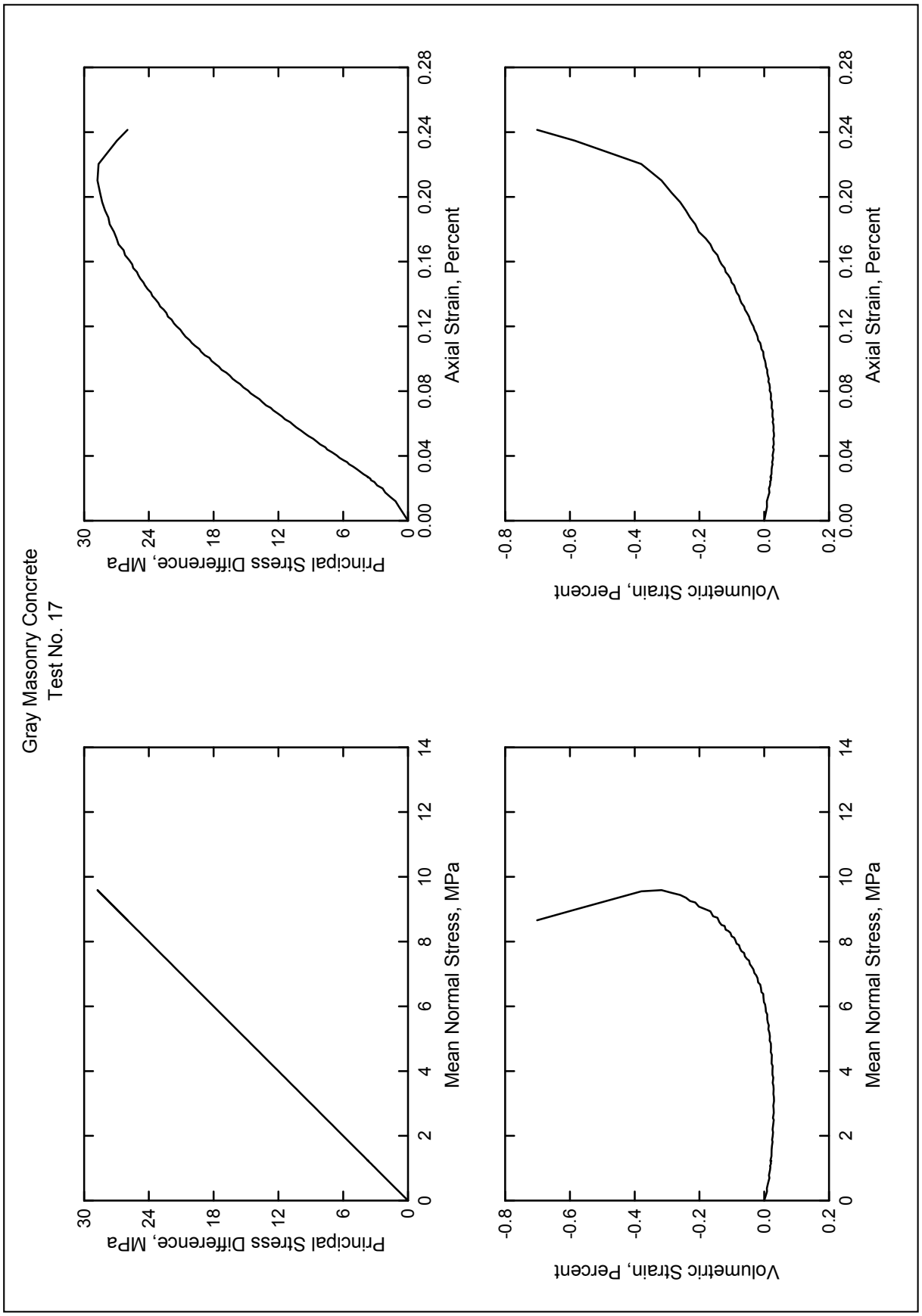
Gray Masonry Concrete
Test No. 17
Principal Stress Difference, MPa
Axial Strain, Percent
Volumetric Strain, Percent
Axial Strain, Percent
Principal Stress Difference, MPa
Mean Normal Stress, MPa
Volumetric Strain, Percent
Mean Normal Stress, MPa

Plate 4

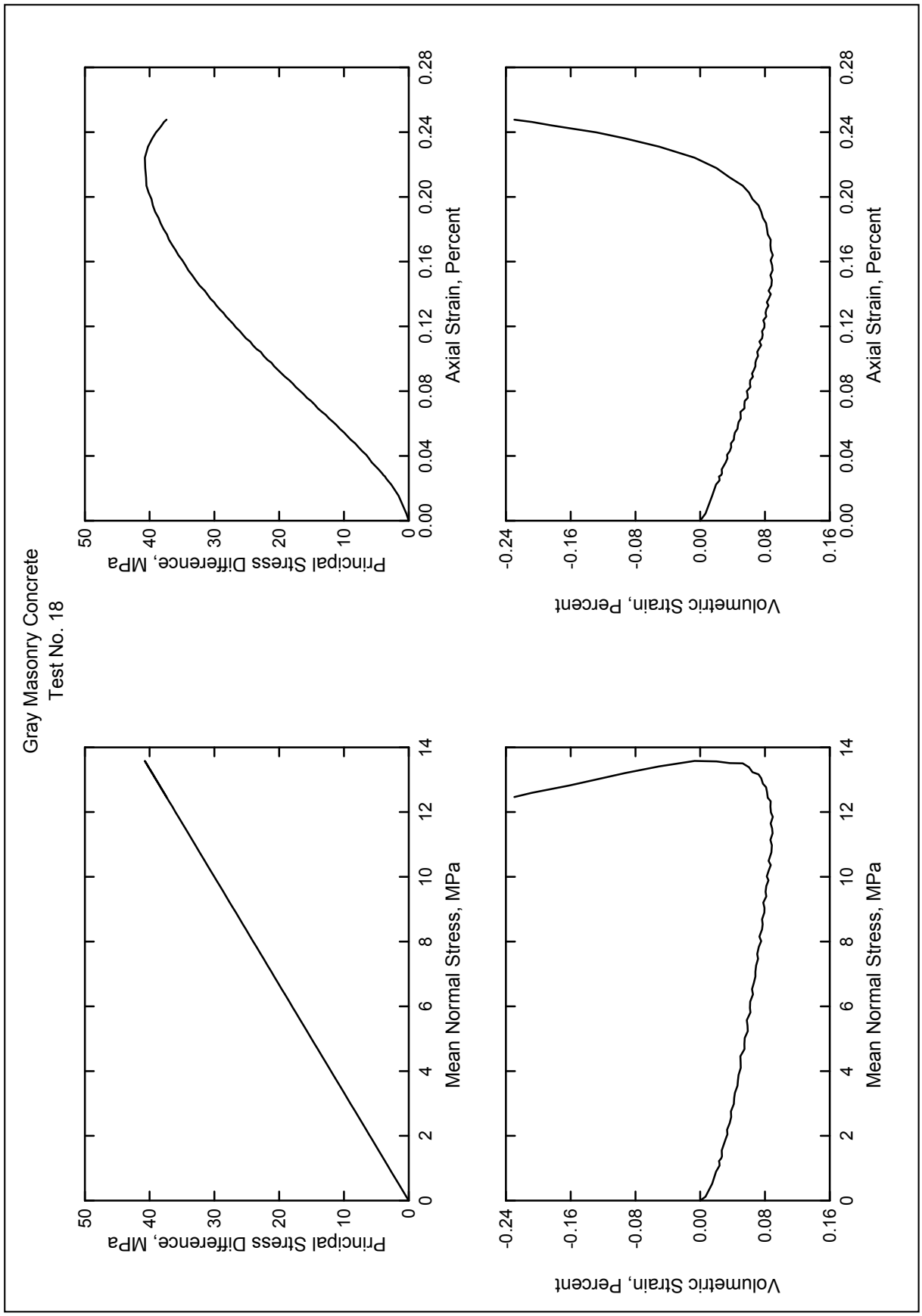
Gray Masonry Concrete
Test No. 18
Principal Stress Difference, MPa
Axial Strain, Percent
Volumetric Strain, Percent
Axial Strain, Percent
Principal Stress Difference, MPa
Mean Normal Stress, MPa
Volumetric Strain, Percent
Mean Normal Stress, MPa

Plate 5

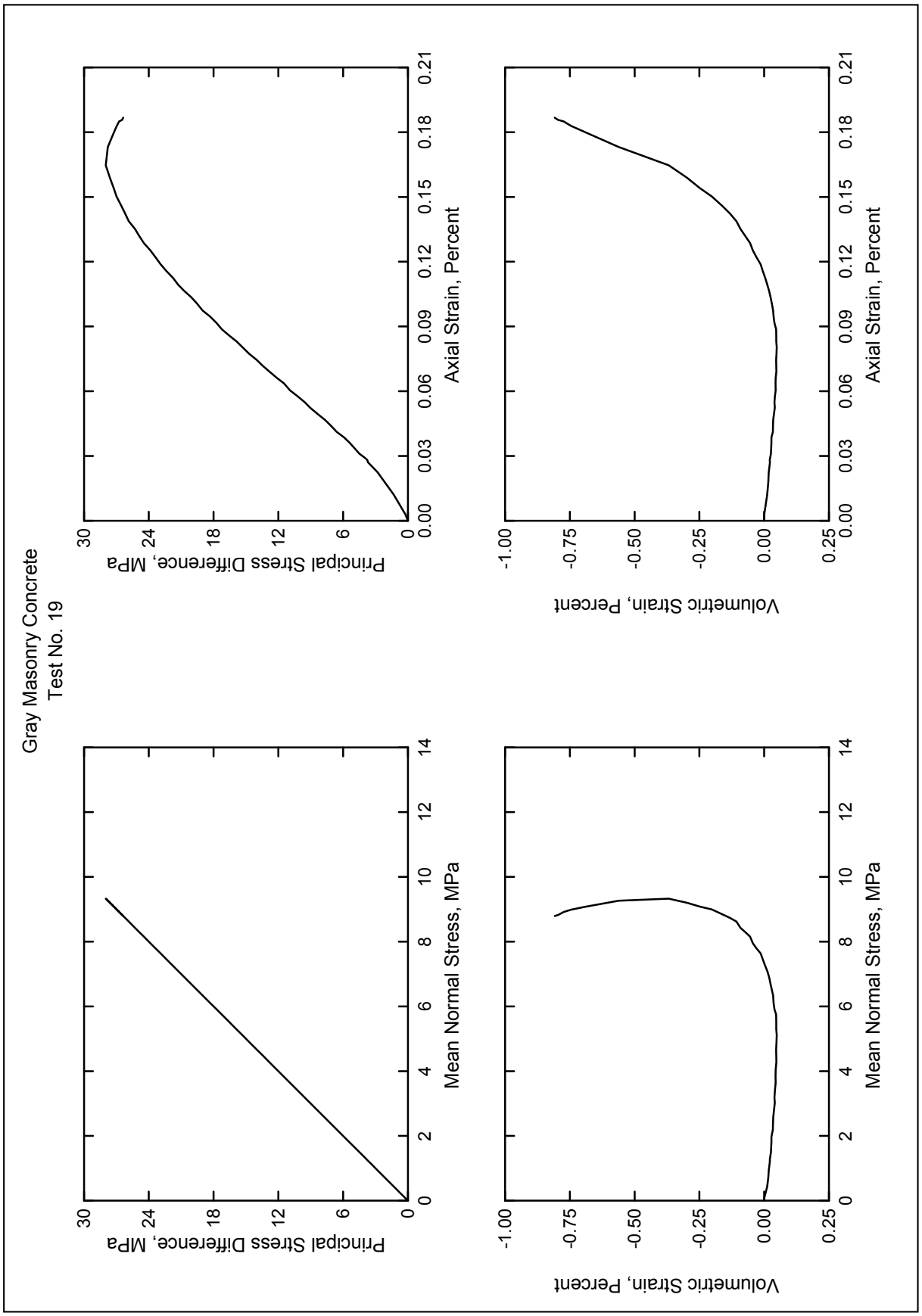
Gray Masonry Concrete
Test No. 19
Principal Stress Difference, MPa
Axial Strain, Percent
Volumetric Strain, Percent
Axial Strain, Percent
Principal Stress Difference, MPa
Mean Normal Stress, MPa
Volumetric Strain, Percent
Mean Normal Stress, MPa

Plate 6

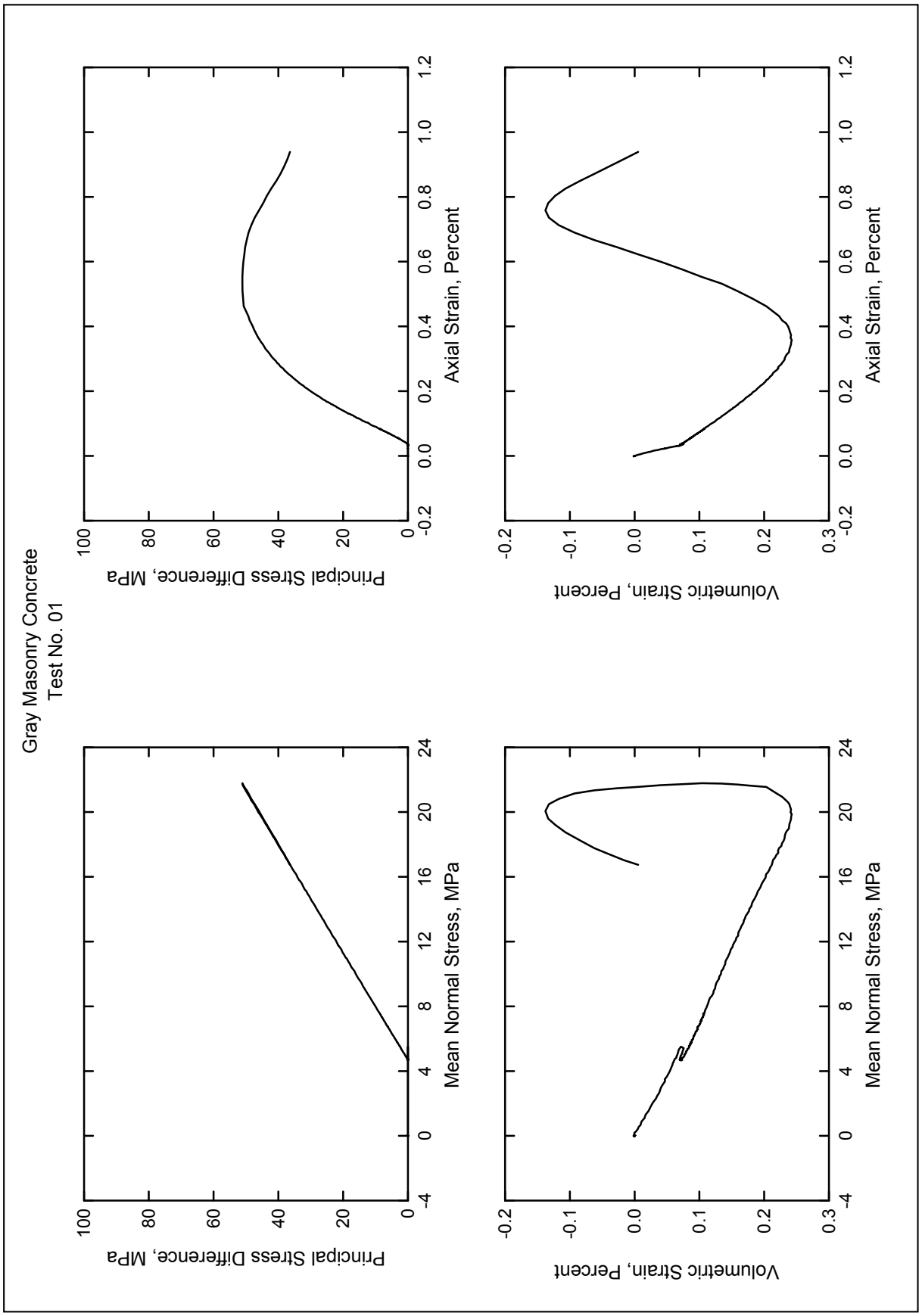
Gray Masonry Concrete
Test No. 01
Principal Stress Difference, MPa
Axial Strain, Percent
Volumetric Strain, Percent
Axial Strain, Percent
Principal Stress Difference, MPa
Mean Normal Stress, MPa
Volumetric Strain, Percent
Mean Normal Stress, MPa

Plate 7

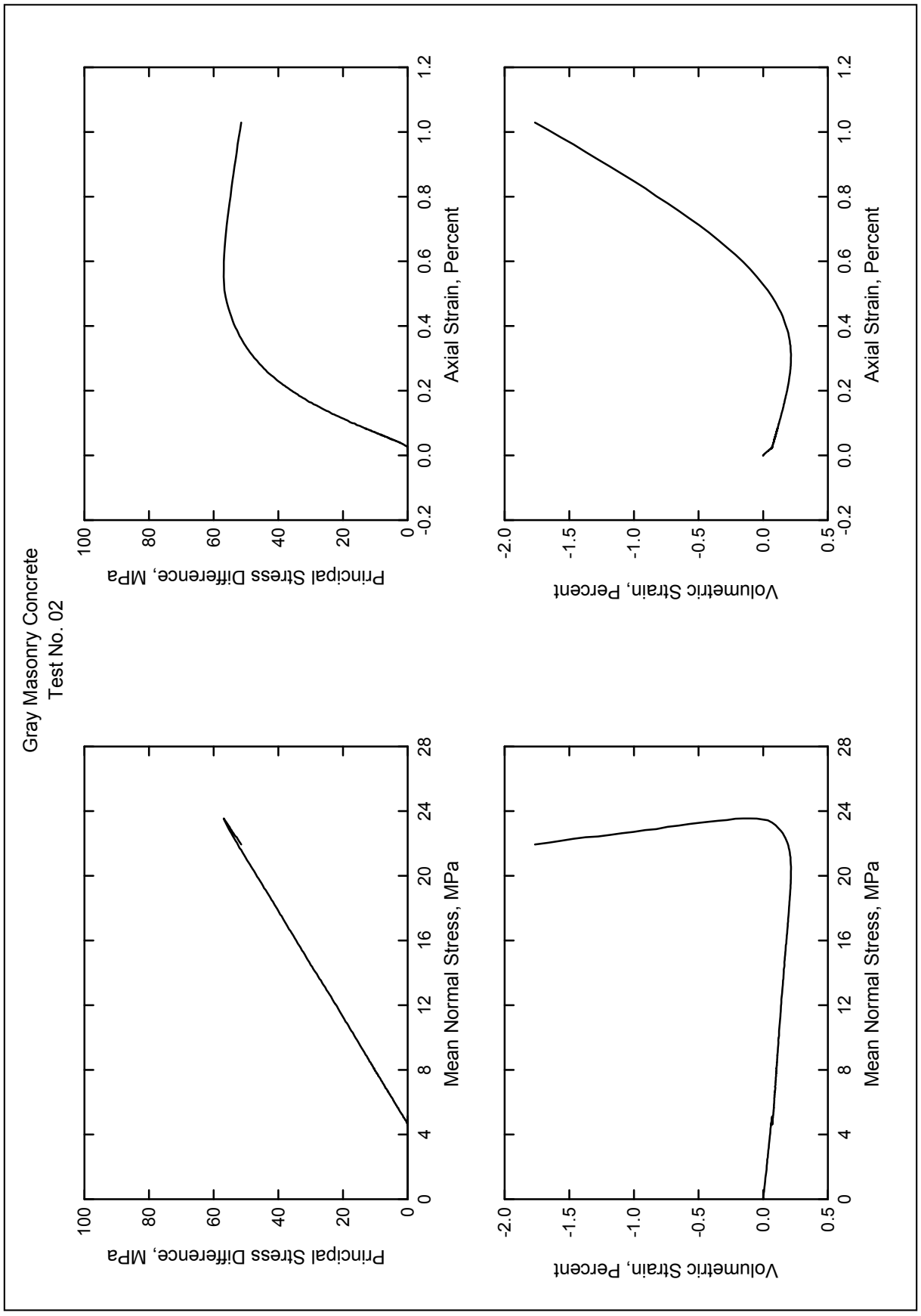
Gray Masonry Concrete
Test No. 02
Principal Stress Difference, MPa
Axial Strain, Percent
Volumetric Strain, Percent
Axial Strain, Percent
Principal Stress Difference, MPa
Mean Normal Stress, MPa
Volumetric Strain, Percent
Mean Normal Stress, MPa

Plate 8

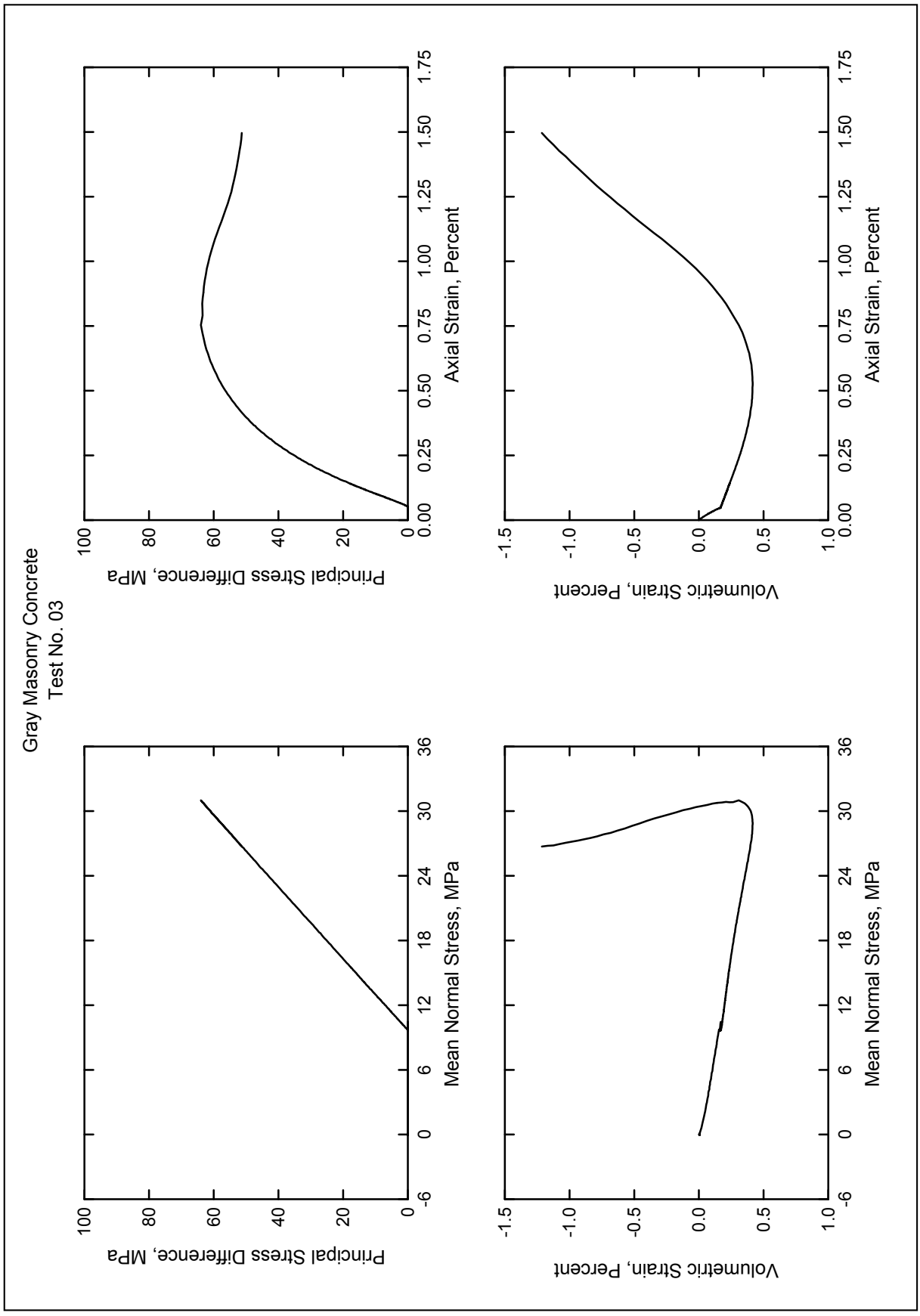
Gray Masonry Concrete
Test No. 03
Principal Stress Difference, MPa
Axial Strain, Percent
Volumetric Strain, Percent
Axial Strain, Percent
Principal Stress Difference, MPa
Mean Normal Stress, MPa
Volumetric Strain, Percent
Mean Normal Stress, MPa

Plate 9

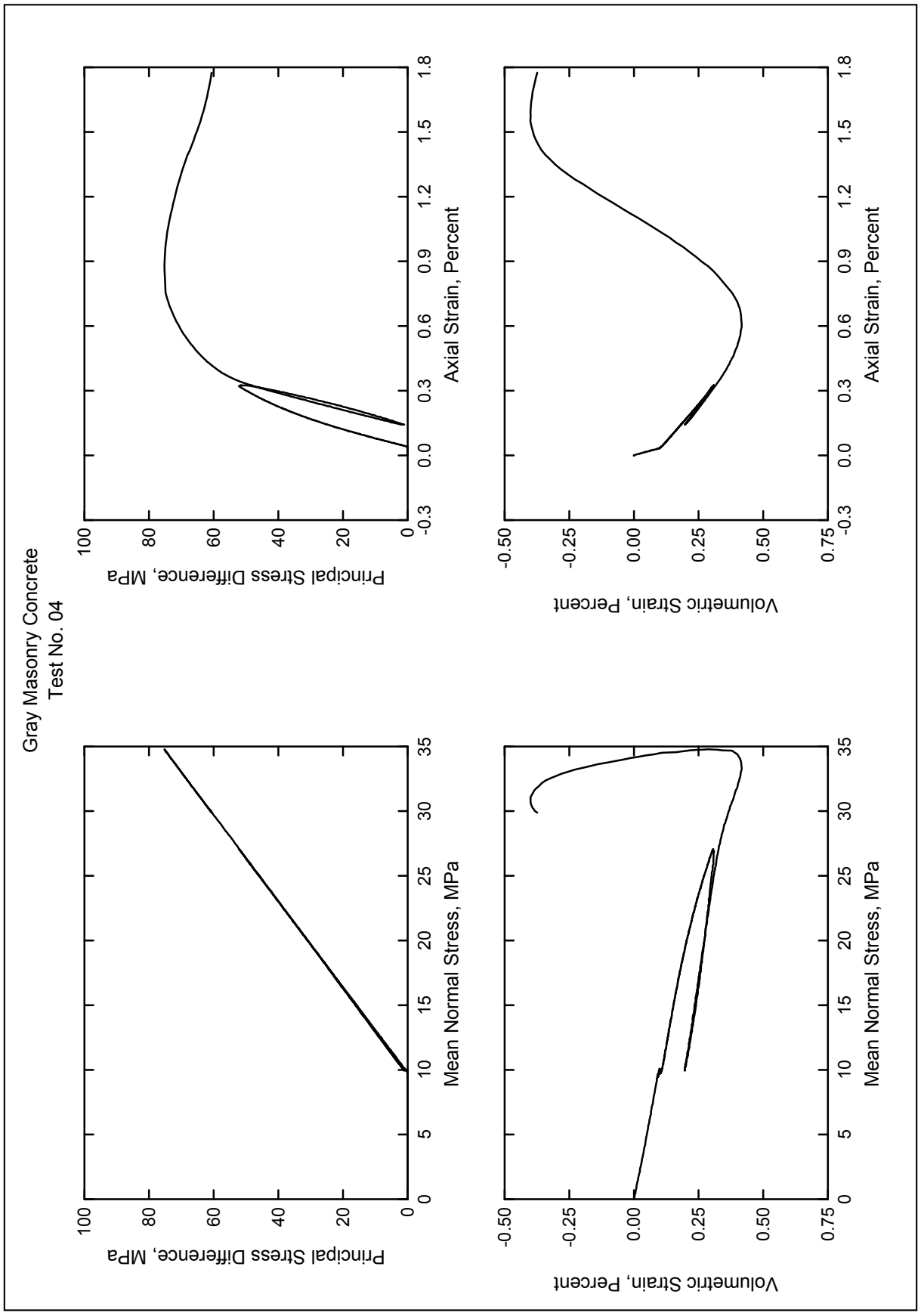
Gray Masonry Concrete
Test No. 04
Principal Stress Difference, MPa
Axial Strain, Percent
Volumetric Strain, Percent
Axial Strain, Percent
Principal Stress Difference, MPa
Mean Normal Stress, MPa
Volumetric Strain, Percent
Mean Normal Stress, MPa

Plate 10

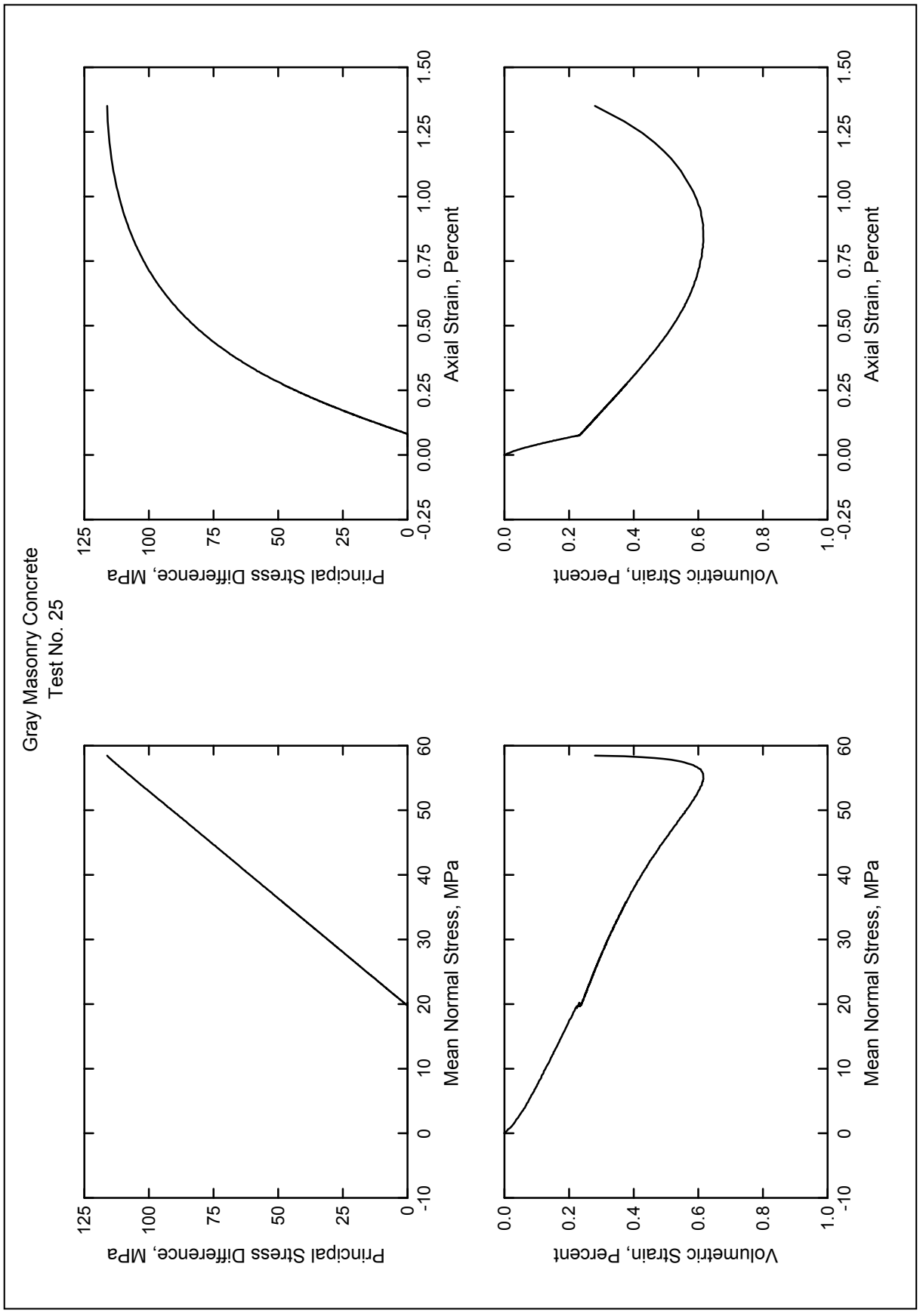
Gray Masonry Concrete
Test No. 25
Principal Stress Difference, MPa
Axial Strain, Percent
Volumetric Strain, Percent
Axial Strain, Percent
Principal Stress Difference, MPa
Mean Normal Stress, MPa
Volumetric Strain, Percent
Mean Normal Stress, MPa

Plate 11

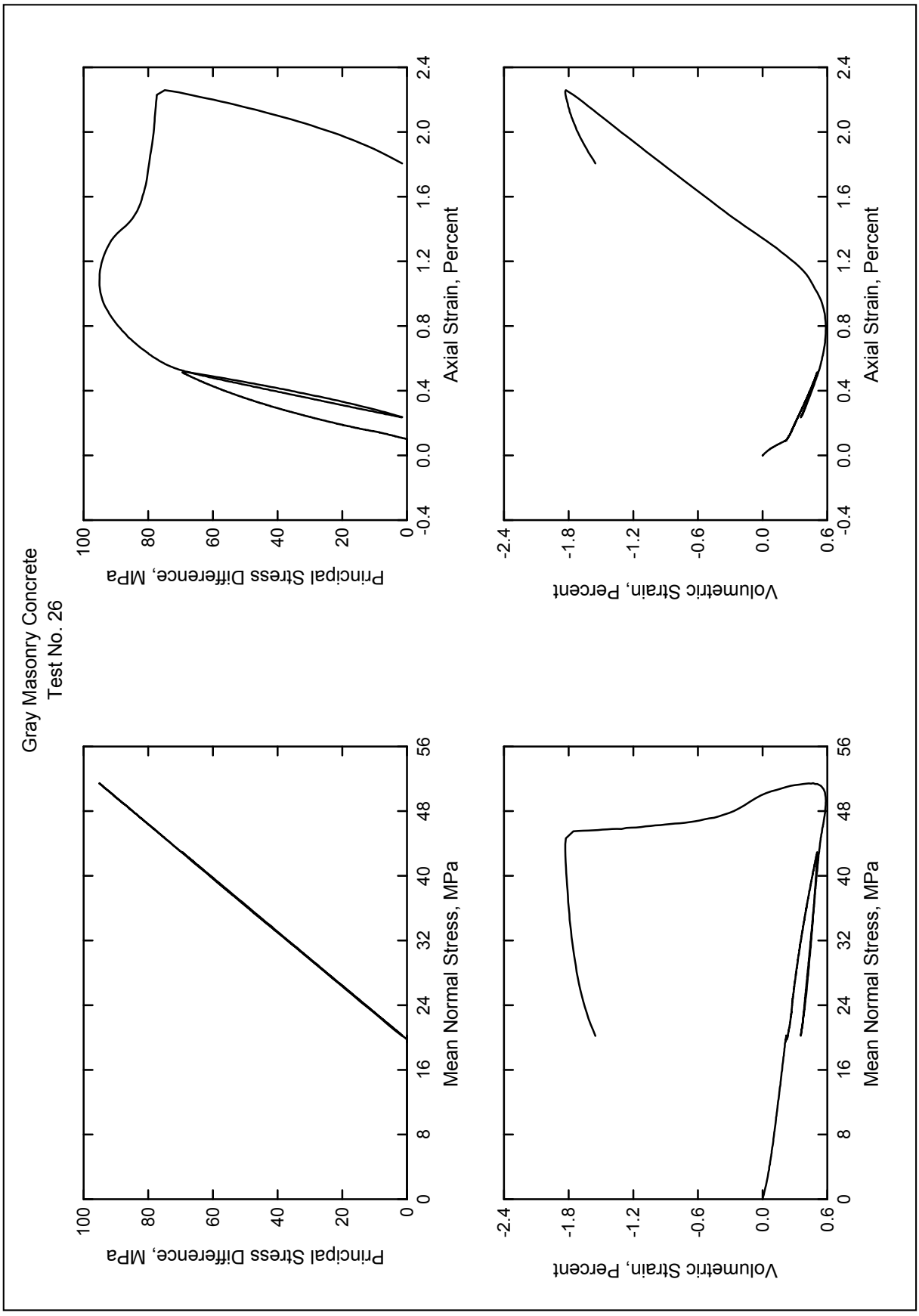
Gray Masonry Concrete
Test No. 26
Principal Stress Difference, MPa
Axial Strain, Percent
Volumetric Strain, Percent
Axial Strain, Percent
Principal Stress Difference, MPa
Mean Normal Stress, MPa
Volumetric Strain, Percent
Mean Normal Stress, MPa

Plate 12

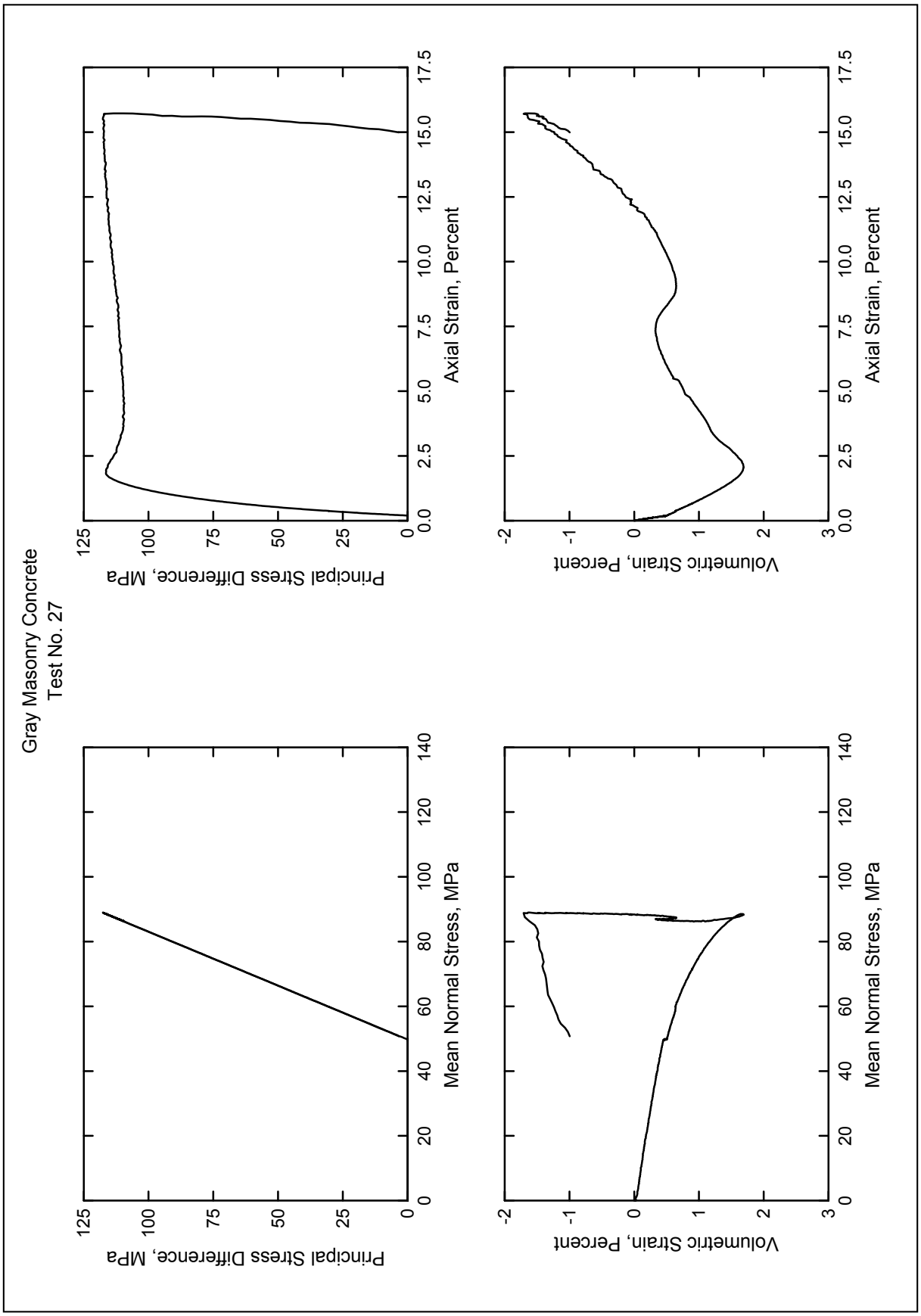
Gray Masonry Concrete
Test No. 27
Principal Stress Difference, MPa
Axial Strain, Percent
Volumetric Strain, Percent
Axial Strain, Percent
Principal Stress Difference, MPa
Mean Normal Stress, MPa
Volumetric Strain, Percent
Mean Normal Stress, MPa

Plate 13

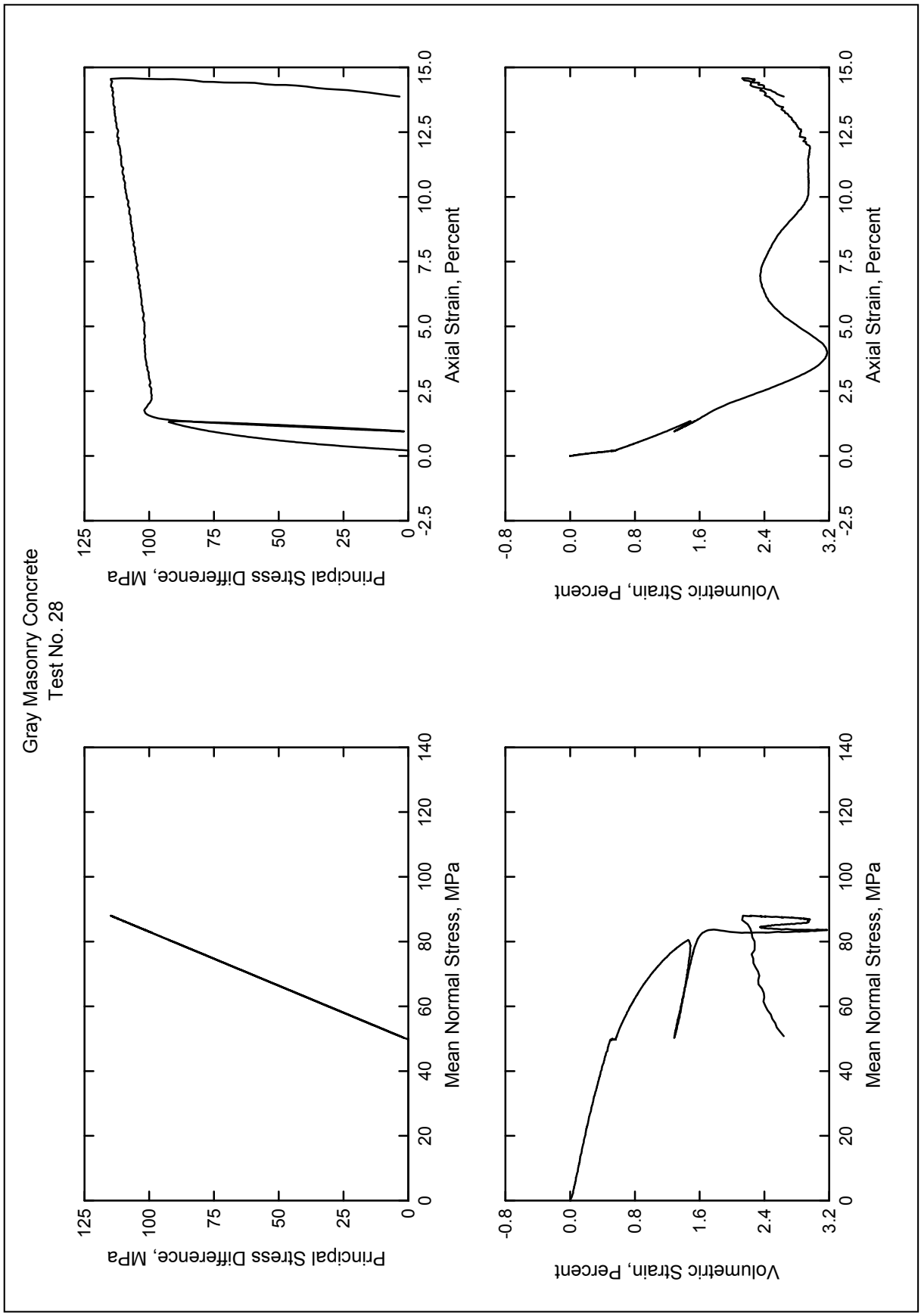
Gray Masonry Concrete
Test No. 28
Principal Stress Difference, MPa
Axial Strain, Percent
Volumetric Strain, Percent
Axial Strain, Percent
Principal Stress Difference, MPa
Mean Normal Stress, MPa
Volumetric Strain, Percent
Mean Normal Stress, MPa

Plate 14

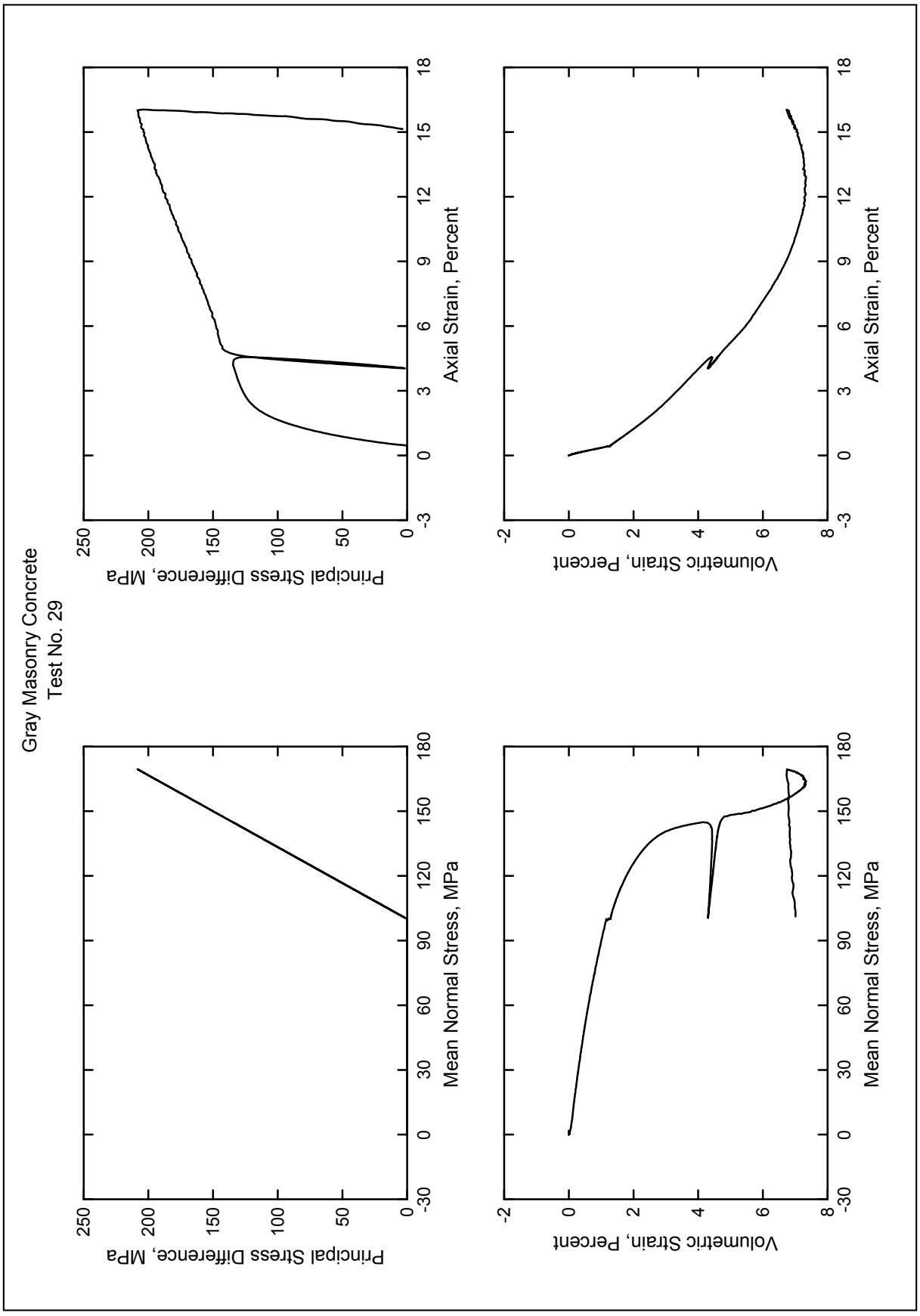
Gray Masonry Concrete
Test No. 29
Principal Stress Difference, MPa
Axial Strain, Percent
Volumetric Strain, Percent
Axial Strain, Percent
Principal Stress Difference, MPa
Mean Normal Stress, MPa
Volumetric Strain, Percent
Mean Normal Stress, MPa

Plate 15

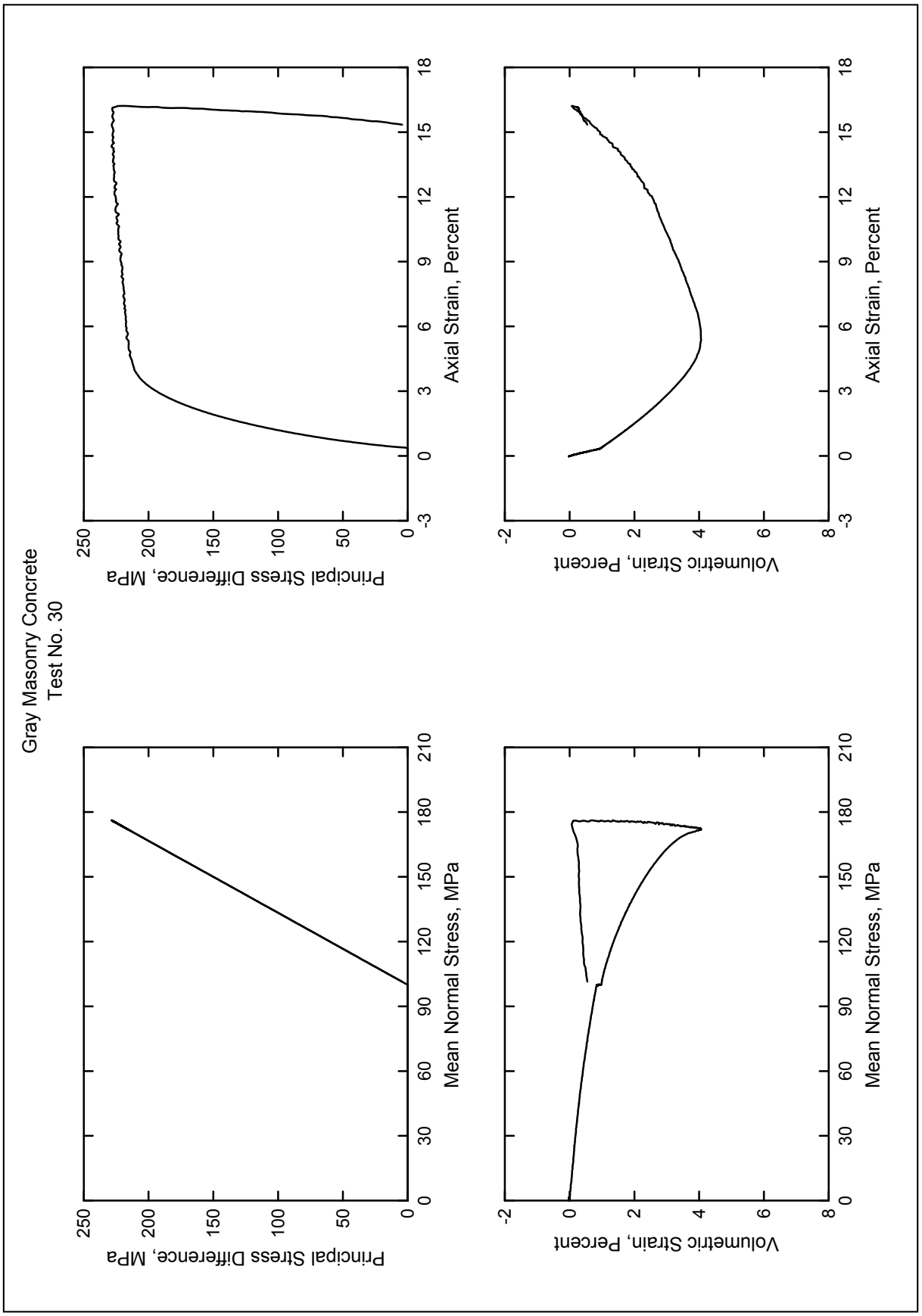
Gray Masonry Concrete
Test No. 30
Principal Stress Difference, MPa
Axial Strain, Percent
Volumetric Strain, Percent
Axial Strain, Percent
Principal Stress Difference, MPa
Mean Normal Stress, MPa
Volumetric Strain, Percent
Mean Normal Stress, MPa

Plate 16

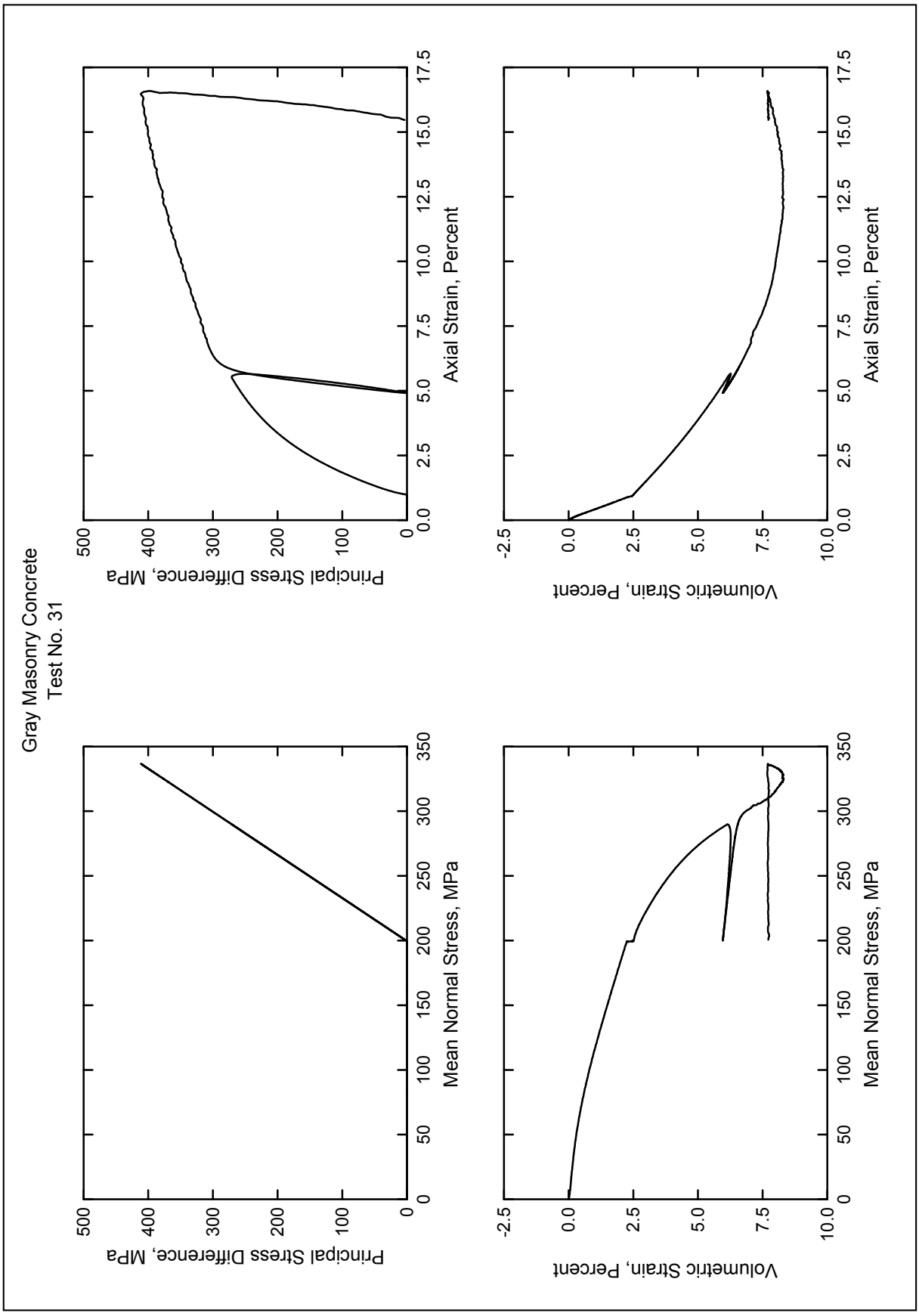
Gray Masonry Concrete
Test No. 31
Principal Stress Difference, MPa
Axial Strain, Percent
Volumetric Strain, Percent
Axial Strain, Percent
Principal Stress Difference, MPa
Mean Normal Stress, MPa
Volumetric Strain, Percent
Mean Normal Stress, MPa

Plate 17

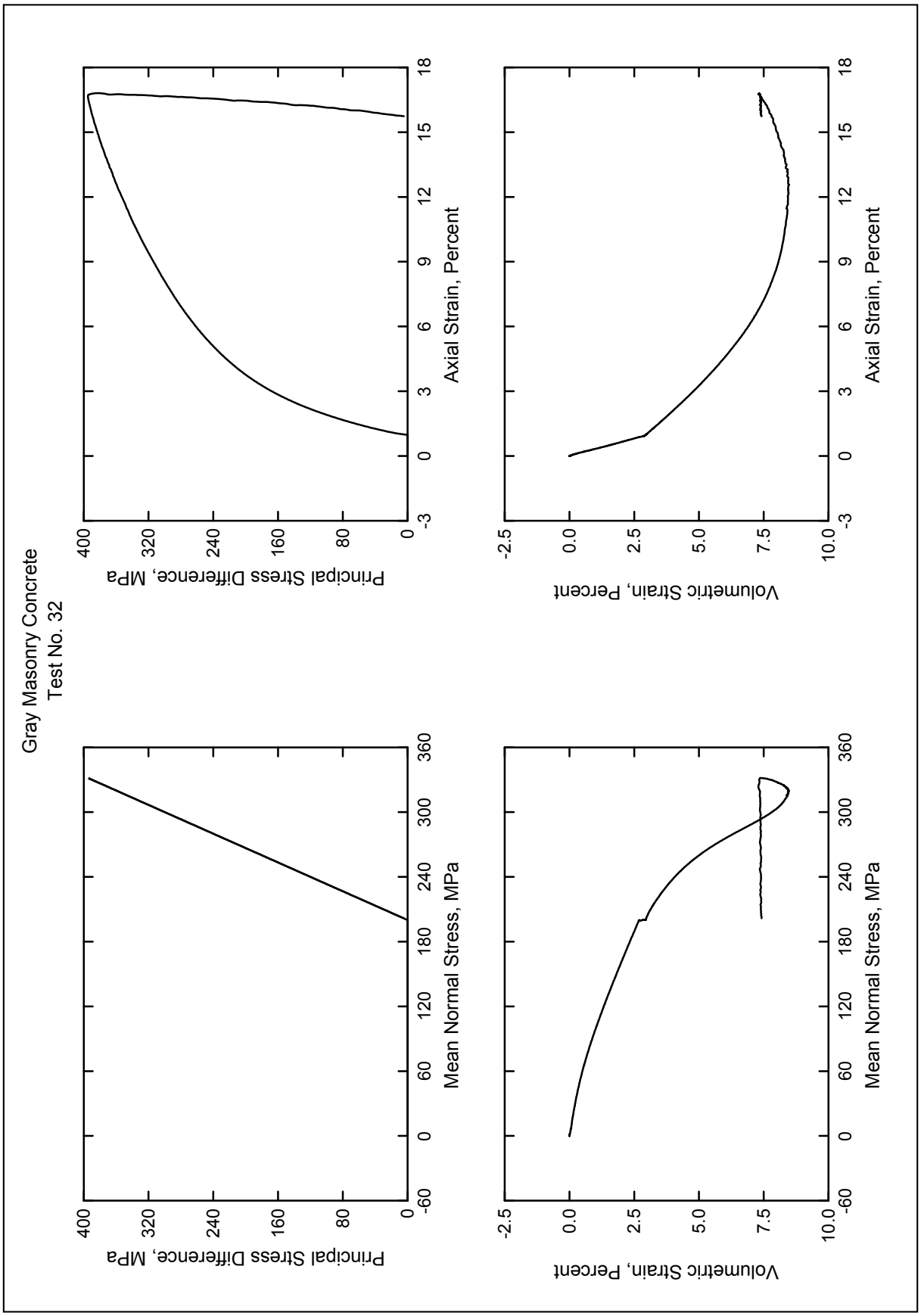
Gray Masonry Concrete
Test No. 32
Principal Stress Difference, MPa
Axial Strain, Percent
Volumetric Strain, Percent
Axial Strain, Percent
Principal Stress Difference, MPa
Mean Normal Stress, MPa
Volumetric Strain, Percent
Mean Normal Stress, MPa

Plate 18

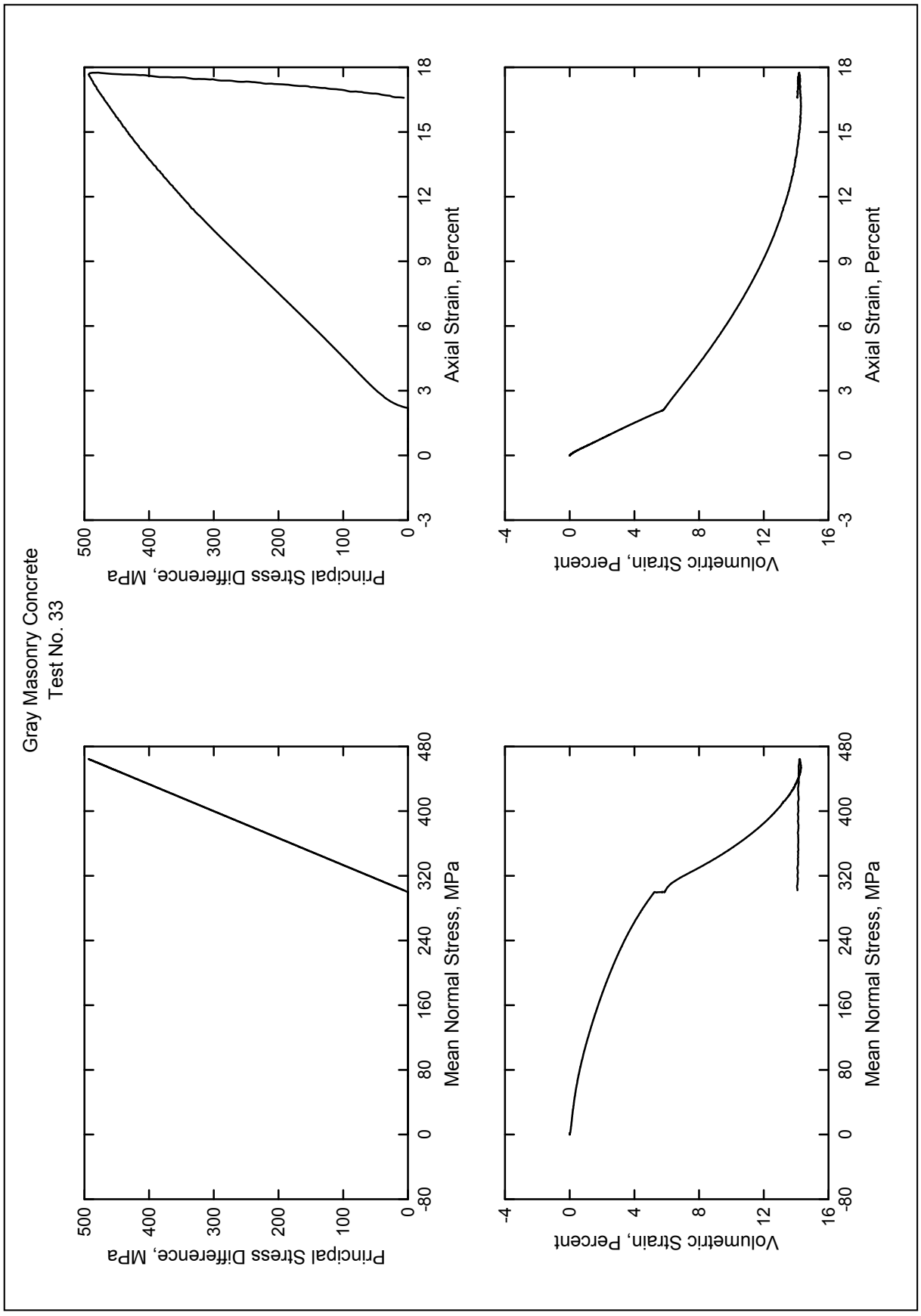
Gray Masonry Concrete
Test No. 33
Principal Stress Difference, MPa
Axial Strain, Percent
Volumetric Strain, Percent
Axial Strain, Percent
Principal Stress Difference, MPa
Mean Normal Stress, MPa
Volumetric Strain, Percent
Mean Normal Stress, MPa

Plate 19

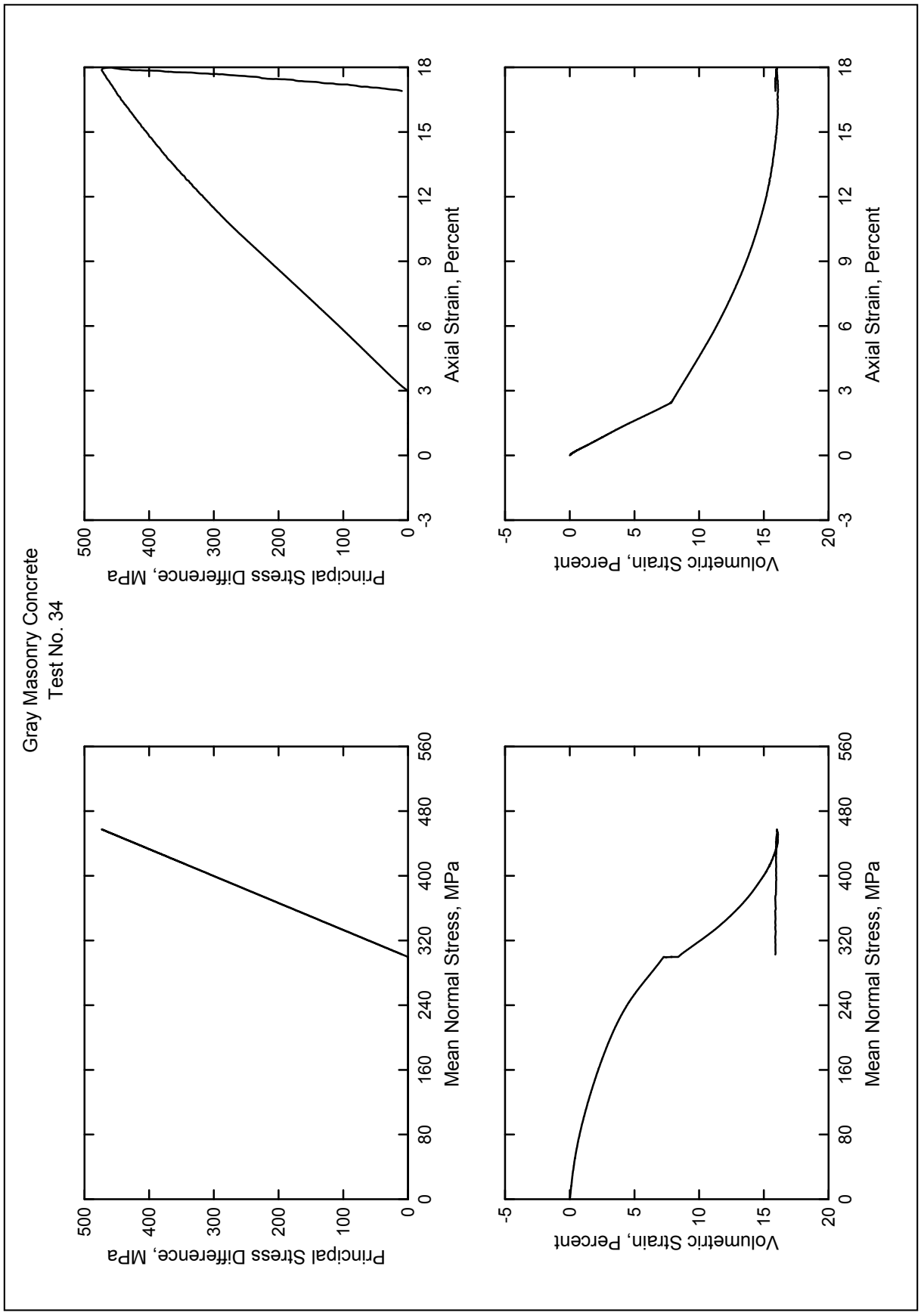
Gray Masonry Concrete
Test No. 34
Principal Stress Difference, MPa
Axial Strain, Percent
Volumetric Strain, Percent
Axial Strain, Percent
Principal Stress Difference, MPa
Mean Normal Stress, MPa
Volumetric Strain, Percent
Mean Normal Stress, MPa

Plate 20

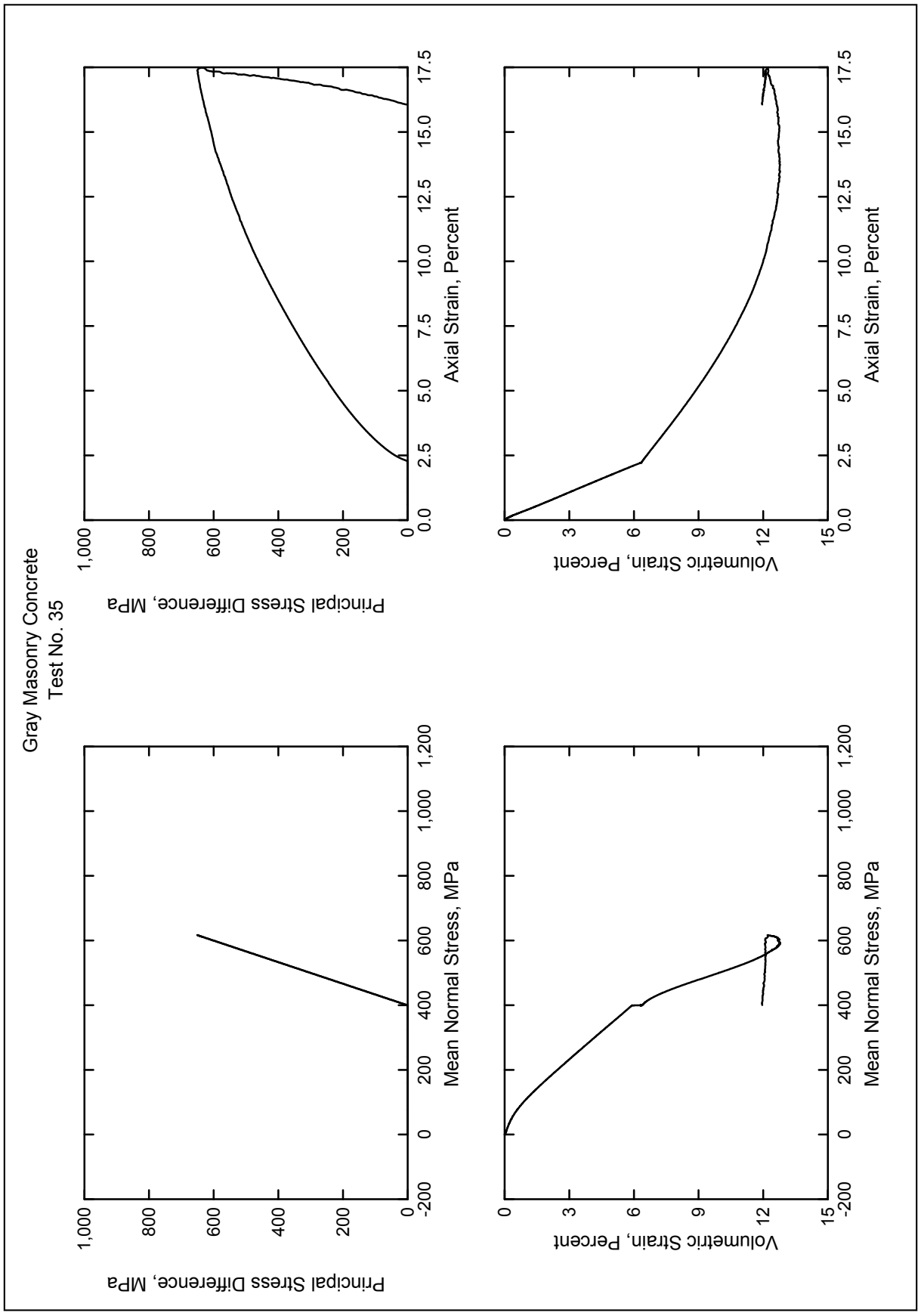
Gray Masonry Concrete
Test No. 35
Principal Stress Difference, MPa
Axial Strain, Percent
Volumetric Strain, Percent
Axial Strain, Percent
Principal Stress Difference, MPa
Mean Normal Stress, MPa
Volumetric Strain, Percent
Mean Normal Stress, MPa

Plate 21

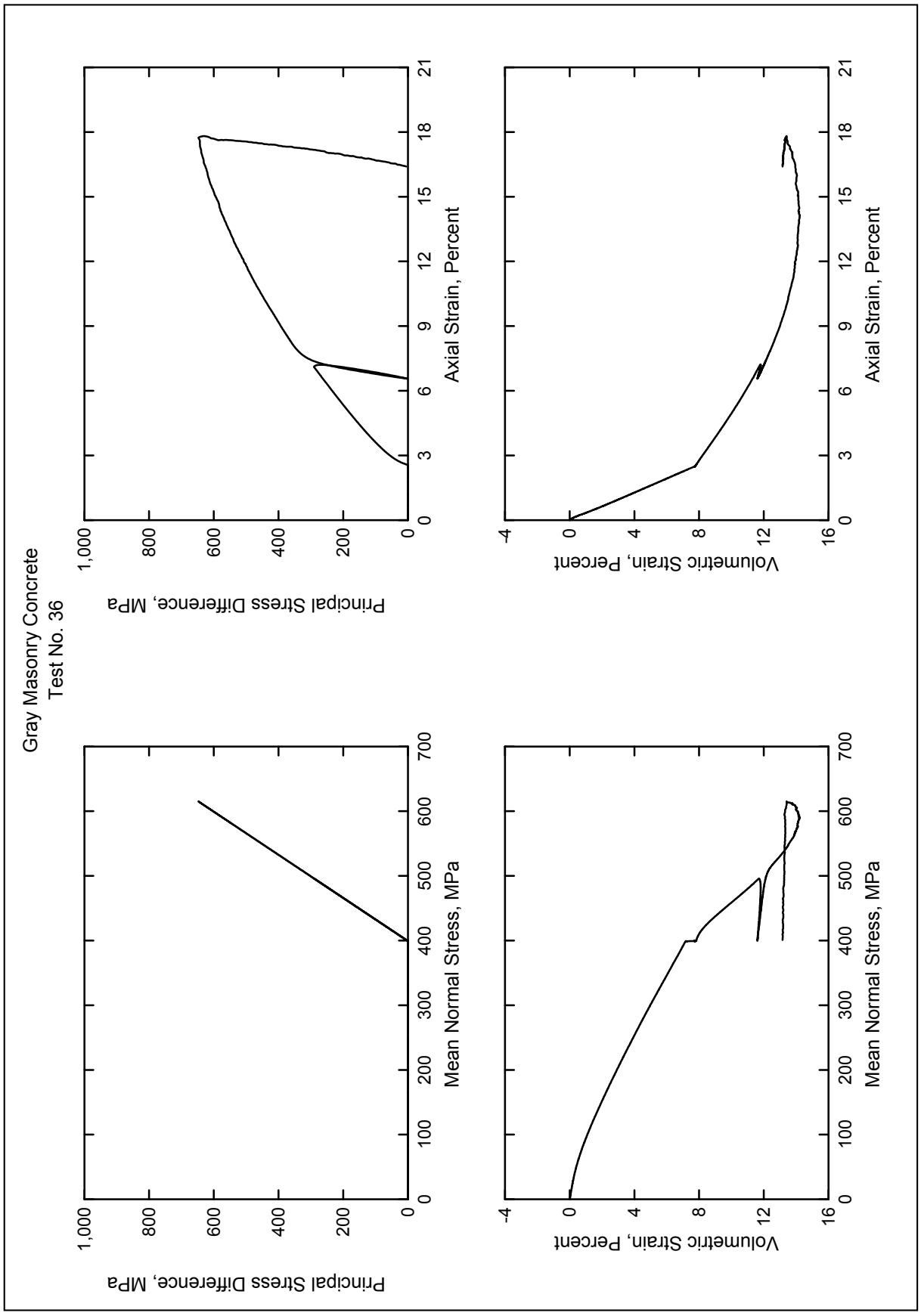
Gray Masonry Concrete
Test No. 36
Principal Stress Difference, MPa
Axial Strain, Percent
Volumetric Strain, Percent
Axial Strain, Percent
Principal Stress Difference, MPa
Mean Normal Stress, MPa
Volumetric Strain, Percent
Mean Normal Stress, MPa

Plate 22

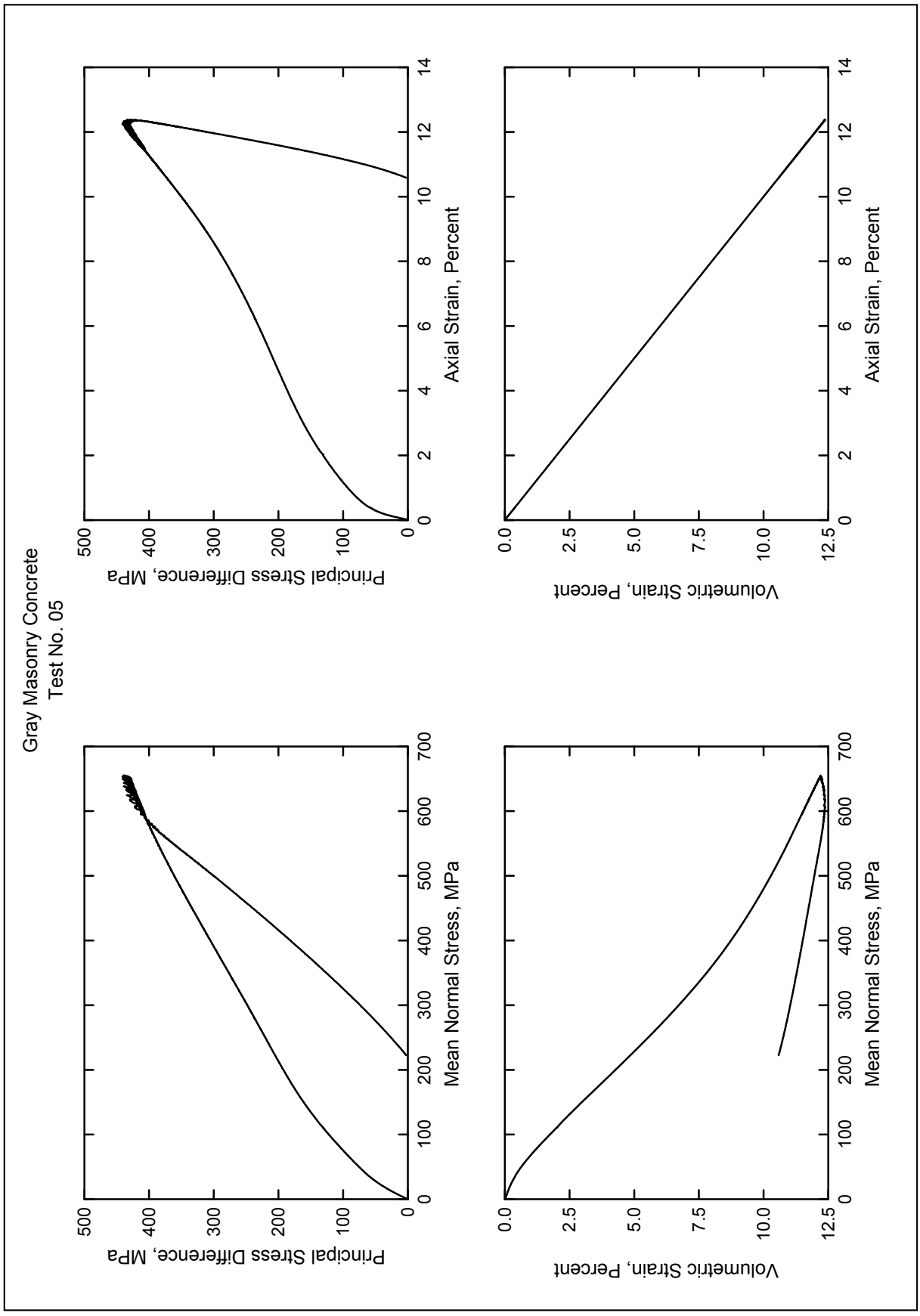
Gray Masonry Concrete
Test No. 05
Principal Stress Difference, MPa
Axial Strain, Percent
Volumetric Strain, Percent
Axial Strain, Percent
Principal Stress Difference, MPa
Mean Normal Stress, MPa
Volumetric Strain, Percent
Mean Normal Stress, MPa

Plate 23

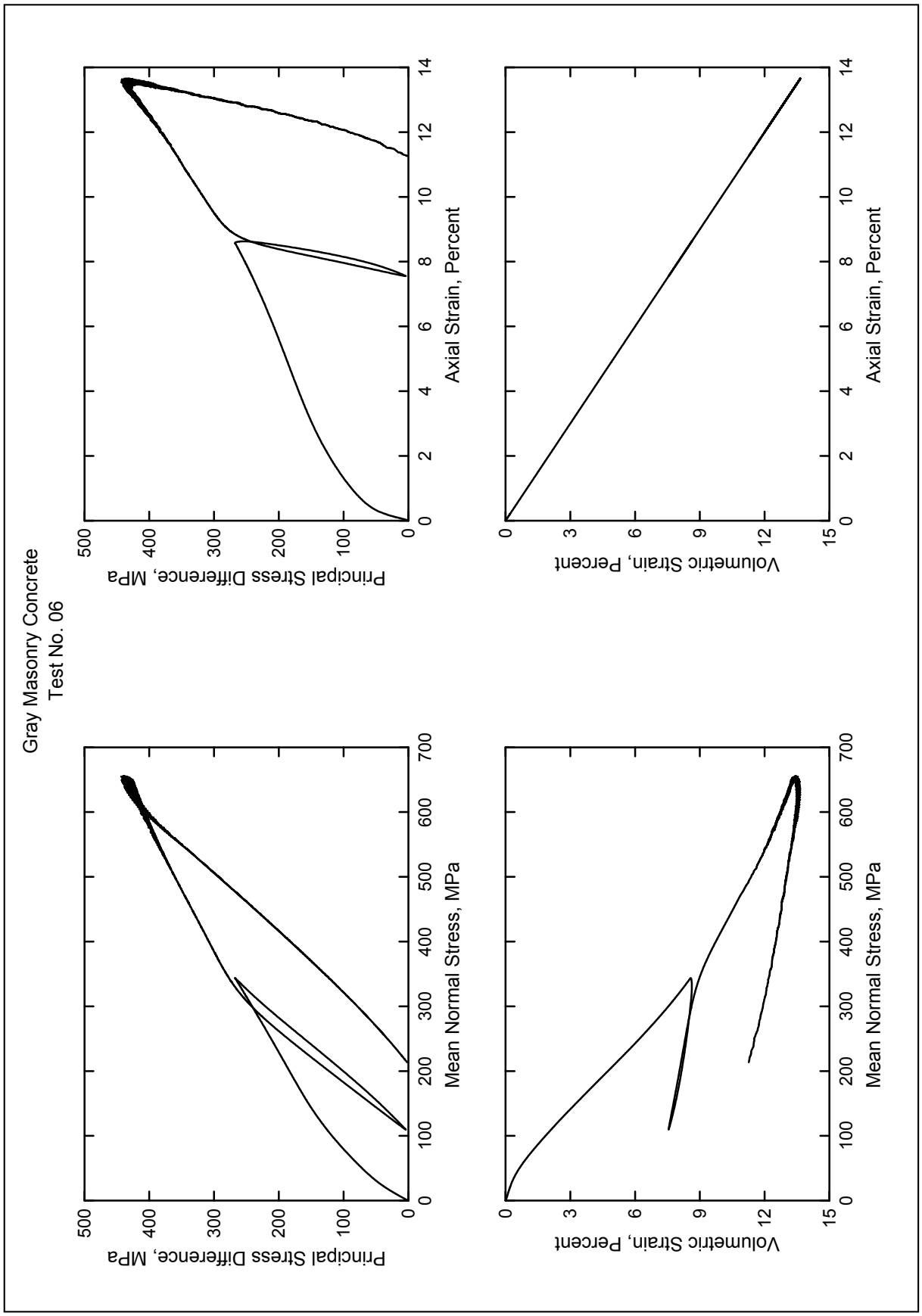
Gray Masonry Concrete
Test No. 06
Principal Stress Difference, MPa
Axial Strain, Percent
Volumetric Strain, Percent
Axial Strain, Percent
Principal Stress Difference, MPa
Mean Normal Stress, MPa
Volumetric Strain, Percent
Mean Normal Stress, MPa

Plate 24

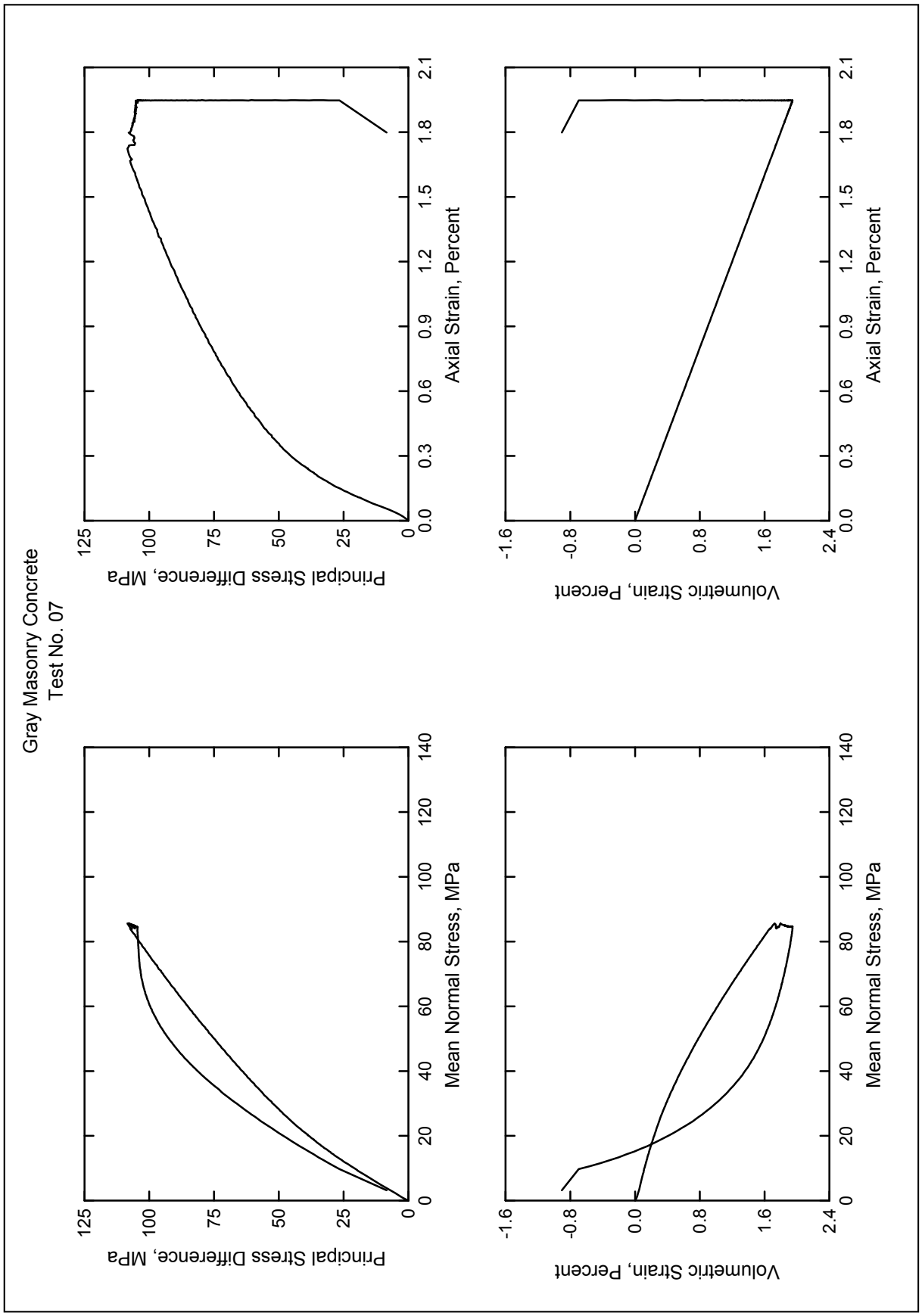
Gray Masonry Concrete
Test No. 07
Principal Stress Difference, MPa
Axial Strain, Percent
Volumetric Strain, Percent
Axial Strain, Percent
Principal Stress Difference, MPa
Mean Normal Stress, MPa
Volumetric Strain, Percent
Mean Normal Stress, MPa

Plate 25

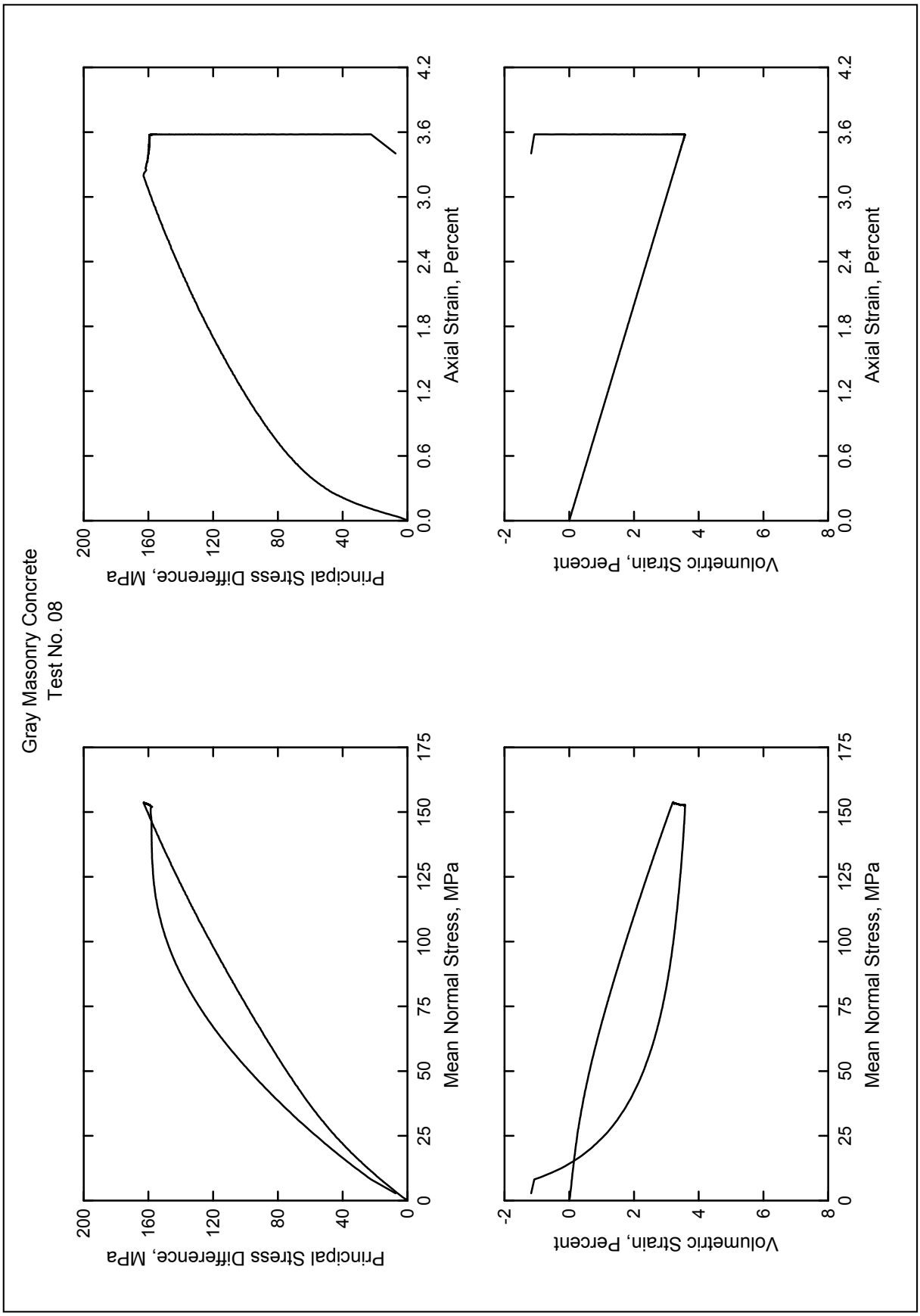
Gray Masonry Concrete
Test No. 08
Principal Stress Difference, MPa
Axial Strain, Percent
Volumetric Strain, Percent
Axial Strain, Percent
Principal Stress Difference, MPa
Mean Normal Stress, MPa
Volumetric Strain, Percent
Mean Normal Stress, MPa

Plate 26

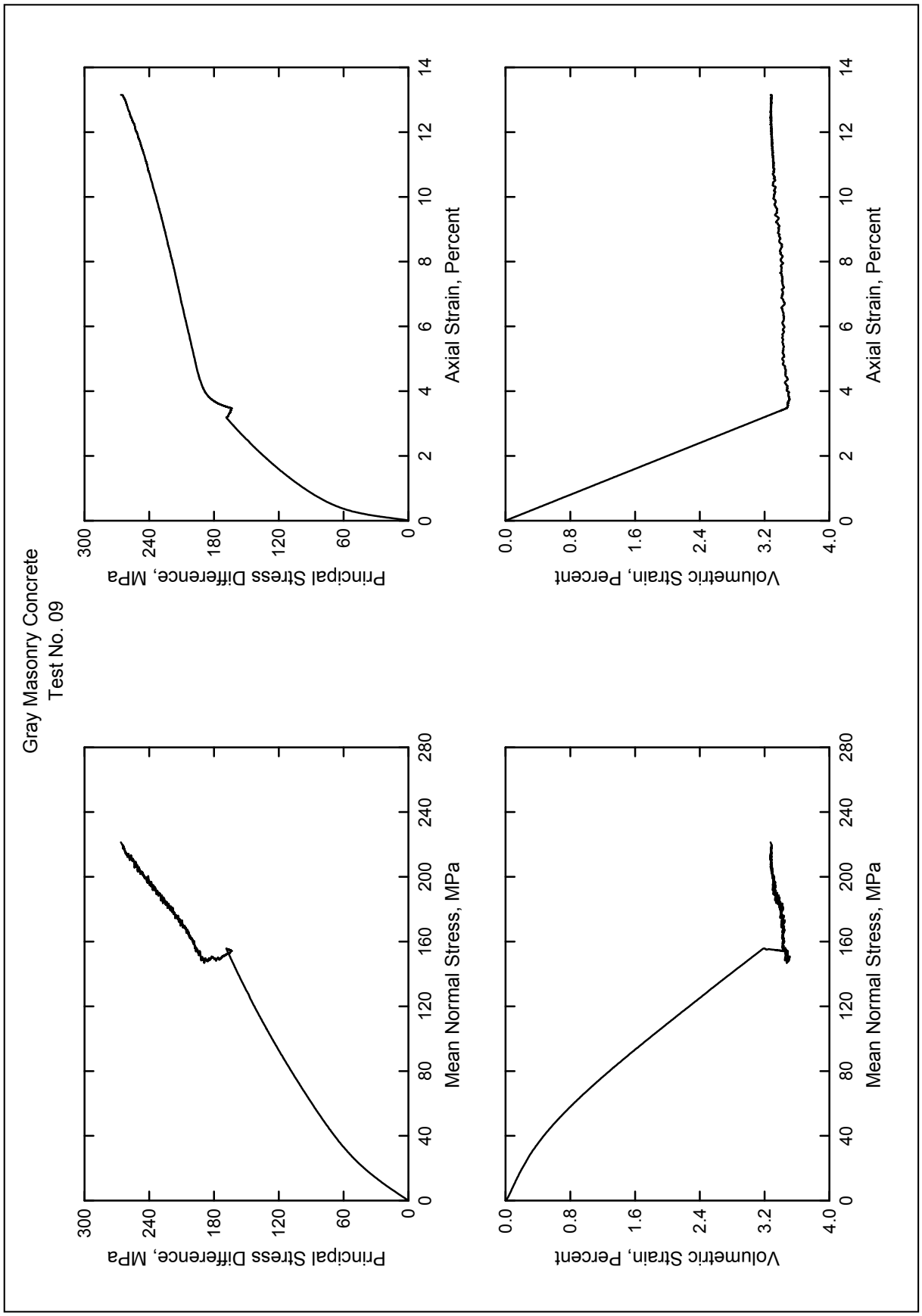
Gray Masonry Concrete
Test No. 09
Principal Stress Difference, MPa
Axial Strain, Percent
Volumetric Strain, Percent
Axial Strain, Percent
Principal Stress Difference, MPa
Mean Normal Stress, MPa
Volumetric Strain, Percent
Mean Normal Stress, MPa

Plate 27

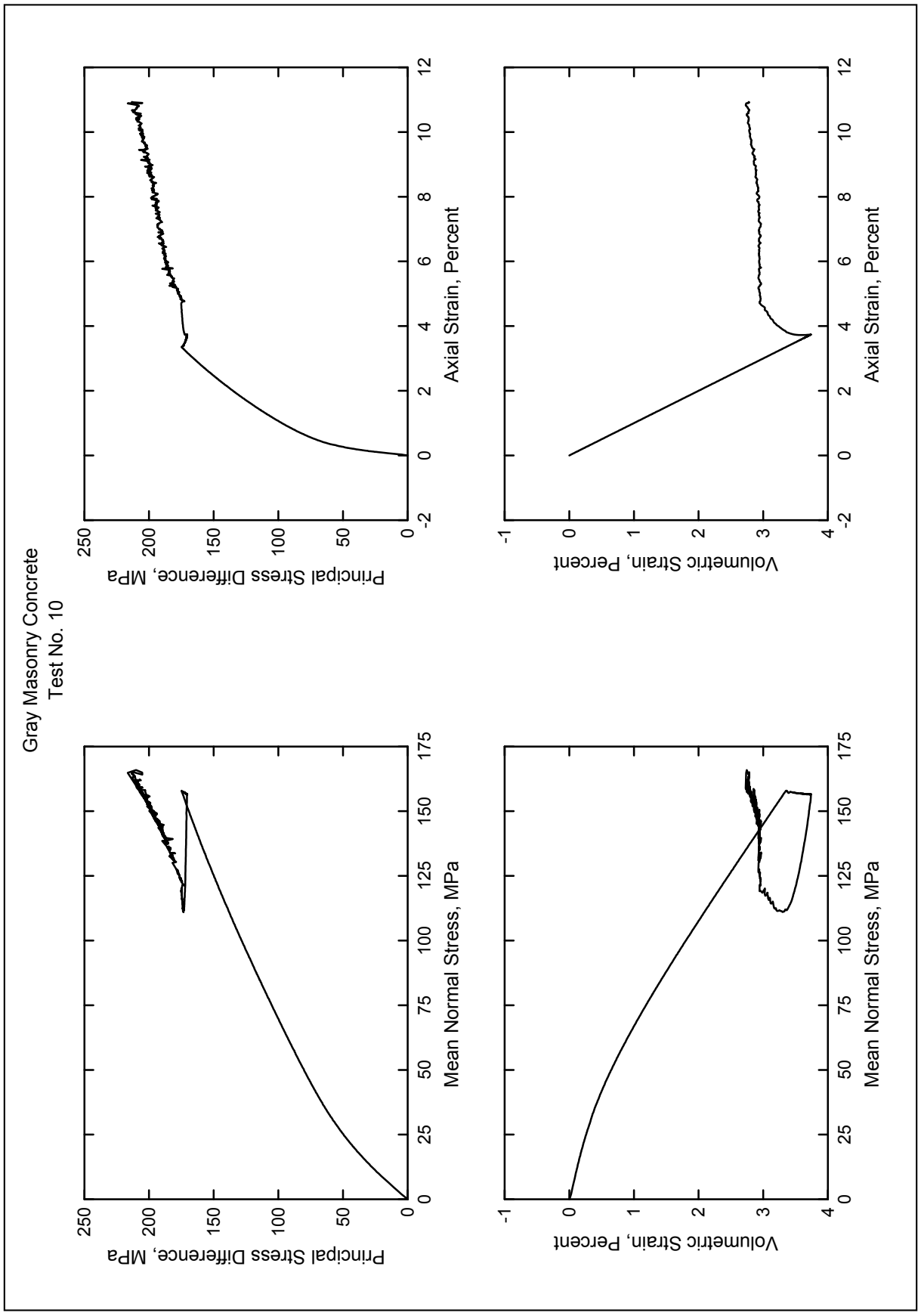
Gray Masonry Concrete
Test No. 10
Principal Stress Difference, MPa
Axial Strain, Percent
Volumetric Strain, Percent
Axial Strain, Percent
Principal Stress Difference, MPa
Mean Normal Stress, MPa
Volumetric Strain, Percent
Mean Normal Stress, MPa

Plate 28

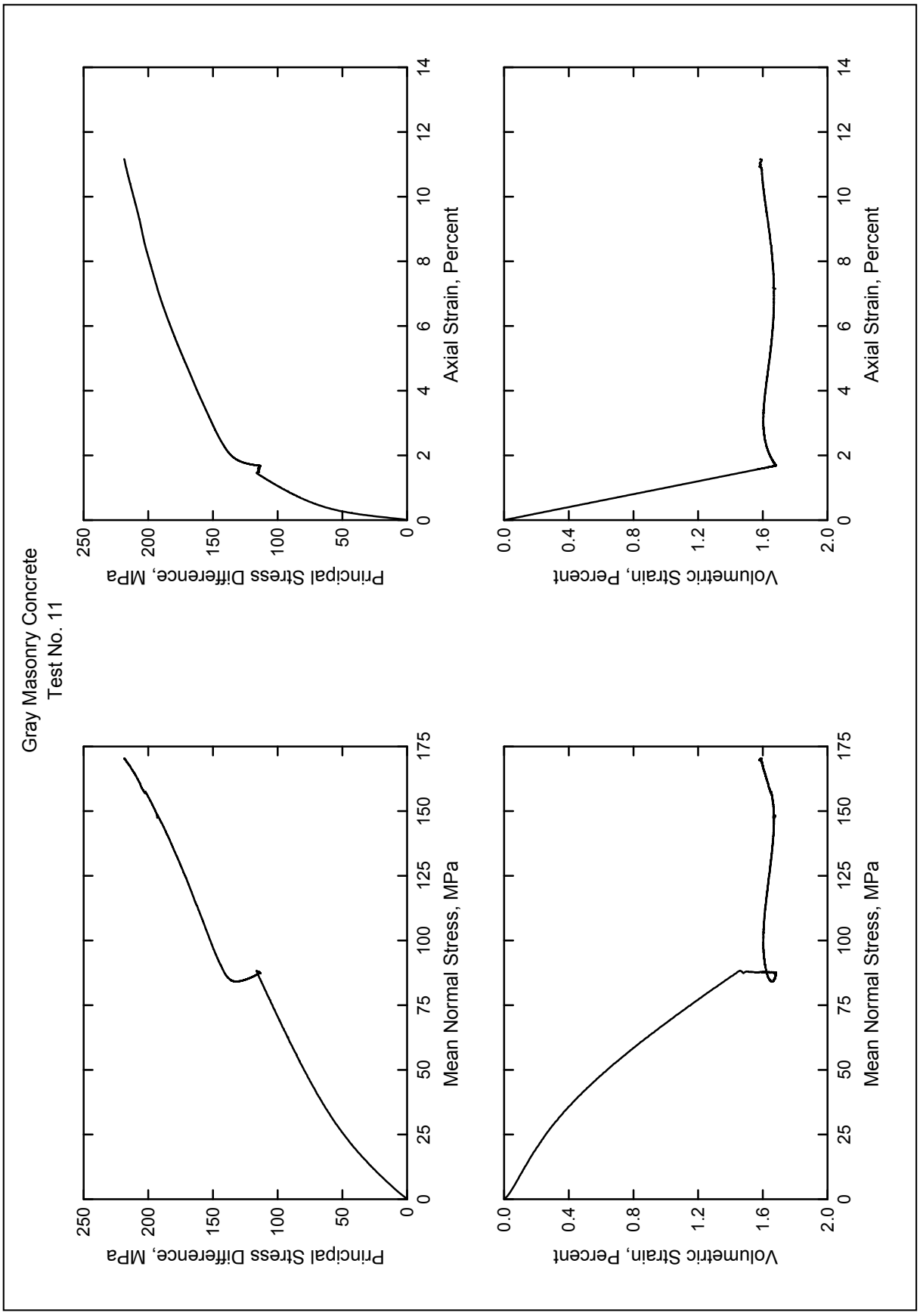
Gray Masonry Concrete
Test No. 11
Principal Stress Difference, MPa
Axial Strain, Percent
Volumetric Strain, Percent
Axial Strain, Percent
Principal Stress Difference, MPa
Mean Normal Stress, MPa
Volumetric Strain, Percent
Mean Normal Stress, MPa

Plate 29

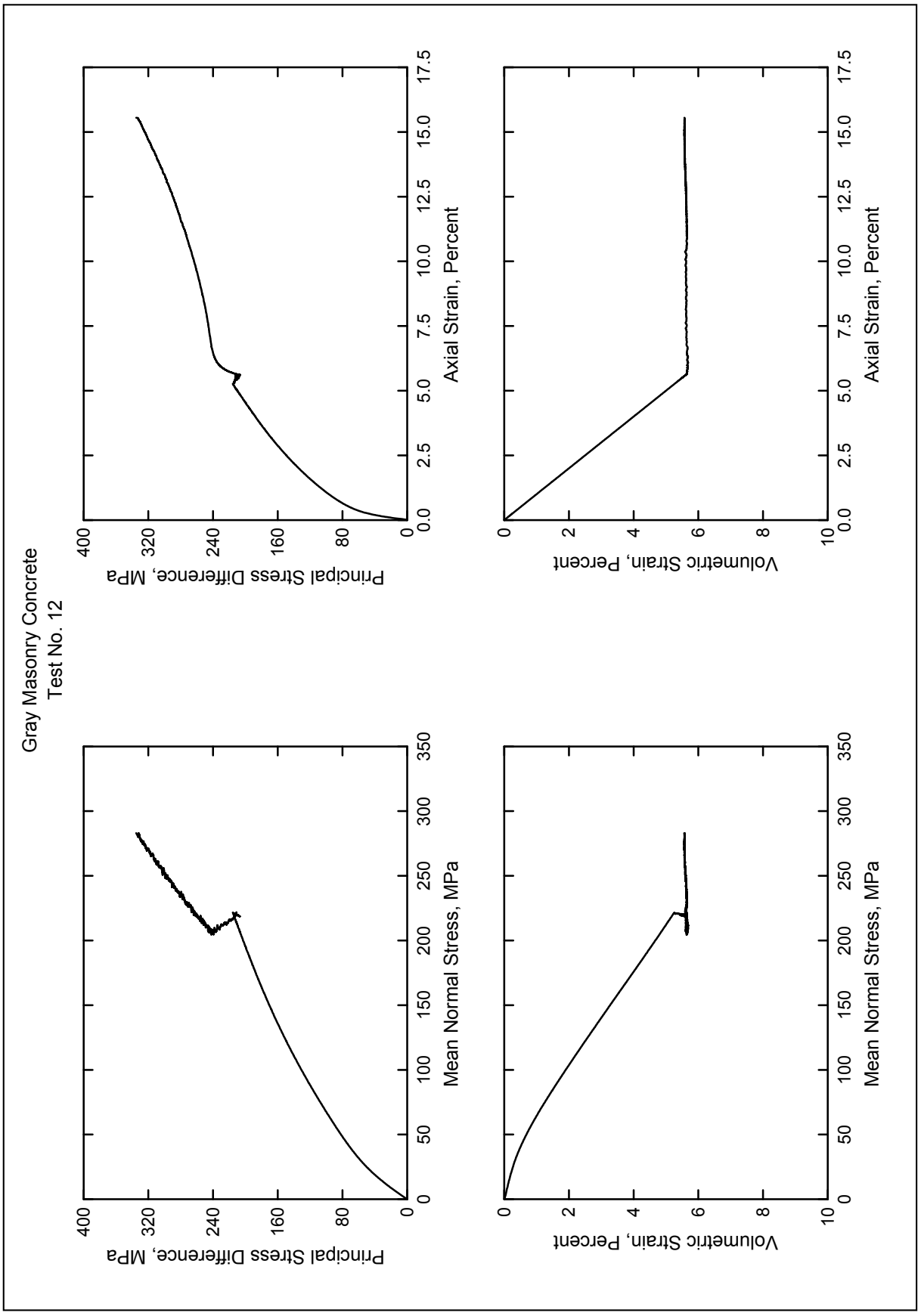
Gray Masonry Concrete
Test No. 12
Principal Stress Difference, MPa
Axial Strain, Percent
Volumetric Strain, Percent
Axial Strain, Percent
Principal Stress Difference, MPa
Mean Normal Stress, MPa
Volumetric Strain, Percent
Mean Normal Stress, MPa

Plate 30

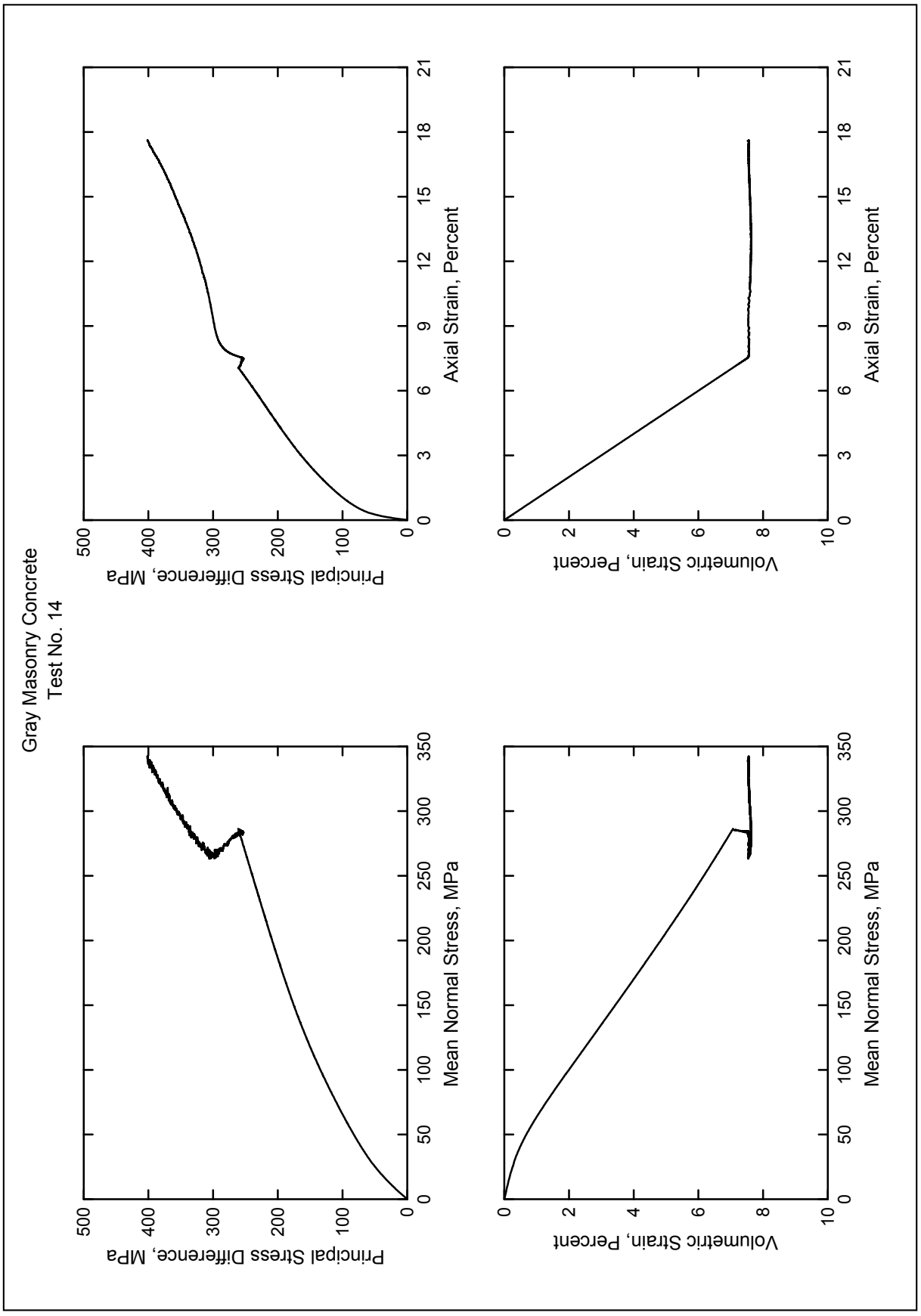
Gray Masonry Concrete
Test No. 14
Principal Stress Difference, MPa
Axial Strain, Percent
Volumetric Strain, Percent
Axial Strain, Percent
Principal Stress Difference, MPa
Mean Normal Stress, MPa
Volumetric Strain, Percent
Mean Normal Stress, MPa

Plate 31

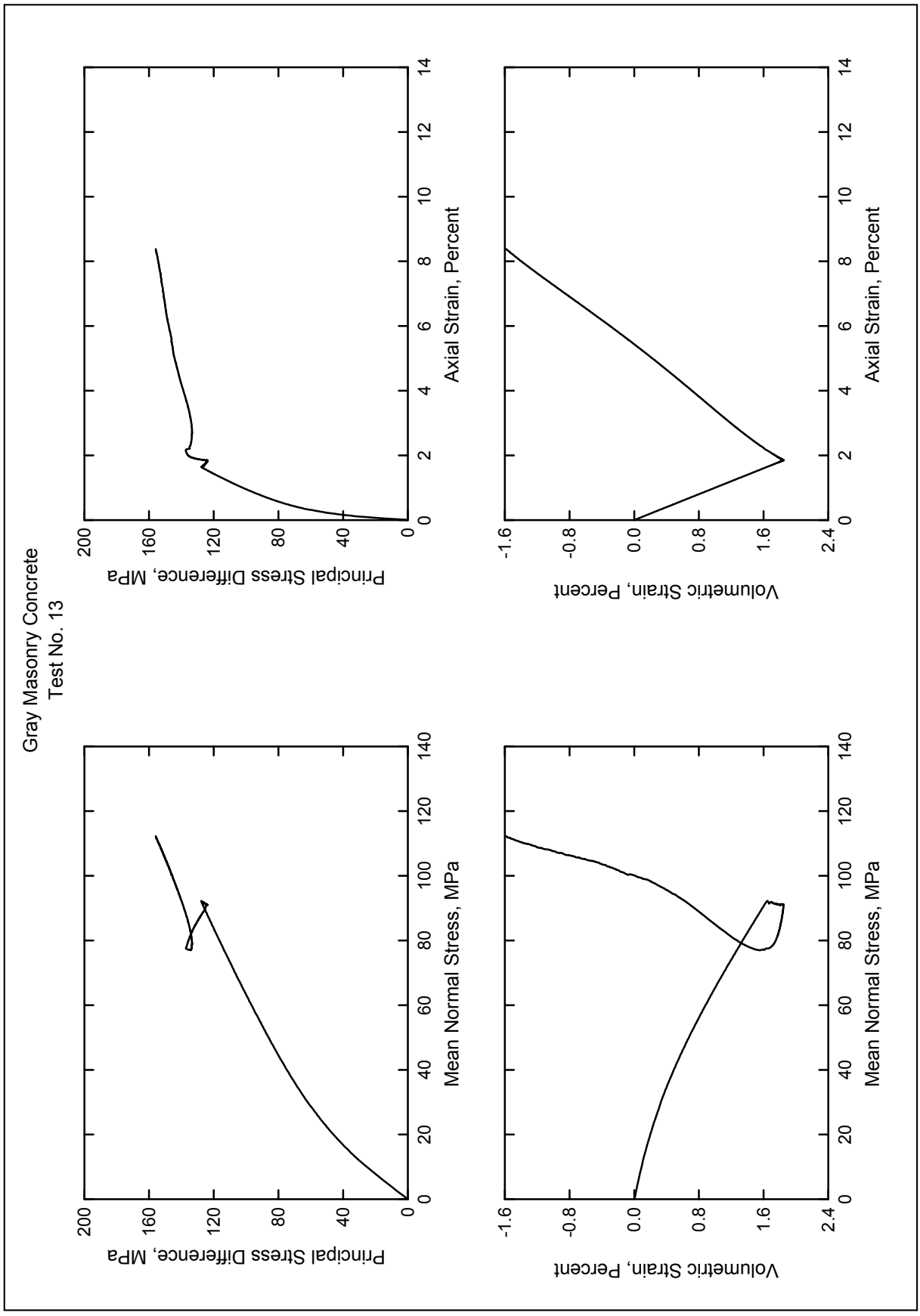
Gray Masonry Concrete
Test No. 13
Principal Stress Difference, MPa
Axial Strain, Percent
Volumetric Strain, Percent
Axial Strain, Percent
Principal Stress Difference, MPa
Mean Normal Stress, MPa
Volumetric Strain, Percent
Mean Normal Stress, MPa

Plate 32

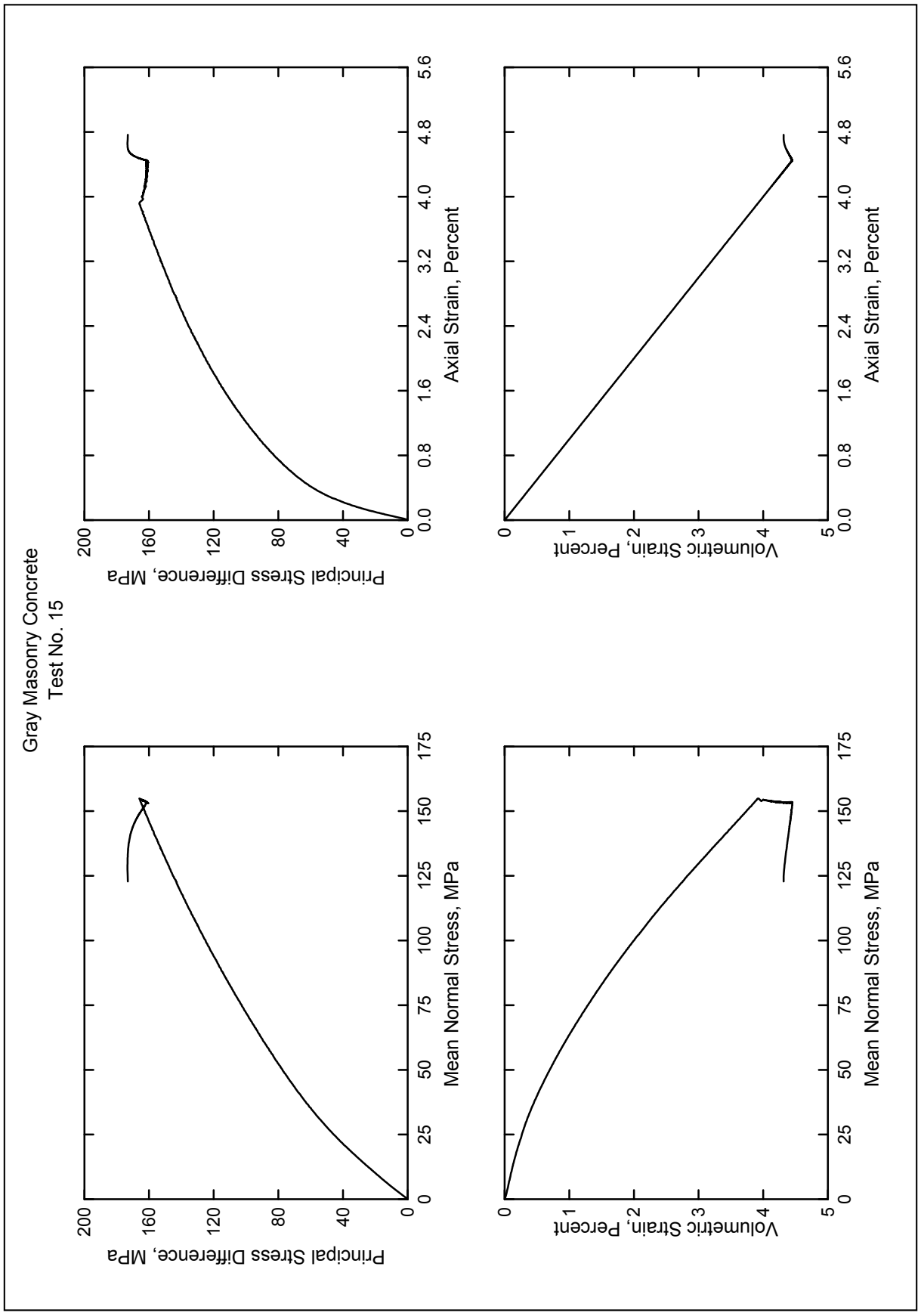
Gray Masonry Concrete
Test No. 15
Principal Stress Difference, MPa
Axial Strain, Percent
Volumetric Strain, Percent
Axial Strain, Percent
Principal Stress Difference, MPa
Mean Normal Stress, MPa
Volumetric Strain, Percent
Mean Normal Stress, MPa

Plate 33

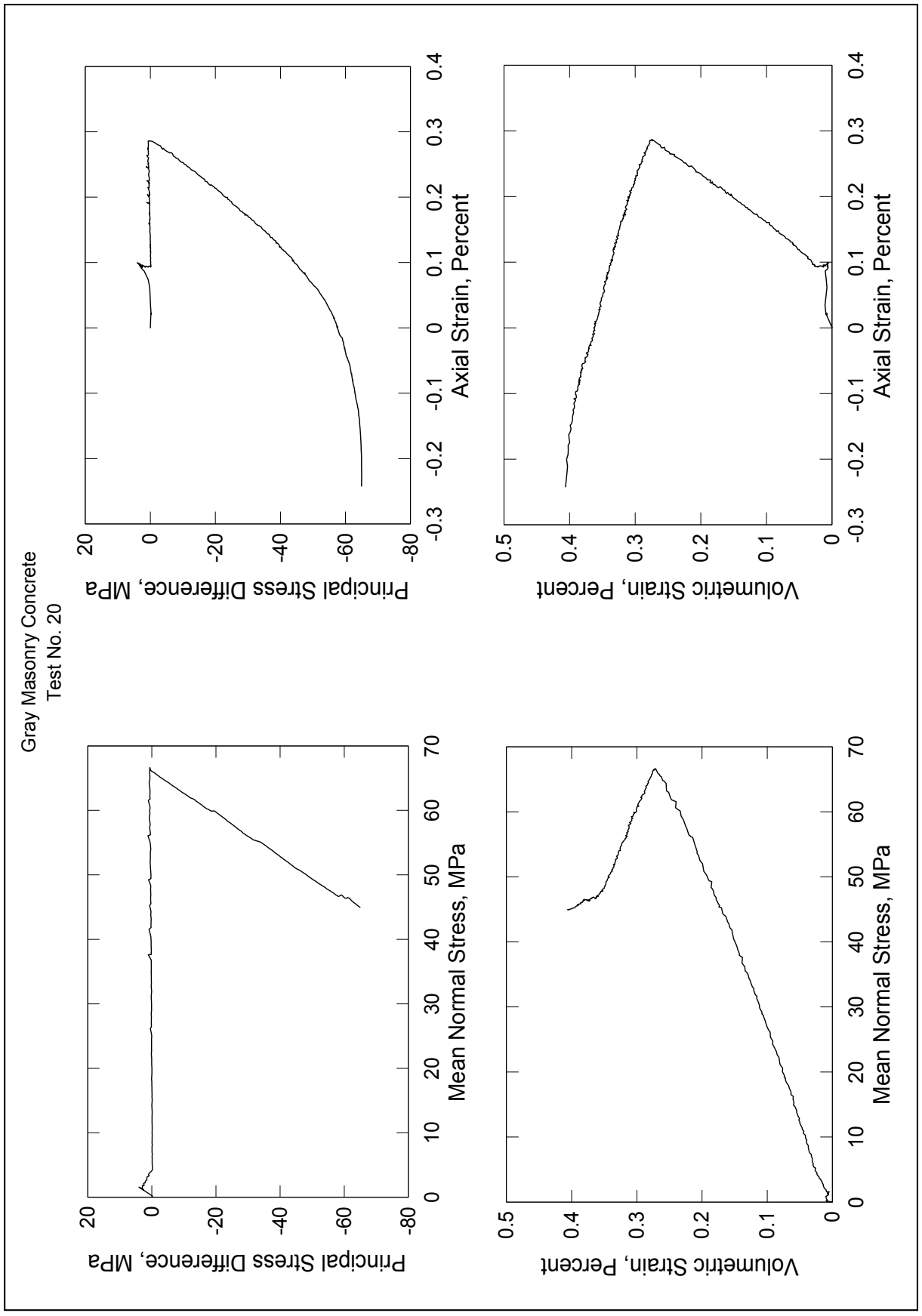
Gray Masonry Concrete
Test No. 20
Principal Stress Difference, MPa
Mean Normal Stress, MPa
Volumetric Strain, Percent
Axial Strain, Percent

Plate 34

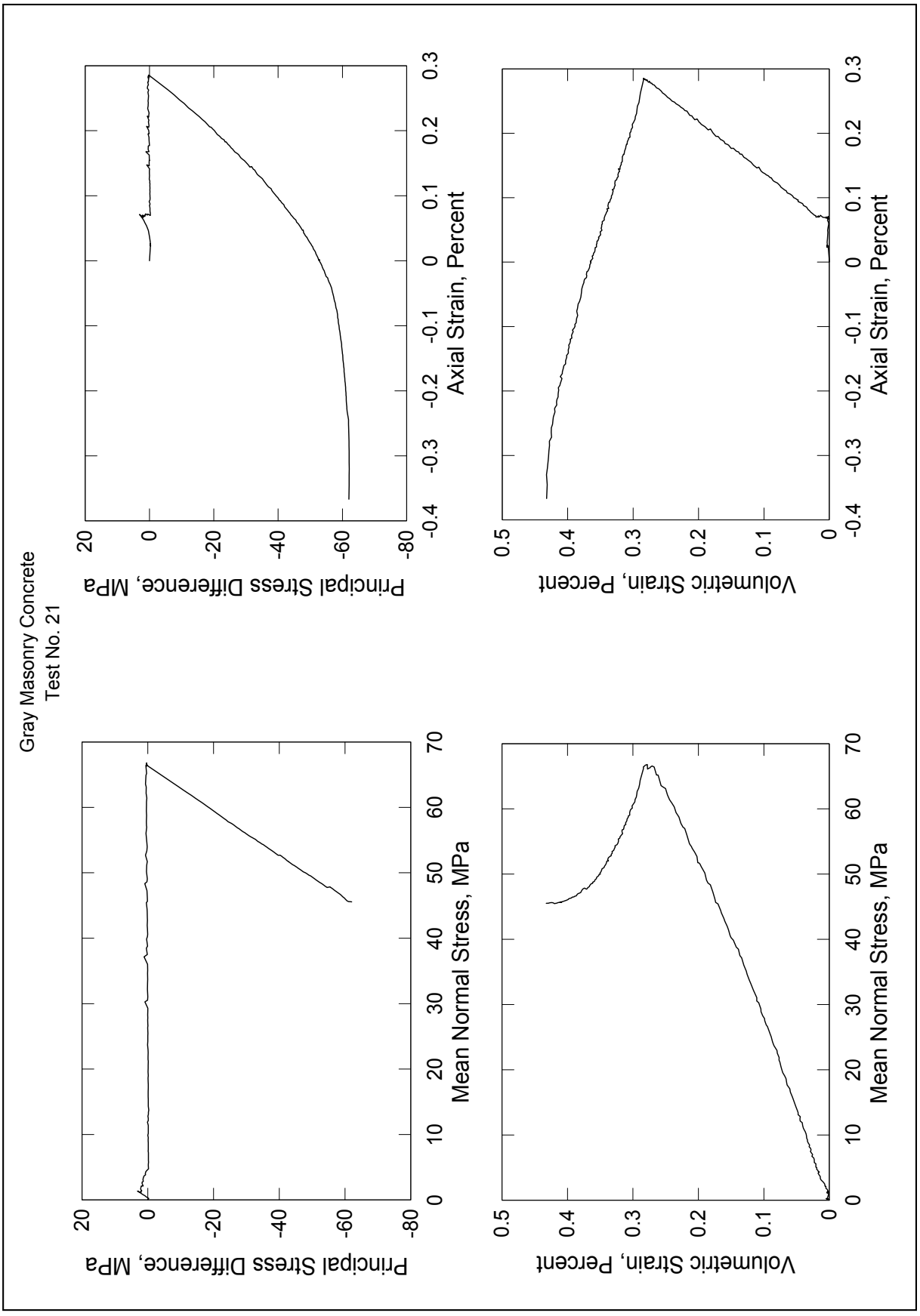
Gray Masonry Concrete
Test No. 21
Principal Stress Difference, MPa
Axial Strain, Percent
Volumetric Strain, Percent
Axial Strain, Percent
Principal Stress Difference, MPa
Mean Normal Stress, MPa
Volumetric Strain, Percent
Mean Normal Stress, MPa

Plate 35

REPORT DOCUMENTATION PAGE

Form Approved
OMB No. 0704-0188

1. REPORT DATE *(DD-MM-YYYY)*	2. REPORT TYPE	3. DATES COVERED *(From - To)*
August 2007	Final report	

4. TITLE AND SUBTITLE

Laboratory Characterization of Gray Masonry Concrete

5a. CONTRACT NUMBER

5b. GRANT NUMBER

5c. PROGRAM ELEMENT NUMBER

6. AUTHOR(S)

Erin M. Williams, Stephen A. Akers, and Paul A. Reed

5d. PROJECT NUMBER

5e. TASK NUMBER

5f. WORK UNIT NUMBER

7. PERFORMING ORGANIZATION NAME(S) AND ADDRESS(ES)

U.S. Army Engineer Research and Development Center
Geotechnical and Structures Laboratory
3909 Halls Ferry Road
Vicksburg, MS 39180-6199

8. PERFORMING ORGANIZATION REPORT NUMBER

ERDC/GSL TR-07-23

9. SPONSORING / MONITORING AGENCY NAME(S) AND ADDRESS(ES)

Headquarters, U.S. Army Corps of Engineers
Washington, DC 20314-1000

10. SPONSOR/MONITOR'S ACRONYM(S)

11. SPONSOR/MONITOR'S REPORT NUMBER(S)

12. DISTRIBUTION / AVAILABILITY STATEMENT

Approved for public release; distribution is unlimited.

13. SUPPLEMENTARY NOTES

14. ABSTRACT

Personnel of the Geotechnical and Structures Laboratory, U.S. Army Engineer Research and Development Center, conducted a laboratory investigation to characterize the strength and constitutive property behavior of a gray masonry concrete. A total of 38 mechanical property tests were successfully completed: two hydrostatic compression tests, four unconfined compression (UC) tests, 16 triaxial compression (TXC) tests, two uniaxial strain tests, two uniaxial strain load/biaxial strain unload tests, five uniaxial strain load/constant volume strain loading (UX/CV) tests, two uniaxial strain load/constant strain ratio (UX/SR) tests, three direct pull tests, and two reduced triaxial extension tests. In addition to the mechanical property tests, nondestructive pulse-velocity measurements were performed on each specimen. The TXC tests exhibited a continuous increase in maximum principal stress difference with increasing confining stress. A compression failure surface was developed from the TXC test results at eight levels of confining stress and from the results of the UC tests. The results of the direct pull and reduced triaxial extension tests were used to develop the extension failure surface. The resulting compression and extension failure surfaces were well defined and nonsymmetric about the mean normal stress axis. Good correlations were observed between the stress paths obtained from the UX/CV and UX/SR strain path tests and the failure surface from the TXC test.

15. SUBJECT TERMS

Compression tests
Extension tests
Masonry concrete
Material characterization
Material properties

16. SECURITY CLASSIFICATION OF:			17. LIMITATION OF ABSTRACT	18. NUMBER OF PAGES	19a. NAME OF RESPONSIBLE PERSON
a. REPORT	b. ABSTRACT	c. THIS PAGE			19b. TELEPHONE NUMBER *(include area code)*
UNCLASSIFIED	UNCLASSIFIED	UNCLASSIFIED		99	